



Statens vegvesen

Ferry free E39 –Fjord crossings Bjørnafjorden

304624

Rev.	Publish date	Description	Made by	Checked by	Project appro.	Client appro.
0	15.08.19	Issued for use	TNNgu			
Client						
 Statens vegvesen						
Contractor			Contract no.:			
Norconsult  DR. TECHN. OLAV OLSEN			18/91094			

Document name:

K12 – Ship impact, pontoons and columns

Document no.:

SBJ-33-C5-OON-22-RE-014-B

Rev.:

0

Pages:

82



CONCEPT DEVELOPMENT FLOATING BRIDGE E39 BJØRNAFJORDEN

K12 - Ship impact, pontoons and columns

Norconsult 

 DR. TECHN.
OLAV OLSEN

 Prodtex
Production / Technology / Excellence

 IFE
Pure Logic
The science of production reasoning

HEYERDAHL ARKITEKTER AS

 H&BB

 MIKO
MARINE AS

 BUKSÉR og
BERGING

 FORCE
TECHNOLOGY

 SWERIM

REPORT

Project name:

CONCEPT DEVELOPMENT FLOATING BRIDGE E39
BJØRNAFJORDEN

Document name:

K12 - SHIP IMPACT, PONTOONS AND COLUMNS

Project number: 5187772/12777
Document number: SBJ-33-C5-OON-22-RE-014-B

Date: 15.08.2019
Revision: 0
Number of pages: 82

Prepared by: Thanh Ngan Nguyen
Controlled by: Eivind Bjørhei
Approved by: Kolbjørn Høyland

Summary

General

The case of a ship impact on the K12 – end-anchored floating bridge with mooring system over Bjørnafjorden, is studied. The report seeks to clarify how the structure responds to ship impact locally on pontoons and columns by explicit nonlinear finite element analysis.

Bow-pontoon collision is studied for a container bow and an ice-strengthened bow. The impact directions are either head-on the pontoon or 90-degree at the transition between straight and curved pontoon wall. Impact with the ice-strengthened bow is also performed 90 degree between bulkheads and frames too obtain a softer behavior. In the local collision analyses, the pontoon is fixed against movements at the boundary of the modelled pontoon.

The pontoon in axis 3 is the basis for all impact simulations documented, since this pontoon is subjected to the largest impact energy. The pontoon width has become slightly larger (17 m) than the pontoon geometry utilized in this report (16 m), but this is considered to have negligible influence on the results.

Forecastle impact with column is not governing for the forecastles of the container and ship bows. The forecastles of the ship bows are subjected to severe damage, while the column is mostly spared.

Impact energies to be dissipated at different parts of the bridge are defined in the Design Basis [1]. The impact energies are based on risk analysis performed by Rambøll and considers annual probability of return and Heinrich factor among others.

Input from local collision response to global collision assessment is the force-displacement curves. The force-displacement curve gives the relationship between the contact force and the indentation between ship deckhouse and bridge girder. These curves are put into the global finite element model of the bridge structure by a non-linear connector element representing the ship and pontoon.

When global assessment has been conducted, several response parameters are revealed for further local damage evaluation. This includes as the most important the amount of energy that is dissipated locally and the indentation between bow and pontoon.

The impact energies defined in the Design Basis are too high to presuppose only local dissipation, and external dynamics must be accounted for. For that reason, this report does not quantify the exact damage of the pontoon, e.g. the number of filled compartments. Reference is made to the global assessment report [2]. Results for local impact response are rather given for chosen parameters as basis for comparison.

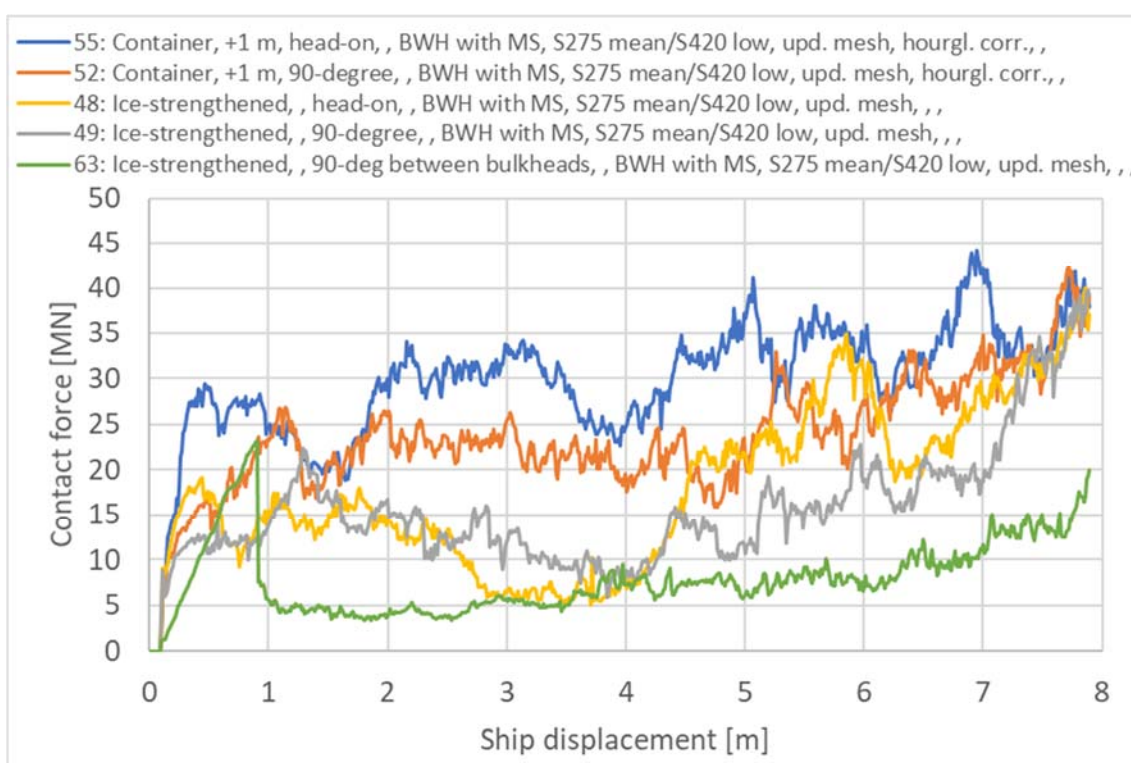
Bow-pontoon collision characteristics

In the local simulations performed, the pontoon dissipates most of the energy while the ship bow is less damaged. The distribution of energy dissipation between the pontoon and the ship bow is in the area 85/15 [%]. This means that the displacement of the connector element obtained from the global assessment can almost be transferred directly as the indentation in the pontoon.

Figure 1 shows the force-displacement curves for the different ship bows and directions investigated. Table 1 evaluates the maximum and mean contact force for the period up to 4 m ship displacement from these curves.

- > Table 1 Maximum and mean contact force [MN] impact bow-pontoon 0-4 m ship displacement

Load case	Max. contact force [MN] 0-4 m	Mean contact force [MN] 0-4 m
Container, head-on	34	27
Container, 90-degree	27	21
Ice-strengthened, head-on	19	11
Ice-strengthened, 90-degree	22	13
Ice-strengthened, 90-degree between bulkheads/frames	23	7



- > Figure 1 Contact force [MN] impact bow-pontoon

Figure 2 shows a graphical presentation of the sensitivity of bow and direction. The maximum contact force defined by a cut-off at ship displacement corresponding 100 MJ is plotted. 100 MJ is about 40 % of the energy to be dissipated for the pontoon in axis 3.

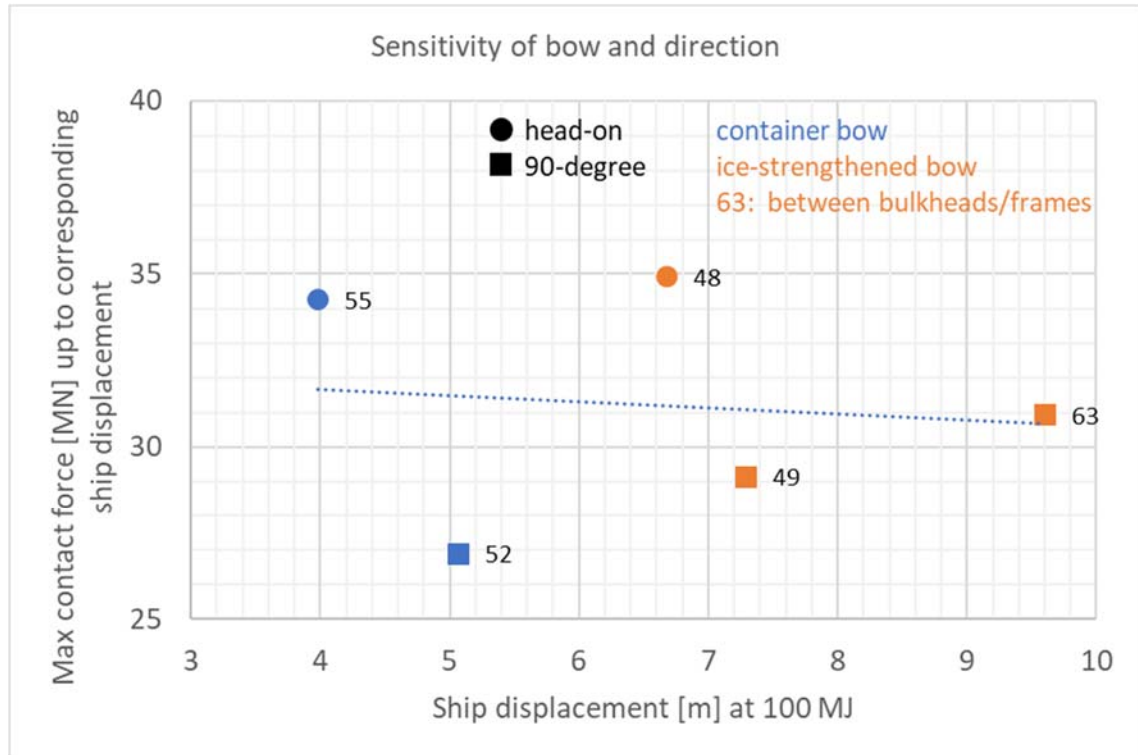


> Figure 2 Sensitivity of ship bow and direction of impact

Force reduction options

Different impact force reduction options have been tested. The damage of the pontoon is regardless severe for a slender design, which is preferred for other load cases and limit states. However, a reduced force level for pontoon collision is beneficial for the bridge girder and column.

The reduction of the force level is limited for the modifications investigated: 2 mm reduction to plate thickness, reduced stiffener height from 320 mm to 240 mm and 0.5 m corrugated bulkhead. The type of ship that hits the pontoon and the direction of the impact is of greater importance but cannot be controlled.

Sensitivity of ship impact response

The ship impact simulations performed are sensitive to several parameters. In addition to type of ship bow and direction and location of impact, sensitivity is studied for material parameters including superduplex steel, material damage models, mesh size, element type, impact height and ship velocity.

The simulation of bow-pontoon collision is sensitive to change in material parameters of the pontoon and less sensitive to change in material parameters of the ship bow. The reason is because the pontoon is more damaged in collision with the ship bow. However, only conventional types of ship bows have been studied. An inverted bow for example may reveal other impact characteristic.

Table of Content

1	INTRODUCTION	9
1.1	Current report	9
1.2	Project context	9
1.3	Project team	9
1.4	Project scope	10
2	INTRODUCTION TO SIMULATIONS	12
2.1	General	12
1.1	Design philosophy.....	12
3	MATERIAL MODELLING	14
3.1	General	14
3.2	Yield surface and plastic work hardening.....	14
3.3	Fracture and necking instability	14
3.4	Verification	16
4	SIMULATION MODELS	20
4.1	Geometry	20
4.2	Materials	26
4.3	Mesh and element formulations	28
4.4	Analysis setup	34
5	SIMULATIONS	37
5.1	Load cases.....	37
5.2	Response parameters.....	40
5.3	Response.....	41
6	INPUT TO GLOBAL COLLISION ASSESSMENT	70
7	SUMMARY AND CONCLUSIONS	71
7.1	Compilation of response	71
7.2	Discussion	72
7.3	Further work	80
8	REFERENCES	81

APPENDIX A – Abaqus terminology
APPENDIX B – Mesh and material sensitivity study
APPENDIX C – Sensitivity of ship impact response

1 INTRODUCTION

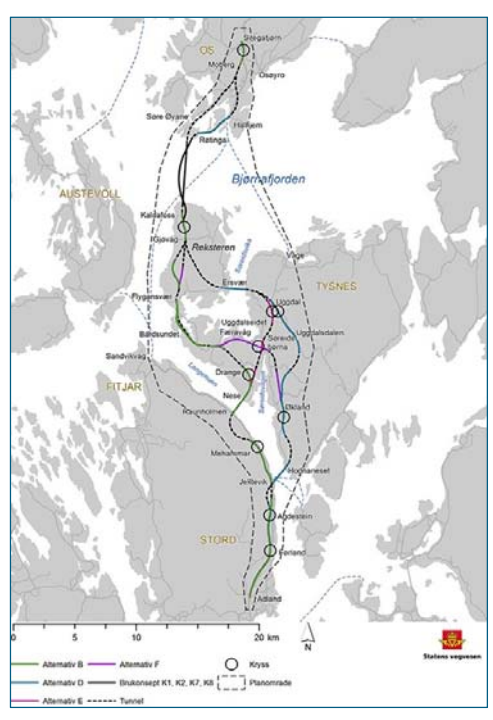
1.1 Current report

This report seeks to clarify how the K12 – end-anchored floating bridge with mooring system over Bjørnafjorden, responds to ship impact locally for pontoons and columns.

1.2 Project context

Statens vegvesen (SVV) has been commissioned by the Norwegian Ministry of Transport and Communications to develop plans for a ferry free coastal highway E39 between Kristiansand and Trondheim. The 1100 km long coastal corridor comprise today 8 ferry connections, most of them wide and deep fjord crossings that will require massive investments and longer spanning structures than previously installed in Norway. Based on the choice of concept evaluation (KVU) E39 Aksdal Bergen, the Ministry of Transport and Communications has decided that E39 shall cross Bjørnafjorden between Reksteren and Os.

SVV is finalizing the work on a governmental regional plan with consequence assessment for E39 Stord-Os. This plan recommends a route from Stord to Os, including crossing solution for Bjørnafjorden, and shall be approved by the ministry of Local Government and Modernisation. In this fifth phase of the concept development, only floating bridge alternatives remain under consideration.



1.3 Project team

Norconsult AS and Dr.techn.Olav Olsen AS have a joint work collaboration for execution of this project. Norconsult is the largest multidiscipline consultant in Norway, and is a leading player within engineering for transportation and communication. Dr.techn.Olav Olsen is an independent structural engineering and marine technology consultant firm, who has a specialty in design of large floating structures. The team has been strengthened with selected subcontractors who are all highly qualified within their respective areas of expertise:

- Prodtex AS is a consultancy company specializing in the development of modern production and design processes. Prodtex sits on a highly qualified staff who have experience from design and operation of automated factories, where robots are used to handle materials and to carry out welding processes.
- Pure Logic AS is a consultancy firm specializing in cost- and uncertainty analyses for prediction of design effects to optimize large-scale constructs, ensuring optimal feedback for a multidisciplinary project team.
- Institute for Energy Technology (IFE) is an independent nonprofit foundation with 600 employees dedicated to research on energy technologies. IFE has been working on high-performance computing software based on the Finite-Element-Method for the industry, wind, wind loads and aero-elasticity for more than 40 years.
- Buksér og Berging AS (BB) provides turn-key solutions, quality vessels and maritime personnel for the marine operations market. BB is currently operating 30 vessels for

harbour assistance, project work and offshore support from headquarter at Lysaker, Norway.

- Miko Marine AS is a Norwegian registered company, established in 1996. The company specializes in products and services for oil pollution prevention and in-water repair of ship and floating rigs, and is further offering marine operation services for transport, handling and installation of heavy construction elements in the marine environment.
- Heyerdahl Arkitekter AS has in the last 20 years been providing architect services to major national infrastructural projects, both for roads and rails. The company shares has been sold to Norconsult, and the companies will be merged by 2020.
- Haug og Blom-Bakke AS is a structural engineering consultancy firm, who has extensive experience in bridge design.
- FORCE Technology AS is engineering company supplying assistance within many fields, and has in this project phase provided services within corrosion protection by use of coating technology and inspection/maintenance/monitoring.
- Swerim is a newly founded Metals and Mining research institute. It originates from Swerea-KIMAB and Swerea-MEFOS and the metals research institute IM founded in 1921. Core competences are within Manufacturing of and with metals, including application technologies for infrastructure, vehicles / transport, and the manufacturing industry.

In order to strengthen our expertise further on risk and uncertainties management in execution of large construction projects Kåre Dybwad has been seconded to the team as a consultant.

1.4 Project scope

The objective of the current project phase is to develop 4 nominated floating bridge concepts, document all 4 concepts sufficiently for ranking, and recommend the best suited alternative. The characteristics of the 4 concepts are as follows:

- K11: End-anchored floating bridge. In previous phase named K7.
- K12: End-anchored floating bridge with mooring system for increase robustness and redundancy.
- K13: Straight side-anchored bridge with expansion joint. In previous phase named K8.
- K14: Side-anchored bridge without expansion joint.

In order to make the correct recommendation all available documentation from previous phases have been thoroughly examined. Design and construction premises as well as selection criteria have been carefully considered and discussed with the Client. This form basis for the documentation of work performed and the conclusions presented. Key tasks are:

- Global analyses including sensitivity studies and validation of results
- Prediction of aerodynamic loads
- Prediction of hydrodynamic loads
- Ship impact analyses, investigation of local and global effects
- Fatigue analyses
- Design of structural elements
- Marine geotechnical evaluations
- Steel fabrication
- Bridge assembly and installation

- Architectural design
- Risk assessment

2 INTRODUCTION TO SIMULATIONS

2.1 General

The case of a ship impact on the K12 – end-anchored floating bridge with mooring system over Bjørnafjorden, is studied. Distribution of impact energies are given in the Design Basis [1].

This report seeks to clarify how the structure responds to ship impact locally for pontoons and columns. Bow-pontoon collision is studied in the depth for the pontoon in axis 3, since this pontoon is subjected to the largest impact energy according to the Design Basis [1].

1.1 Design philosophy

Ship impacts are defined as accidental load conditions related to a recurrence period of 10 000 years. The Norwegian Public Roads Administration (NPRA) has in handbook N400 [3] set this as the limit where less likely events are disregarded.

In the Accidental Limit State (ALS) all loads are applied with partial load factors of 1.0, and structures may be designed utilizing lower material safety factors than in Ultimate Limit State (ULS) and Serviceability Limit State (SLS). Local collapse is acceptable, provided the global stability can be maintained to prevent total collapse. For the pontoons, this means that some compartments can be filled with water, as long as the bridge can sustain a post-impact phase according to NS-EN 1991-1-7 [4].

Impact loads depend on the relationship between the incoming ships mass and velocity (total impact energy) and the system response. The system response is depending on the mass (m), the combined stiffness (k) of the structure and ship, and the system damping (c). Simplified it can be described with the equation of motion below, where the impact load F varies over time.

$$m\ddot{x} + c\dot{x} + kx = F(t)$$

The dynamic response from the impact energy depend on ship stiffness and mass and mass of the structure. To ensure a ductile design the analysis considers the differences in stiffness. This is done by transferring the energy through the following steps:

1. Ship bow-pontoon/deckhouse-girder impact. Represented by a force-displacement curve, based on local analysis.
2. Bridge structure. Represented by global finite element model.

By combining the stiffness and mass in different parts of the system in one model, we obtain a realistic energy distribution. For the connection between ship and bridge girder this can be illustrated with the graph in Figure 2-1. The graph shows that the mobilized resistance is equal in the two systems, and that this balance, together with the force-displacement relations, give the corresponding deformations and energy absorption in each part of the system.

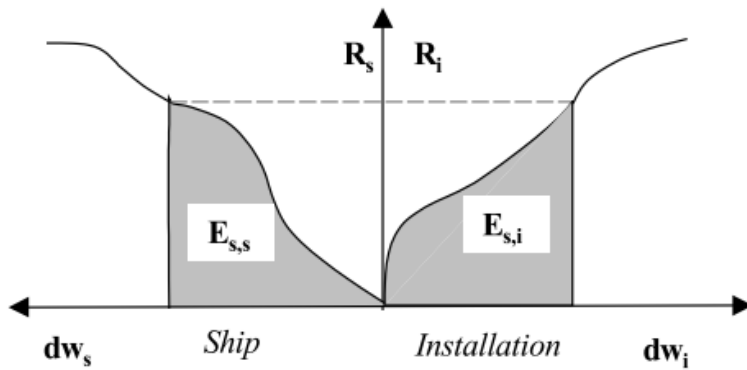


> Figure 2-1 Force equilibrium based on force-displacement curves (from [5])

Figure 2-2 shows an overview of the workflow used for the ship impact analysis, here presented by the screening analysis of girder impacts.

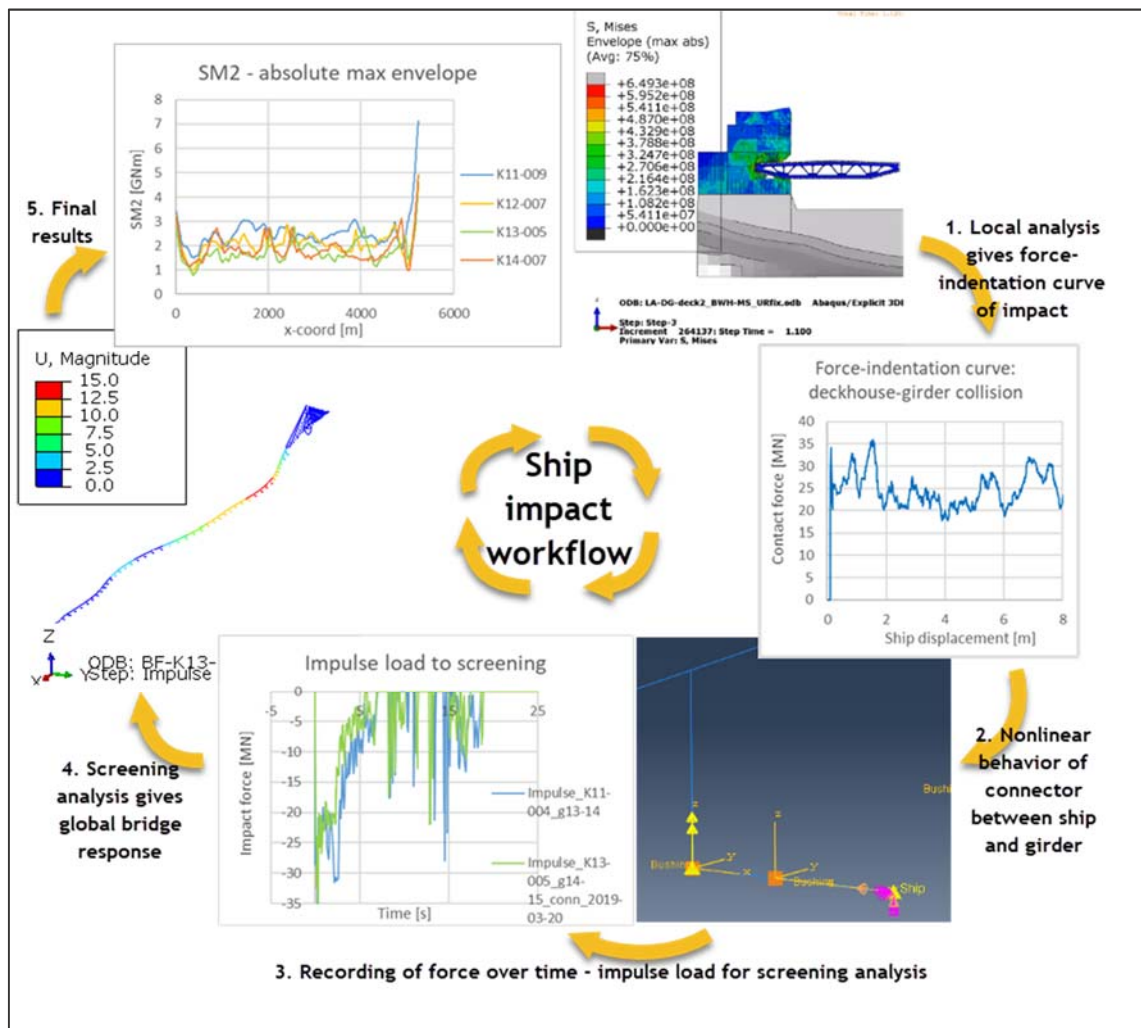


> Figure 2-2 Ship impact workflow. Local analysis: step 1. Global analysis and post-processing step 2-5.

3 MATERIAL MODELLING

3.1 General

A well-defined and robust material model is essential in the simulations of local response for the ship impact scenarios. Robustness of the material model in this context imply e.g. that the material model is not sensitive to small changes in simulation set-up. Due the nature of the concept development, the actual material properties are not known.

To obtain a representative response for the design materials it is chosen to use parameters according to DNVGL-RP 208 [6], DNVGL-OS-B101 [7], isotropic hardening and the Bressan-Williams-Hill (BWH) instability criteria.

3.2 Yield surface and plastic work hardening

Material description in the elastic range is applied using the standard material module in Abaqus [8].

Properties defining the material in the plastic range and damage evolution is defined through a subroutine developed at NTNU. The subroutine is provided by the Client and is described in Kevin Ofstads master thesis [9], and further description of the material model is given in [10]. For simplicity this material model is in this report referred to as the BWH model.

The von Mises yield surface is used for the isotropic materials. The yield surface defines when plastic strains are generated.

Isotropic hardening is applied to define how the yield surface changes for plastic strain. The isotropic hardening is considered a suitable model for problems with large plastic straining and where the strain does not continuously reverse direction sharply [8]. The rate-independent plasticity model uses associated flow. The hardening rule is given as:

$$\sigma_{eq} = Kp^n$$

where K is the power law modulus, p is the plastic strain and n is the power law exponent.

It is chosen not to include strain-rate dependence in the material. The effect of strain-rate hardening can according to [11] be significant, but the effect is less on complex structures than on uniaxial test.

3.3 Fracture and necking instability

In recent work performed at NTNU [9] [12] [13] [14] and in phase 3 of the Bjørnafjorden project [15] two main damage evolution models have been used in ship impact analysis, i.e. the Bressan-Williams-Hill (BWH) instability criterium and the Rice-Tracy-Cockcroft-Latham (RTCL) criterium. In the current work it is chosen to use the BWH criterium due to computation time, availability and compatibility with the Abaqus software. The material model is described in short, for details it is referred to [9] and [10] For verification of the received model, simulations have also been performed with both strain- and stress-based material models in Abaqus, see Appendix B [16] for results.

The BWH model combine Hill's criterion for onset of local necking and Bressan-William's criterion for shear failure. Strain-rate effects are not included in the instability model.

The failure criterion in the subroutine is stress-based and can be written with regards to critical major principle stress:

$$\sigma_1 = \begin{cases} \frac{2K}{\sqrt{3}} \frac{1+\frac{1}{2}\beta}{\sqrt{1+\beta+\beta^2}} \left(\frac{2}{\sqrt{3}} \frac{\hat{\varepsilon}_1}{1+\beta} \sqrt{1+\beta+\beta^2} \right)^n & \text{for } \beta \in (-1, 0] \\ \frac{2}{\sqrt{3}} K \frac{\left(\frac{2}{\sqrt{3}} \hat{\varepsilon}_1 \right)^n}{\sqrt{1-\left(\frac{\beta}{2+\beta}\right)^2}} & \text{for } \beta \in (0, 1] \end{cases}$$

where $\hat{\varepsilon}_1$ is the critical strain and assumed equal to the power law exponent n , and β is the strain increment ratio given as:

$$\beta = \frac{d\varepsilon_2^p}{d\varepsilon_1^p}$$

where ε_1^p and ε_2^p are the major and minor principle plastic strain respectively.

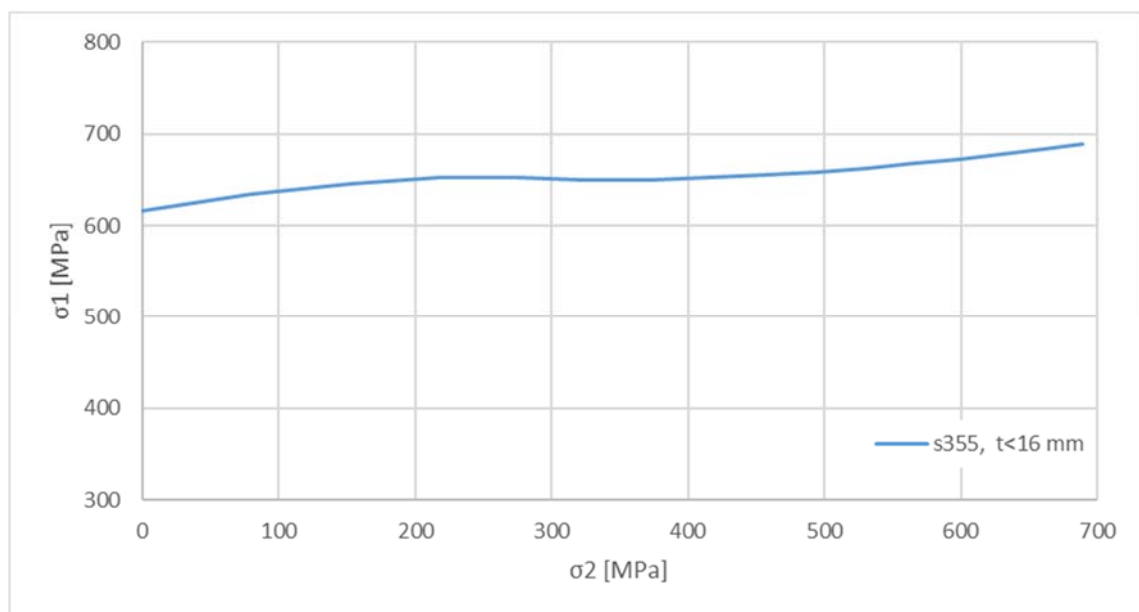


> Figure 3-1 BWH failure criterion for plane-stress conditions. Exemplified with S355 steel.

The parameter $\hat{\varepsilon}_1$ have element size dependent qualities and Alsos et. al. [14] included a scaling factor that have been implemented in the applied subroutine. With the assumption that $\hat{\varepsilon}_1$ equal to n , the mesh scaling is included by doing the following replacement in the expression for σ_1 above:

$$\hat{\varepsilon}_1 = \frac{1}{2} \left(1 + \frac{t_e}{l_e} \right) * n$$

where t_e is the element thickness and l_e is the element length at initial configuration. The effect of this scaling factor has been investigated in section 3.4.2.

3.4 Verification

Verification of the material model is sought through available literature and by comparison with other well-defined material models.

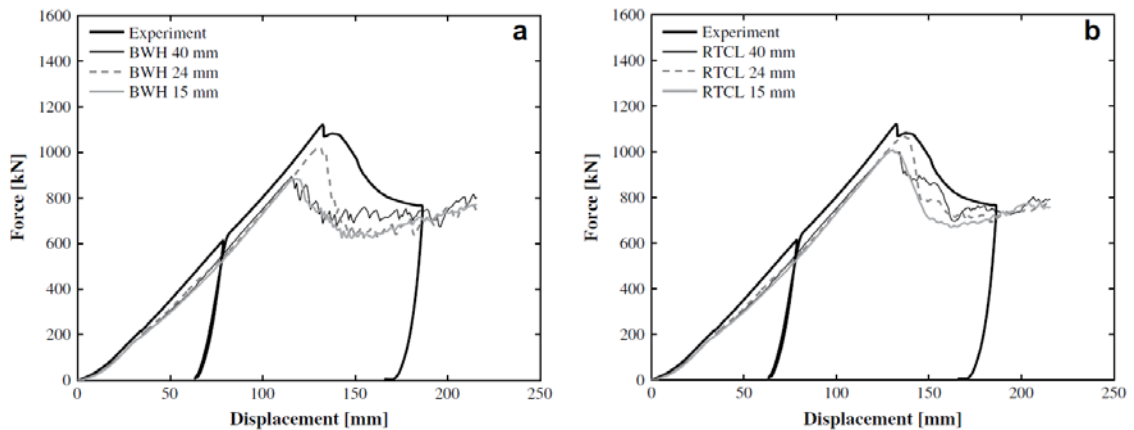
3.4.1 Numerical simulations compared with experimental tests

A study by Alsos, Amdahl and Hopperstad [14] have compared the BWH instability criterion and RTCL fracture criterion with experimental tests presented in [17]. The experimental test is done with a scaled down plate section without stiffeners, with flat bar stiffeners and HP stiffeners. Figure 3-2 show the plate with two HP stiffeners after fracture.



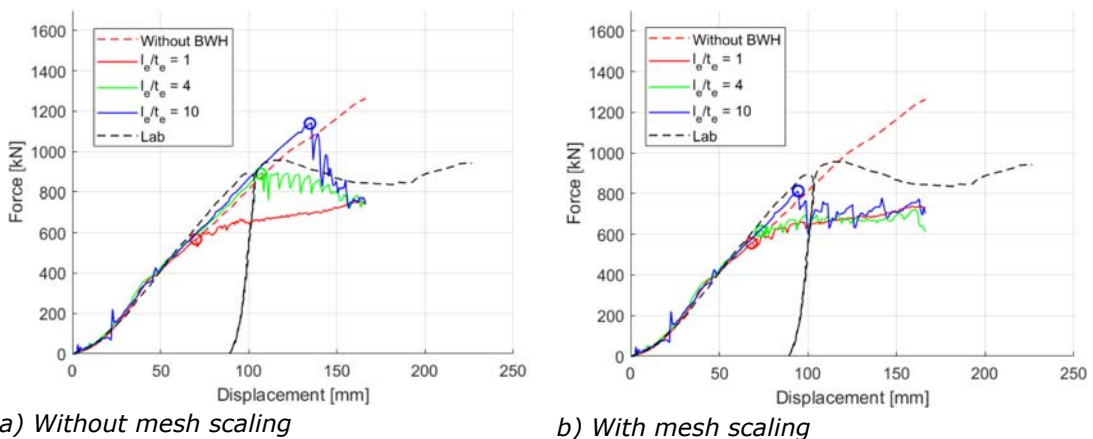
> Figure 3-2 Experimental test. Indentation of panel with 2 HP-stiffeners [17].

Simulations of the plate with two HP stiffeners show that the result is quite mesh dependent for the BWH model, see Figure 3-3. The thickness of the plate is 5 mm and the stiffeners have thickness 6 mm.



- > Figure 3-3 Force-displacement behavior of panel 2-FB. Failure criterion scaling is used at the plate–stiffener junctions: (a) simulations using the BWH criterion, (b) simulations using the RTCL criterion [14]. Plate thickness 40 mm, 24 mm and 15 mm give a l/t -ratio of 8, 4.8 and 3 respectively.

As seen in Figure 3-3 the simulations with the BWH criterion is sensitive to mesh size. Ofstad [9] compared analysis results for the BWH model with both formability tests and the stiffened plate experiment presented by Alsos and Amdahl [17]. Where mesh scaling is applied it is applied for all elements in the model. The simulations show that the mesh scaling underestimate the capacity compared with the experiment presented by Alsos and Amdahl. It should be noted that weld elements are applied in the model. The weld elements get a yield concentration that may occur due to pore element geometry, i.e. length/width ratio. Summary of the results from analysis on the stiffened plate are given in Figure 3-4.



- > Figure 3-4 Force-displacement curves for plate with two HP stiffeners from test and simulations with different mesh size. [9]

Ofstad also apply the BWH model in simulations of the result of another experiment with a stiffened plate subjected to low-velocity impact. This test specimen has 6 L-stiffeners and a planar geometry of 1375 mm x 1250 mm, see [9] for details. In the simulations of this case weld elements are not used. The results show far better agreement with respect to force level at fracture compared with the simulations including weld elements, see Figure 3-5.

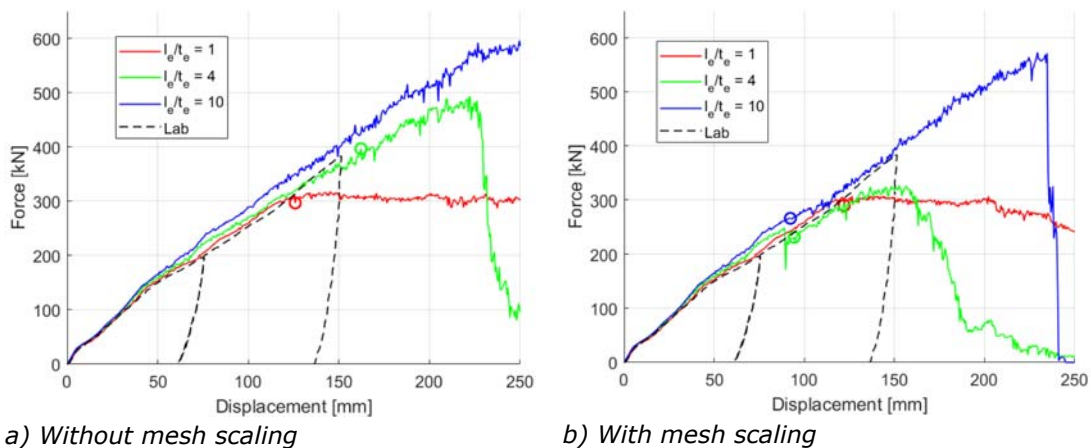


> Figure 3-5 Force-displacement curves for clamped plate with 6 L stiffeners from test and simulations with different mesh size. [9]

From the results discussed above the BWH model is considered suitable for the ship impact analyses performed with mesh scaling applied and no special weld elements.

3.4.2 Sensitivity analyses for material model, effects of mesh size and mesh scaling

To verify the BWH subroutine received from NTNU simulations have been performed on a limited model with the same characteristics as the ship impact models, see Figure 3-6. For more details and additional results see Appendix B [16].

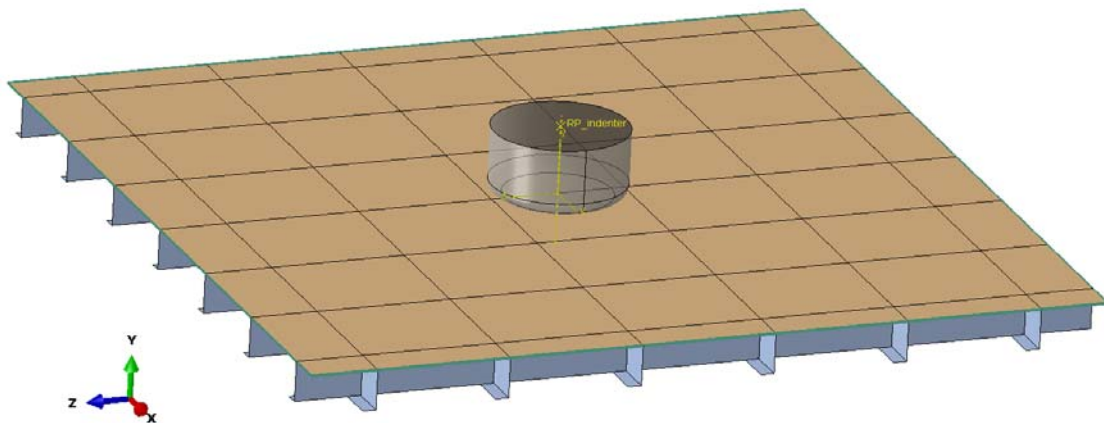


> Figure 3-6 Geometry of model for mesh sensitivity study

The simulations show that the response is sensitive with respect to mesh size. The mesh size influence in particular damage evolution and fracture.

The tested material models FLD (Forming Limit Diagram) and FLSD (Forming Limit Stress Diagram) with Swift instability predict fracture at approximately the same level as BWH without mesh scaling. The FLD material with Store and Rice bifurcation model predict fracture at a higher force level, see Appendix B [16] for material description and results.

The received ship models have typical element-length/thickness (l/t) ratio between 5 and 10 and the same l/t -ration is used when meshing the pontoons and bridge girder.

A mesh sensitivity study is performed for l/t -ratios from 1 to 50.

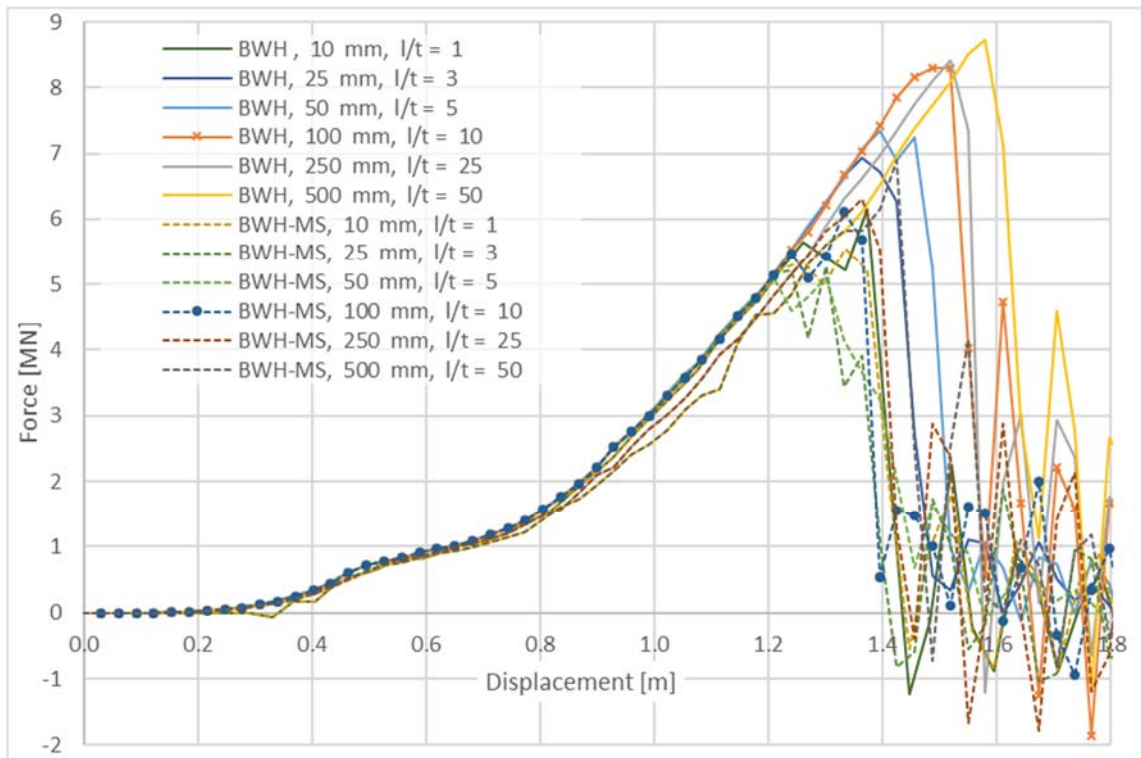


> Figure 3-7 Sensitivity study for BWH. MS – mesh scaling.

The difference in force level at collapse is more significant in simulations using materials without mesh scaling than for the simulations where mesh scaling is applied. The results for $l/t=1$ without mesh scaling is in the same range as results with mesh scaling and l/t -ratio of 1-25.

With respect to the effect of mesh size it is chosen to use the BWH model with l/t -ratio of 5-10 and apply mesh scaling to the full analysis.

4 SIMULATION MODELS

The software Abaqus/Explicit [8] is utilized for the local ship impact analyses.

4.1 Geometry

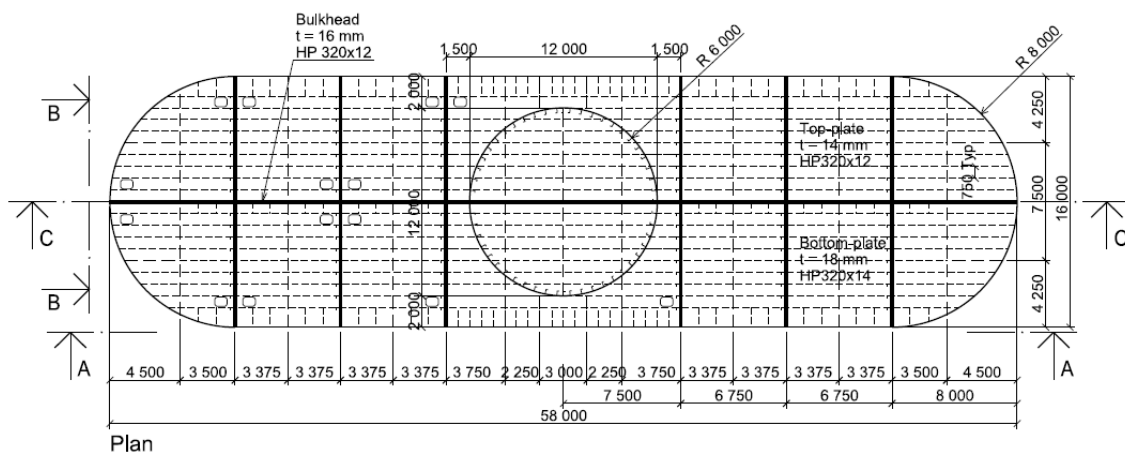
4.1.1 Pontoon and ship bows

The simulation models for local response of bow-pontoon collision consist of two parts, a ship bow and a pontoon.

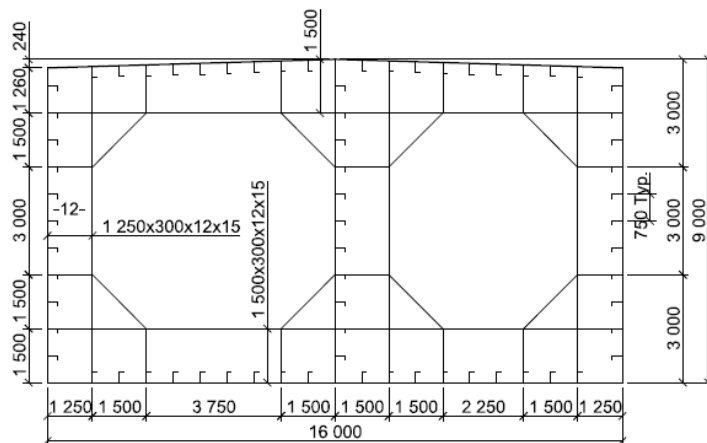
Two models of representative ship bows are provided by the Client and described in the Design Basis [1]. A container bow with a conventional bulb and an ice-strengthened bow with a stiffer and smaller bulb.

The geometry of the pontoon is taken from the K7 end-anchored floating bridge in phase 3 of the Bjørnafjorden project, drawings K7-057 [18] and K7-063 [19]. Later, an assessment should be made of whether the final geometry of the pontoons will change the results in this report. The pontoon design documented in [20] has larger width (17.0 m) than the pontoon geometry utilized for ship impact in this report (16.0 m). The larger width is considered to have negligible influence on the results.

It is chosen to model and analyze the largest pontoon, i.e. the pontoon in axis 3 (16.0 m), because a larger impact area is considered conservative in terms of impact force and energy level.

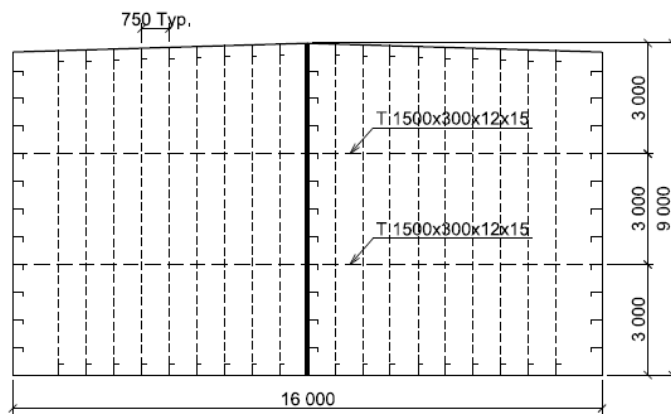


- > Figure 4-1 Plan of the pontoon in axis 3, from drawing K7-057 [18]. The pontoon width has become slightly larger (17 m) than the pontoon geometry utilized in this report (16 m), but this is considered to have negligible influence on the results.



Section D-D₋₀₅₇

- > Figure 4-2 Frame and bulkhead in pontoon in axis 3, from drawing K7-063 [19]



Section E-E₋₀₅₇

- > Figure 4-3 Bulkhead in pontoon in axis 3, from drawing K7-063 [19]

Pontoon finite element model data overview:

- Length modelled: 21.5 m (6 compartments)
- Plate thicknesses: 14 mm (top), 16 mm (walls and bulkheads), 18 mm (bottom)
- Frames: 1500x300x12x15 and 1250x300x12x15
- Stiffeners: HP320x12 for all plates

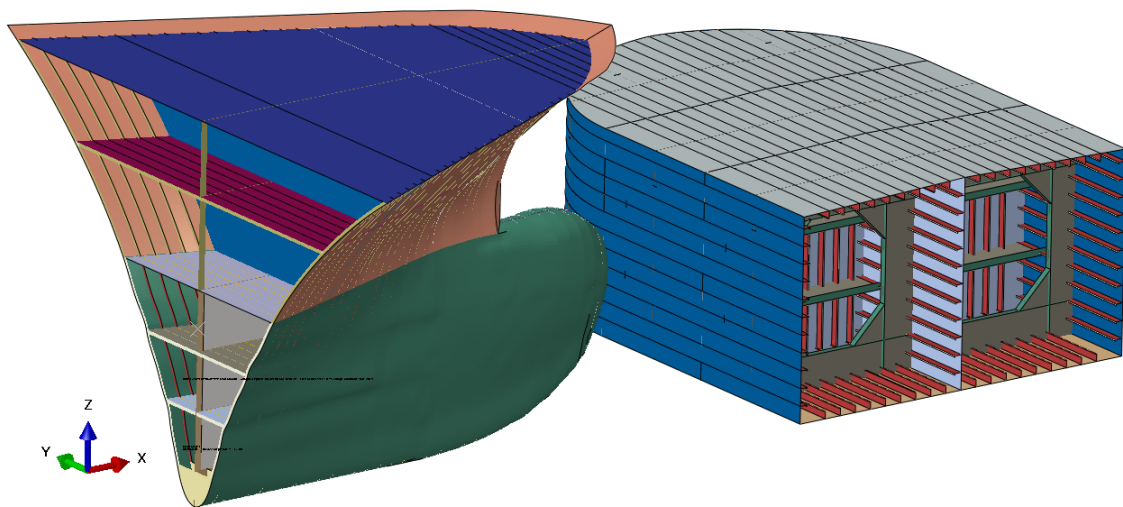


> Figure 4-4 Pontoon finite element model with container bow 90-degree impact

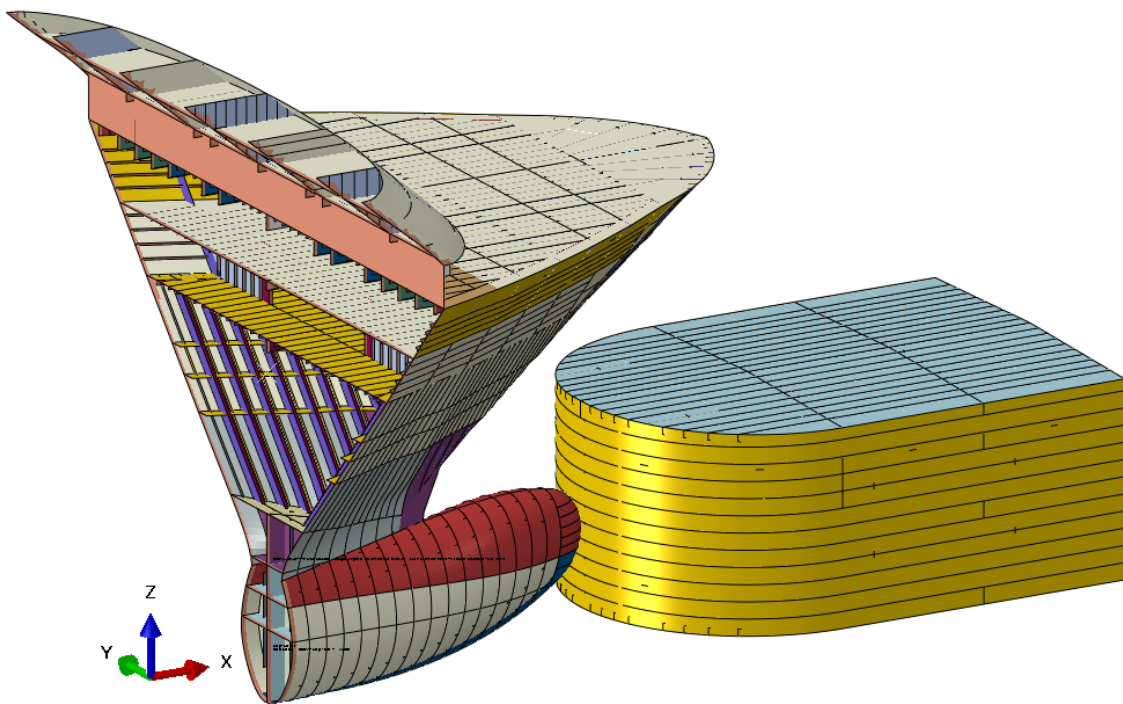


> Figure 4-5 Pontoon finite element model with ice-strengthened bow head-on impact

The modelled length of the pontoon is considered sufficiently for local response investigation since the stresses are in the elastic area at the boundary.

Drawings show stiffeners HP 320x14 in the bottom plate, but all stiffeners are modelled as HP320x12. The difference is considered negligible. The HP320x12 stiffeners are modelled as L-stiffeners with length 320 mm and 58 mm of the two legs. The thickness of the short leg is set to twice the radius of the HP stiffener.

Modifications to the pontoon geometry have been conducted to investigate possible reductions to the impact force. This includes:

- Reduced plate thicknesses to 12 mm (top), 14 mm (walls and bulkheads) and 16 mm (bottom)
- Reduced stiffeners to HP240x12 for all plates
- Corrugated bulkheads in the front of the pontoon, shown in Figure 4-6 and Figure 4-7

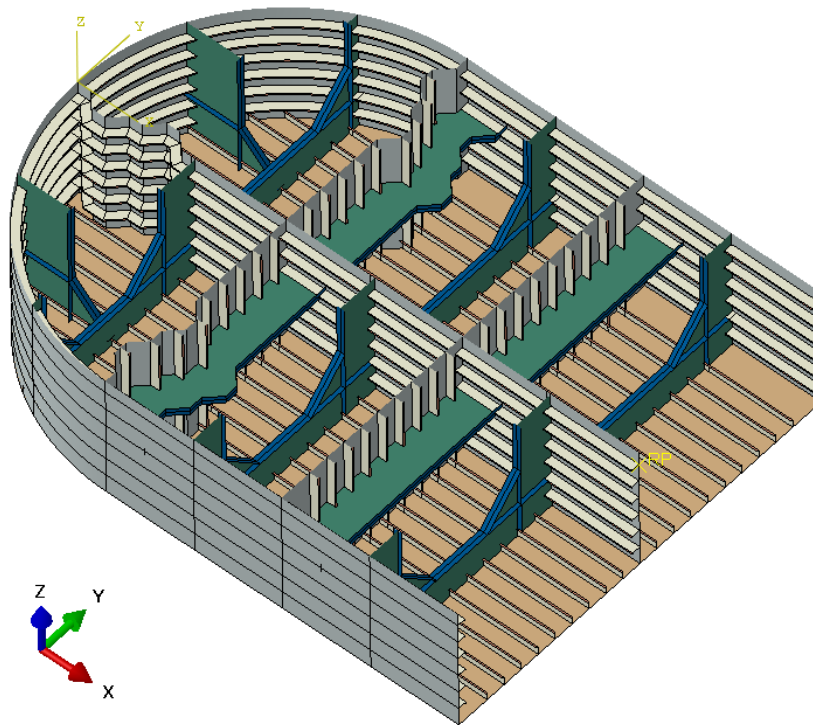


> *Figure 4-6 Corrugated pontoon finite element model*

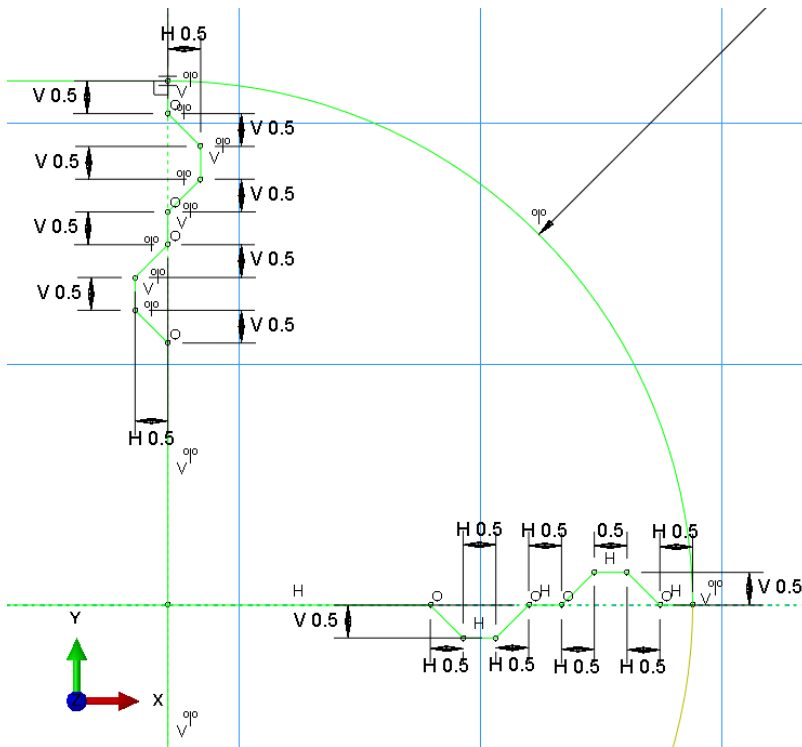


> Figure 4-7 Dimensions [m] of the corrugated plates

4.1.2 Column

The simulation models for local response of forecastle-column collision consist of two parts, the ship bows from section 4.1.1 and a column.

The columns are generally 4 m x 12 m, shown in Figure 4-8. Three vertical bulkheads run throughout the length of the column, in addition to stiffeners with height 0.4 m.

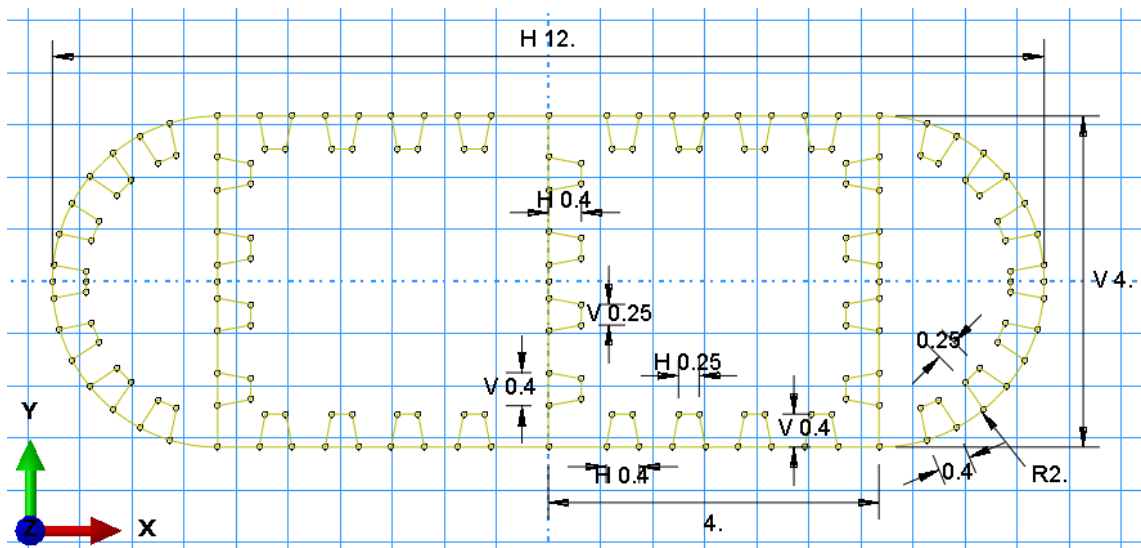


> Figure 4-8 Plan of the column, dimensions in [m]

Column finite element model data overview (not final design):

- Length modelled: 14 m (short column at low bridge)
- Plate thickness: 20 mm
- Horizontal bulkheads: every 4 m, 14 mm
- Vertical bulkheads: 3 pieces, 14 mm
- Stiffeners: 400 x 400 mm

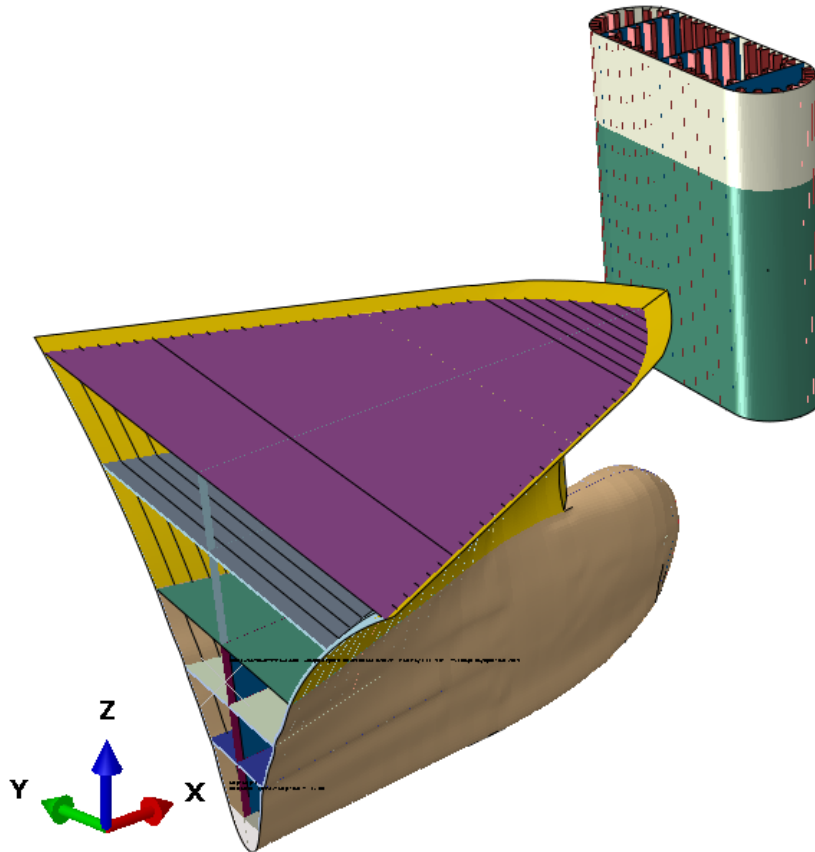


> Figure 4-9 Column finite element model with container bow 90-degree impact

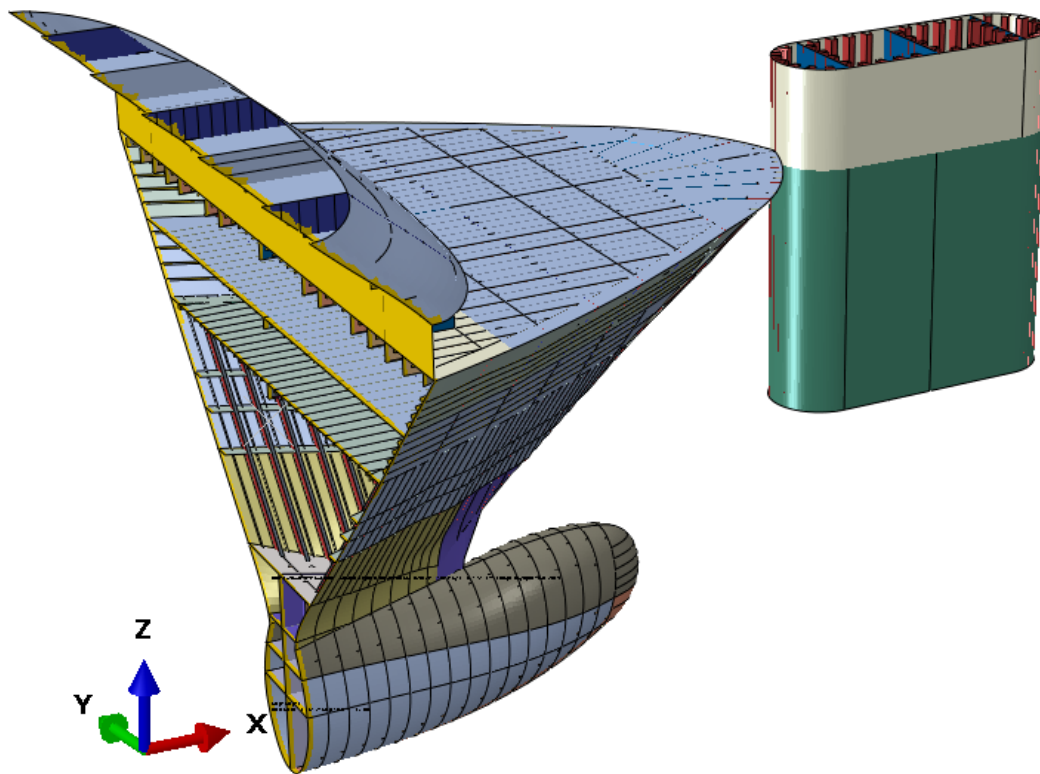


> Figure 4-10 Column finite element model with ice-strengthened bow head-on impact

4.2 Materials

It has been performed a large amount of sensitivity analyses related to material model and material quality. With reference to chapter 3, the Bressan-Williams-Hill (BWH) instability criteria is considered as the most reliable material model tested.

Mainly two sets of material parameters to define the isotropic hardening have been utilized in the analyses:

1. *Low deckhouse, low bridge girder*: Low fracture material parameters according to DNVGL-RP-C208 [6] section 4.6.6
2. *Mean deckhouse, low bridge girder* (but higher than low bridge girder in bullet 1): "Mean-low" material parameters with
 - a. Yield stress according to DNVGL-RP-C208 [6], mean value of S275 (section 7.8) and low fracture value of S355 and S420 (section 4.6.6)
 - b. $\epsilon_{\text{plateau}}$ according to DNVGL-RP-C208 [6] (sections 4.6.6 and 7.8)
 - c. Hardening parameters K and n based on formulas mentioned by Storheim [21] section 3.7.3:

$$n = \ln(1 + \epsilon_{\text{UTS}} - \epsilon_{\text{plateau}})$$

$$K = \sigma_{\text{UTS}} \cdot \left(\frac{\epsilon}{n}\right)^n$$

where ϵ_{UTS} is the maximum uniform strain (elongation) from a tensile test and σ_{UTS} is the associated ultimate tensile strength

- d. ϵ_{UTS} and σ_{UTS} from DNVGL-OS-B101 [7]

The material parameters in bullet number 2 defines the base case material and are summarized in Table 4-1. Figure 4-11 shows the evaluated stress-strain curves. True stress-strain curves are utilized as oppose to engineering stress-strain curves.

> Table 4-1 Base case: "Mean-low" material parameters

	Steel quality	Yield stress ¹	$\epsilon_{\text{plateau}}$	K	n
Ship bows	S275	331.8 MPa	0.017	764 MPa	0.185
Pontoon stiffeners	S355	357 MPa	0.015	796 MPa	0.178
Pontoon plates	S420	422.5 MPa	0.012	827 MPa	0.155
Pontoon splash zone ²	superduplex	530 MPa	0.01	1260 MPa	0.215

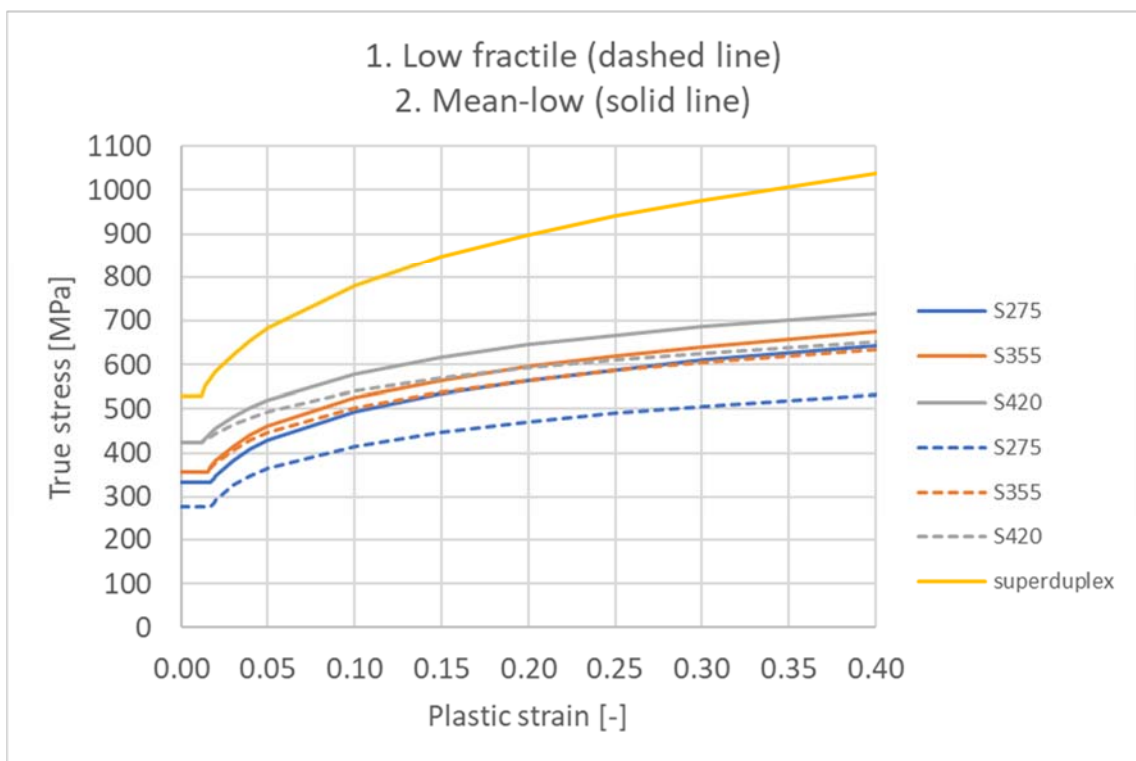


> Figure 4-11 True stress-strain curves of the steel materials, solid lines define the base case materials utilized

Stress-strain curve for the superduplex steel is also evaluated in the equal manner, based on yield stress, tensile strength (low) and elongation for the "Forta SDX 100" material by Outokumpu.

Mean material parameters according to DNVGL-RP-C208 [6] have also been tested. In addition, a set of "mean-high" material parameters with mean yield stress (according to [6])

¹ For thicknesses 16 mm and below

² Only for sensitivity analyses. The splash zone is from 1.3 m below to 1.7 m above water level.

and high K for S355 and S420, is tested. Yield stress, $\epsilon_{\text{plateau}}$ and K for S275 in the “mean-high” set of material parameters are equal to S275 in Table 4-1. See Appendix C sections 2 and 3 [22] for details.

The reason for choosing low yield stress and K for the pontoons is because the “mean-high” material parameters are considered too conservative. Note that the low values chosen are still higher than low fracture values according to DNVGL-RP-C208 [6]. Since the bridge is designed utilizing low material properties, it seems more holistic to utilize low material properties for the pontoons when evaluating the ship impact response. The “mean-low” material parameters are furthermore close to the material parameters chosen for the work performed at NTNU [12] and by the suspension bridge group [15] in the previous phases of the Bjørnafjorden project.

The choice of material parameters defining the isotropic hardening can affect the ship impact response significantly. Generally, a higher material curve also represents a higher force and energy level. To lower the uncertainties regarding higher material quality than accounted for, an opportunity is to specify the maximum values to yield and ultimate tensile stress to the supplier of the bridge steel materials. This is checked with SSAB that it is possible [23]. SSAB also states that typical maximum yield strength for S355 and S420 is 40-60 MPa above minimum value [23]. Minimum and maximum tensile strength is usually specified in the supplier’s data sheets or standards, for example DNVGL-OS-B101 [7].

Following material characteristics are also utilized for the simulations:

- Mesh scaling as a part of the BWH model, described in section 3.3 and 3.4, is applied to the entire model.
- Young’s modulus $E = 210 \text{ GPa}$, Poisson’s ratio $\nu = 0.3$ and density $\rho = 7850 \text{ kg/m}^3$ are chosen for all materials.

4.3 Mesh and element formulations

The finite element model consists of mainly S4R elements, which are linear shell elements with reduced integration. A few S3R elements occur. Full integration for all triangular and rectangular elements in the finite element model is tested for sensitivity analysis.

The characteristic element size of both ship models is 100-150 mm. The element size of the stiffeners in the container bow model is 130-210 mm, with typically one element over the height of the stiffener. The element size of the stiffeners in the ice-strengthened bow model is 70-140 mm, with typically two-three elements over the height of the stiffener.

For the pontoon model, the characteristic element size is 100 mm at impact areas. The element size of the stiffeners in the pontoon model is 80-110 mm, with typically three-four elements over the height of the stiffener.

For the column model, the characteristic element size is 100 mm. The element size of the stiffeners in the column model is 100 mm, with typically four elements over the height of the stiffener.

Sensitivity analysis is performed for a refined mesh of the pontoon model with characteristic element size 50 mm. This means that the element size of the stiffeners is also reduced to the half, and the number of elements over the height of the stiffeners is doubled.

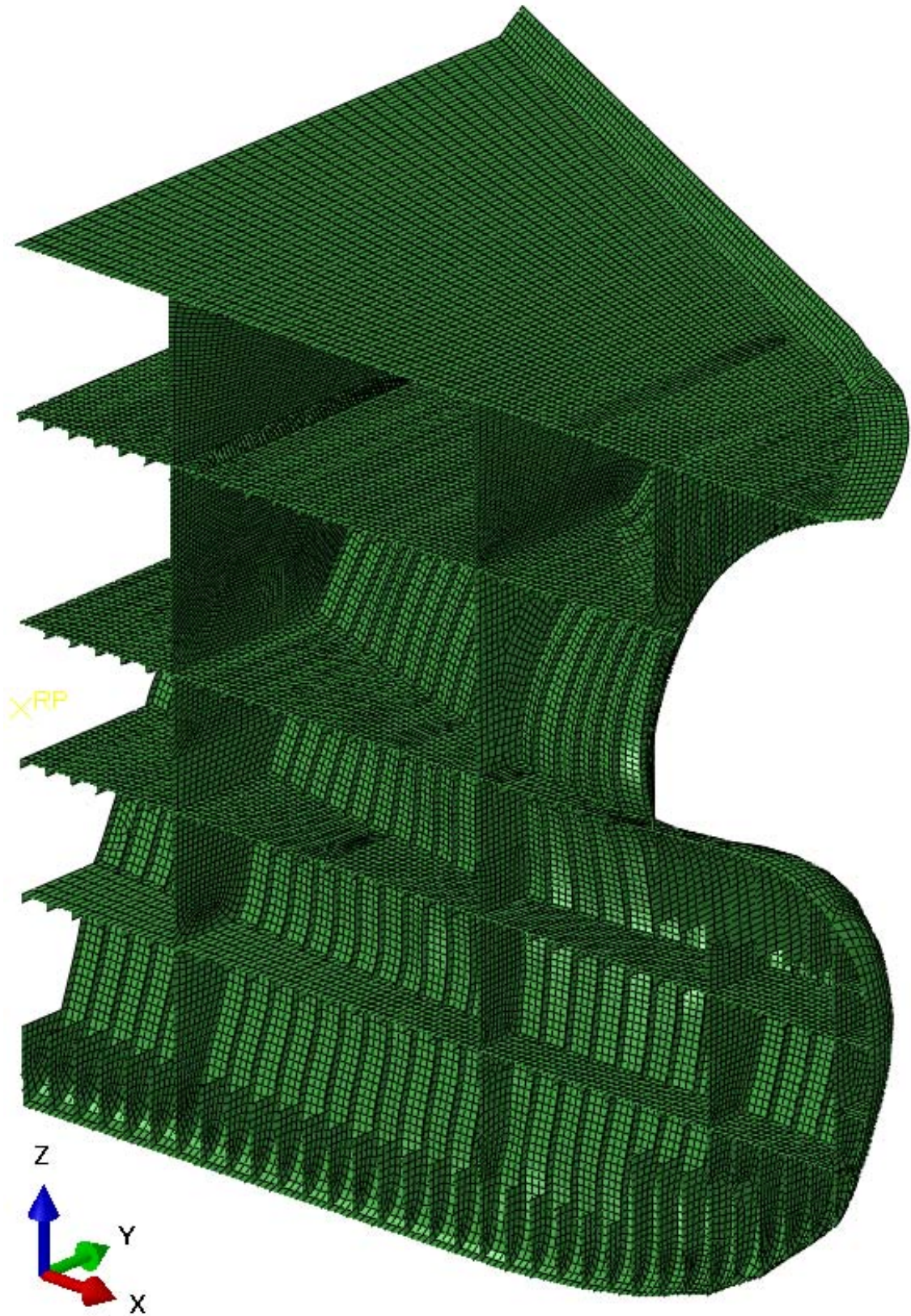


> Figure 4-12 Mesh of the container bow, shown cut in half

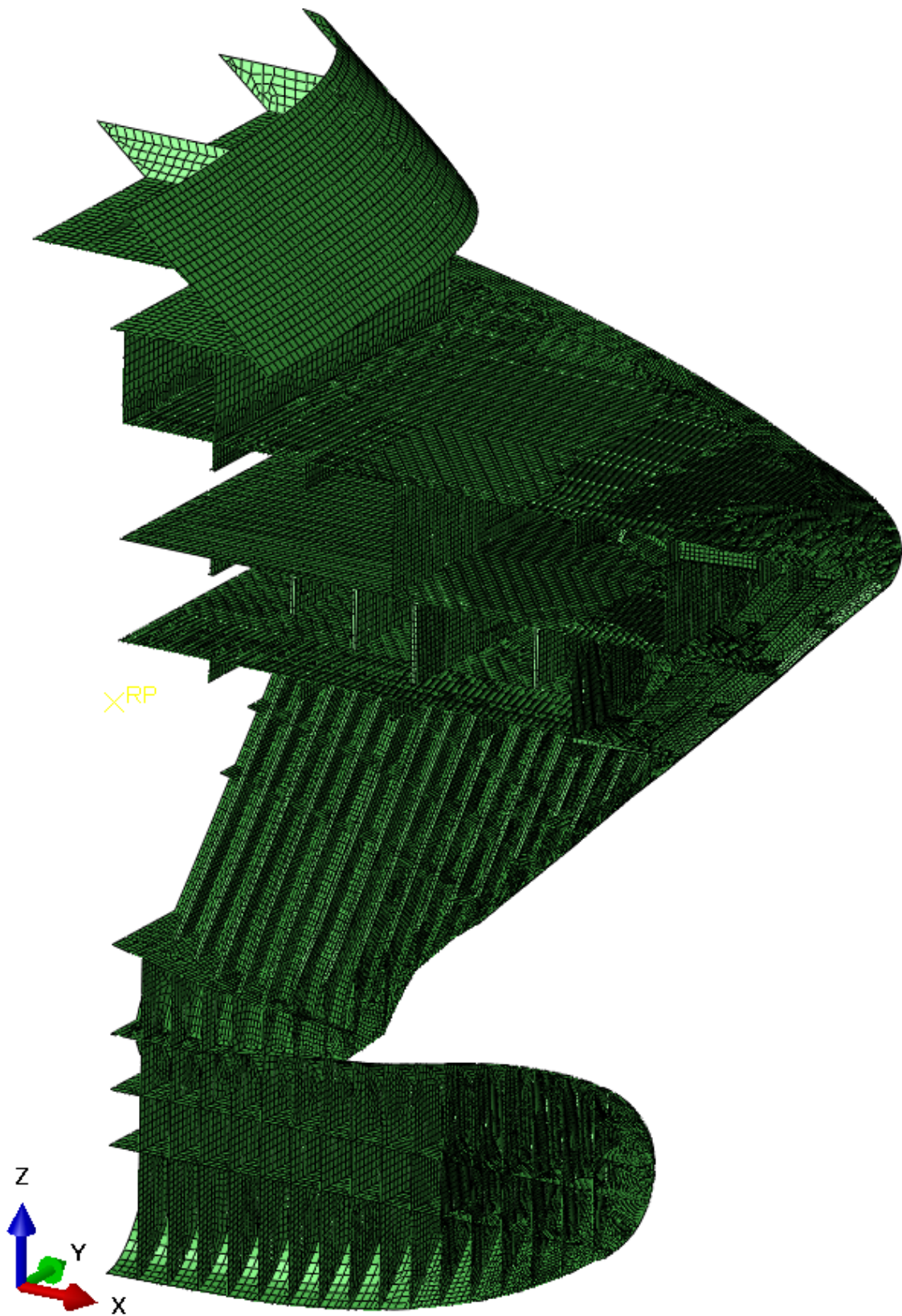


> Figure 4-13 Mesh of the ice-strengthened bow, shown cut in half

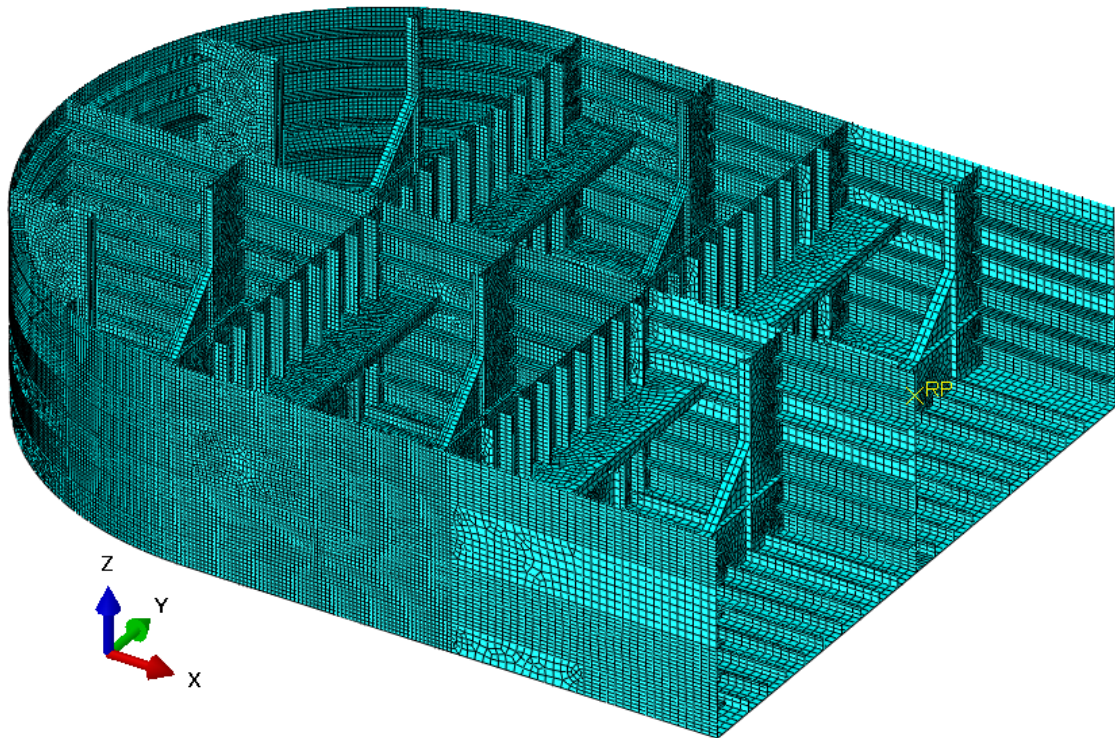


> Figure 4-14 Mesh of the pontoon, shown cut in half

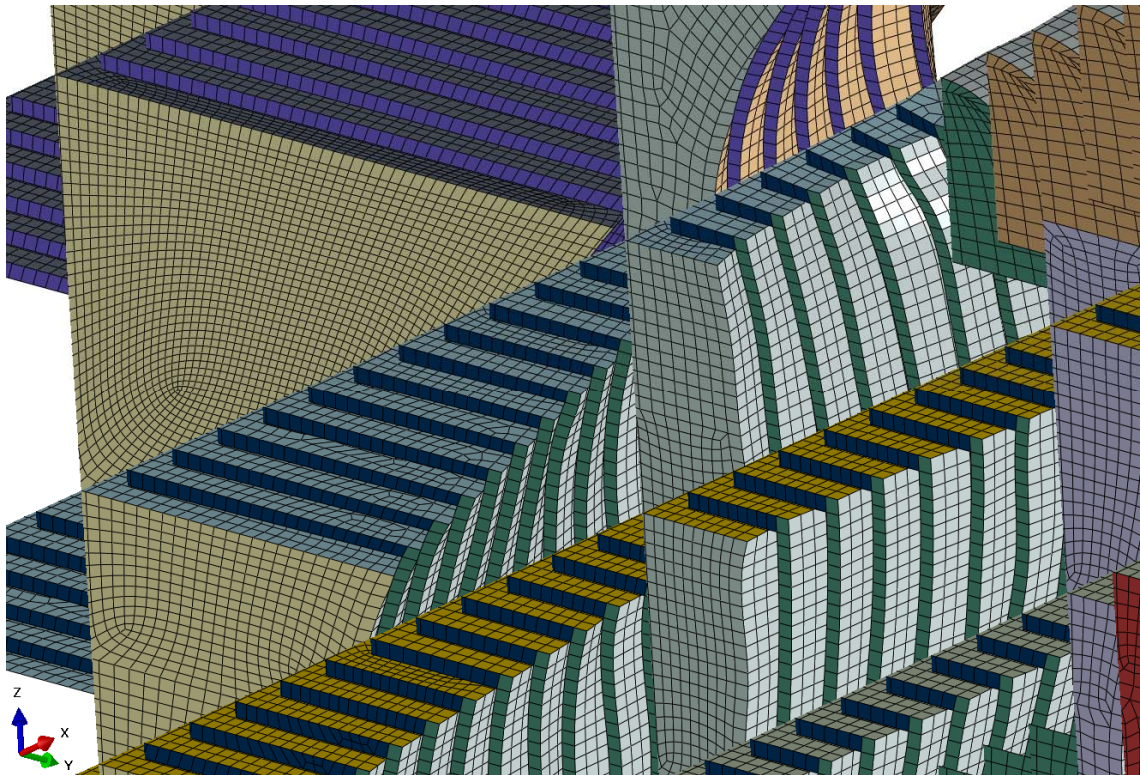


> Figure 4-15 Detailed mesh of the container bow

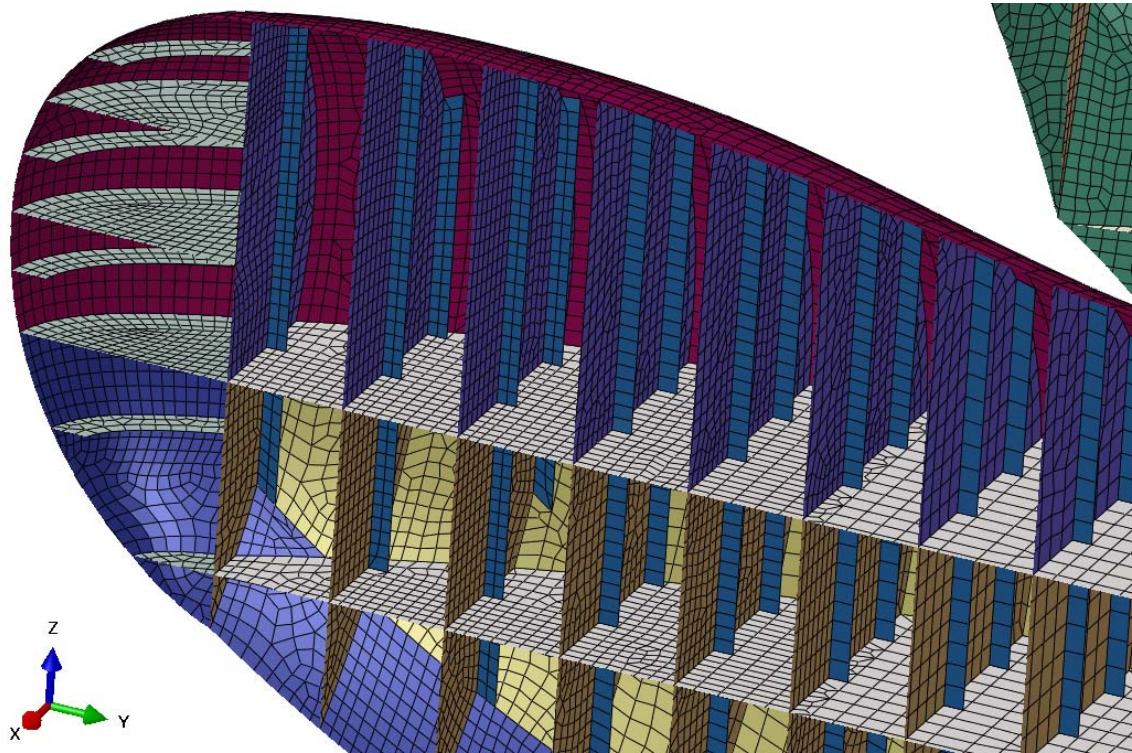


> Figure 4-16 Detailed mesh of the ice-strengthened bow

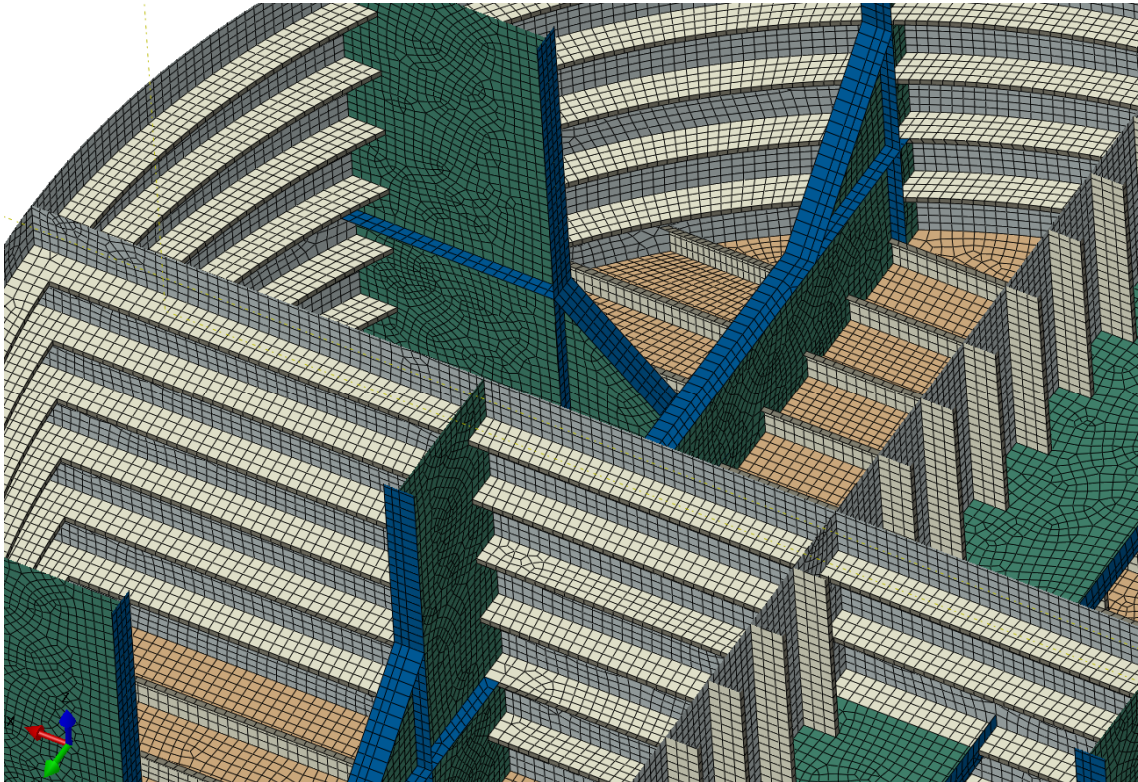


> Figure 4-17 Detailed mesh of the pontoon

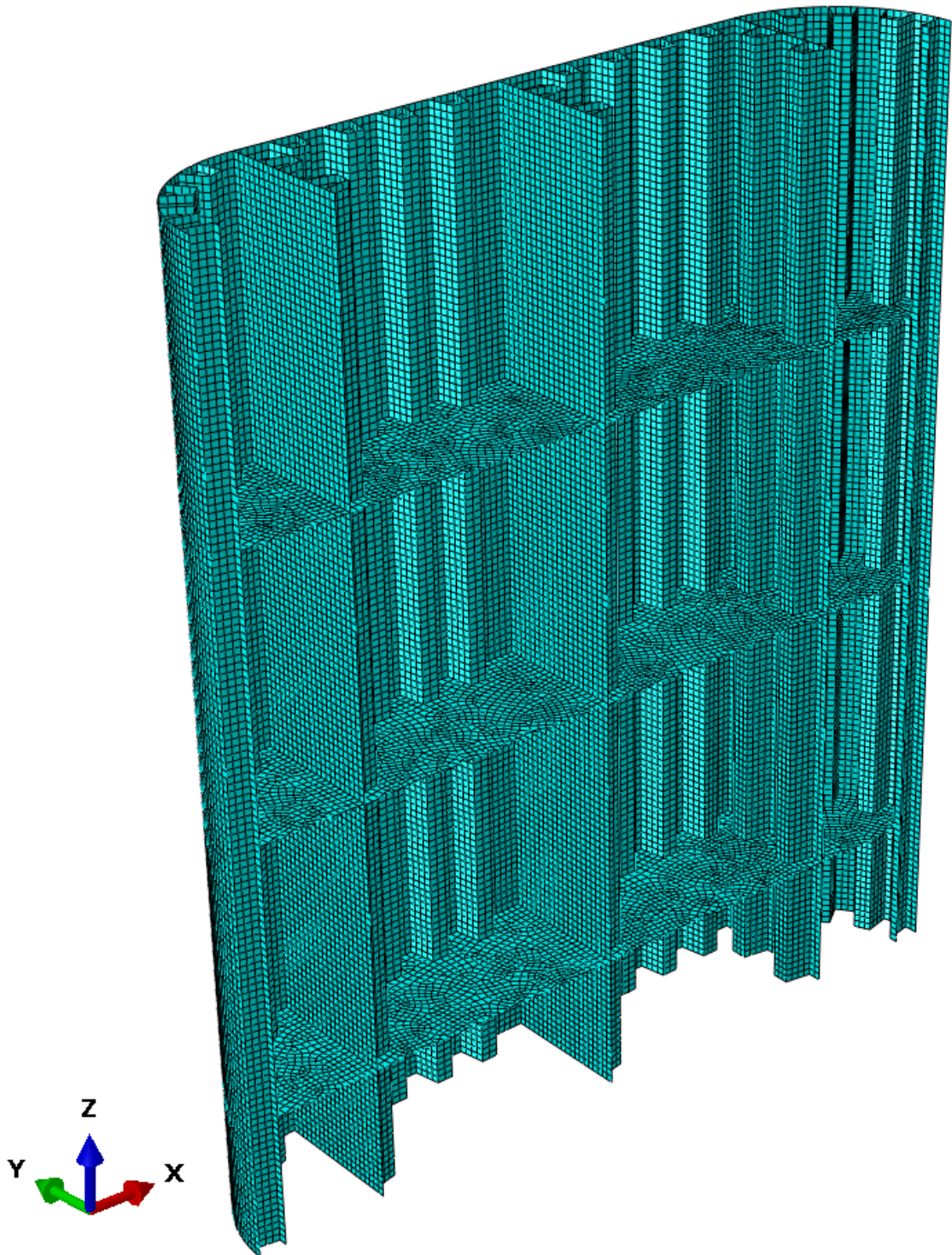


> Figure 4-18 Mesh of the column, shown cut in half

4.4 Analysis setup

4.4.1 Boundary conditions

The pontoon is modelled fixed at the boundary cut-off as illustrated in Figure 4-19. The cut boundary is constrained with a kinematic coupling to a reference point. Fixed boundary is satisfactorily to use because the stresses at the boundary are low, see section 5.3.1.

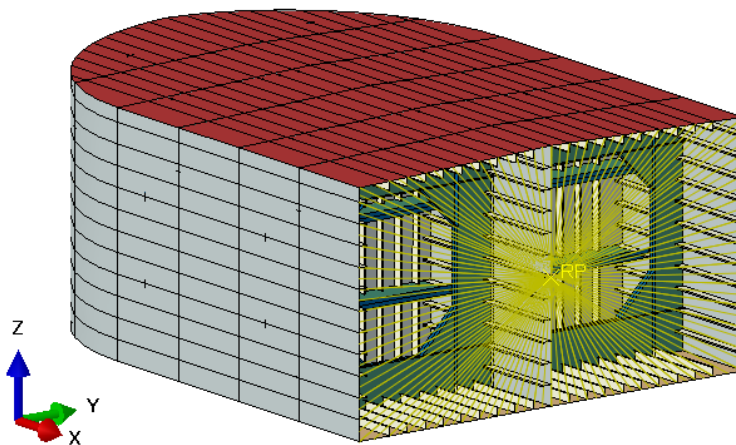


> Figure 4-19 Boundary condition at the cut-off boundary of the pontoon

Boundary conditions for the ship bow are shown in Figure 4-20 for the container bow. The ship bow is fixed in all rotational degrees of freedom in a reference point at the back end of the modelled bow. The back end is constrained as a rigid body to the reference point. Fixed boundaries are satisfactorily to use because the stresses at the boundary are low, see section 5.3.1.

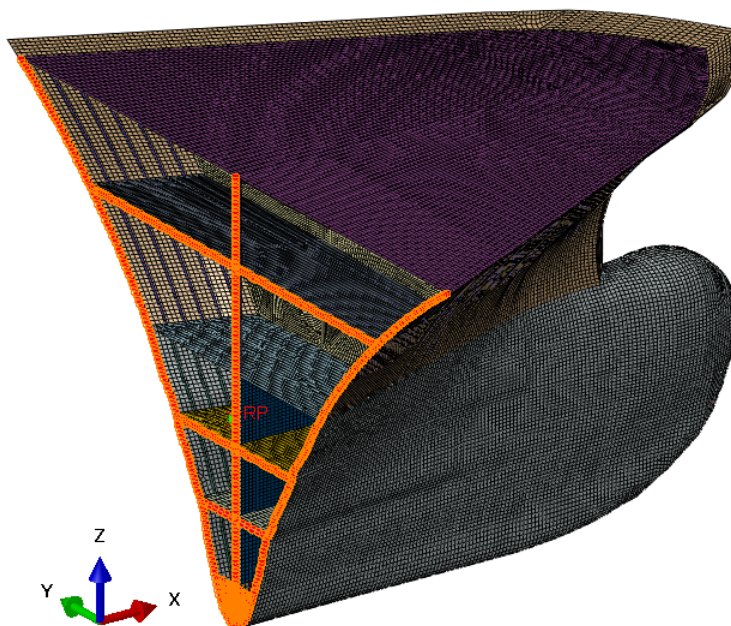


> Figure 4-20 Boundary condition at the cut-off boundary of the ship bow

The column is modelled fixed at the boundary cut-off as illustrated in Figure 4-21. The cut boundaries are constrained with a kinematic coupling to a reference point. Fixed boundaries are satisfactorily to use because the stresses at the boundary are low, see section 5.3.4.

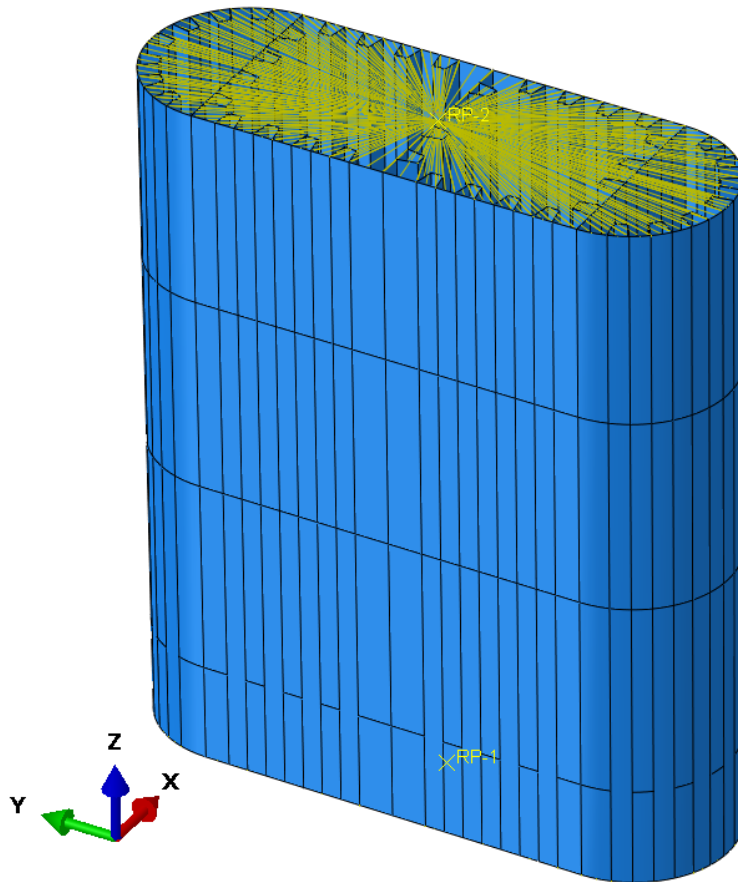


> Figure 4-21 Boundary conditions at the cut-off boundaries of the column

4.4.2 Loads

The only load applied in the simulations models is velocity to the ship bow. This is performed in two steps prior to the impact to avoid unwanted dynamic effects. In step one, velocity is applied to the entire ship bow model. In step two, the velocity is "turned off" for the ship bow, except for a point at the rear end rigidly fixed to the bow. The ship bow will still move towards the pontoon which happens in step three.

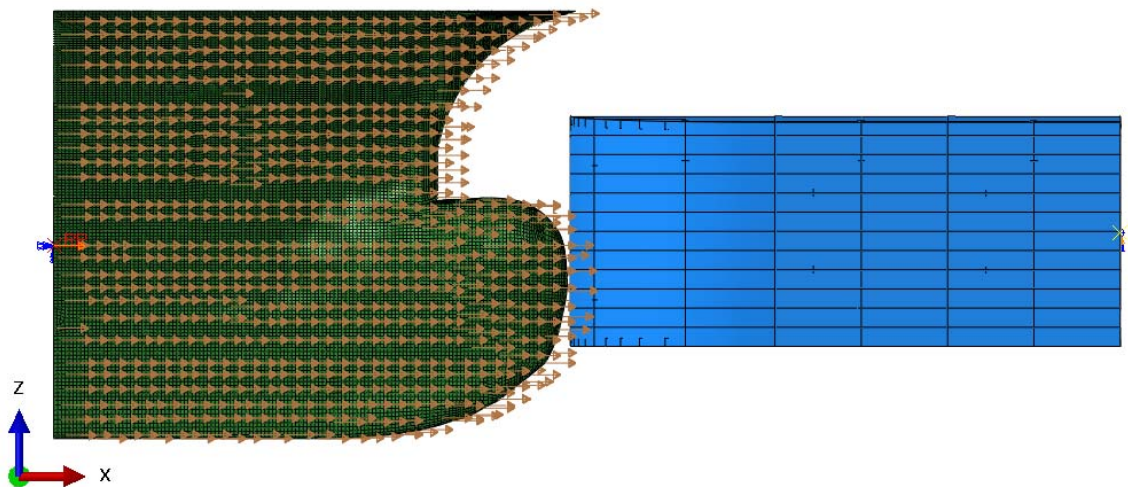


> Figure 4-22 Velocity applied to the container bow in step one

4.4.3 Interactions

A general contact condition is applied to the entire model, including both sides of the surface of all elements in the model. The normal behavior is "hard" contact and the friction coefficient is 0.3.

4.4.4 Output parameters

Output parameters of interest are:

- *Contact force*: Total force due to contact pressure
- *Frictional dissipation*: Frictional dissipated energy
- *Strain energy*: Elastic strain energy
- *Plastic dissipation*: Inelastic dissipated energy
- *Artificial energy*: Artificial strain energy related to hourglass control and drilling rotation control
- *Internal energy*: Or total strain energy. For the simulations in this report, the internal energy is the sum of strain energy, plastic energy and artificial energy.

5 SIMULATIONS

5.1 Load cases

Table 5-1 gives the impact energy for the relevant pontoon. This energy is to be dissipated locally and globally for a collision event.

The pontoon spacing has been changed from 100 m to 120 m during the concept phase, but this is not implemented into the local analysis. According to the Design Basis [1], the impact velocity for pontoon spacing 125 m is 5.7 m/s. In Appendix C section 6 [22], it is seen that the local ship impact simulation is not very sensitive to a small change of the impact velocity. The velocity is not updated from 5.6 to 5.7 m/s. The displacement mass of the ship has no effect on the force-indentation relation obtained from the local ship impact simulations.

> *Table 5-1 Impact energy for bridge concept K12, CC 100 m*

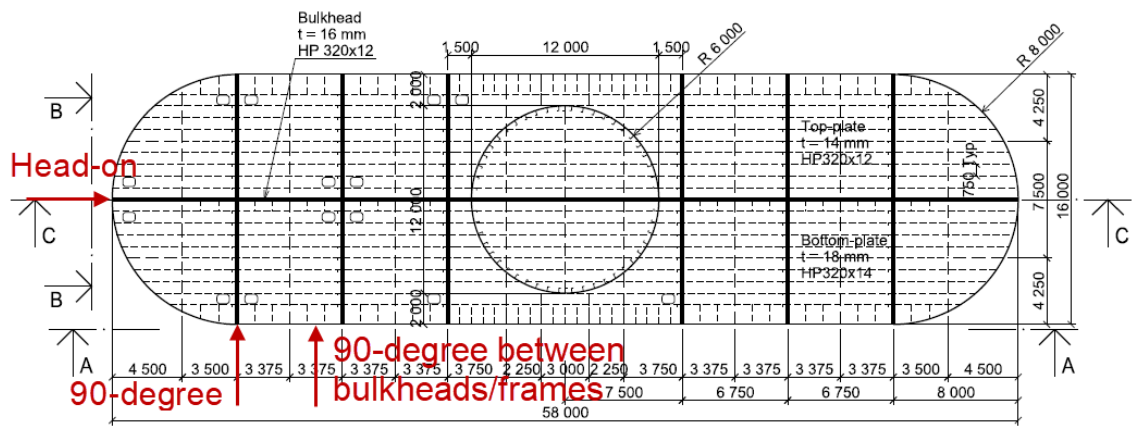
Element	Displacement	Velocity	Impact energy ³
Pontoon in axis 3	14 933 ton	5.6 m/s	246 MJ

Table 5-2 gives the base impact cases for local response of bow-pontoon collision. Ships can collide with the pontoons in any directions, however head-on and 90-degree are considered as the most critical directions.

> *Table 5-2 Impact scenarios bow-pontoon collision*

Load case	Type of ship bow	Height of bow	Direction on pontoon
A	Container bow	Design draught (8.6 m)	Head-on
B	Container bow	Design draught (8.6 m)	90-degree
C	Ice-strengthened bow	Design draught (6.8 m)	Head-on
D	Ice-strengthened bow	Design draught (6.8 m)	90-degree
E	Ice-strengthened bow	Design draught (6.8 m)	90-degree between bulkheads and frames

³ Included 5 % added mass



> Figure 5-1 Illustration of head-on and 90-degree directions

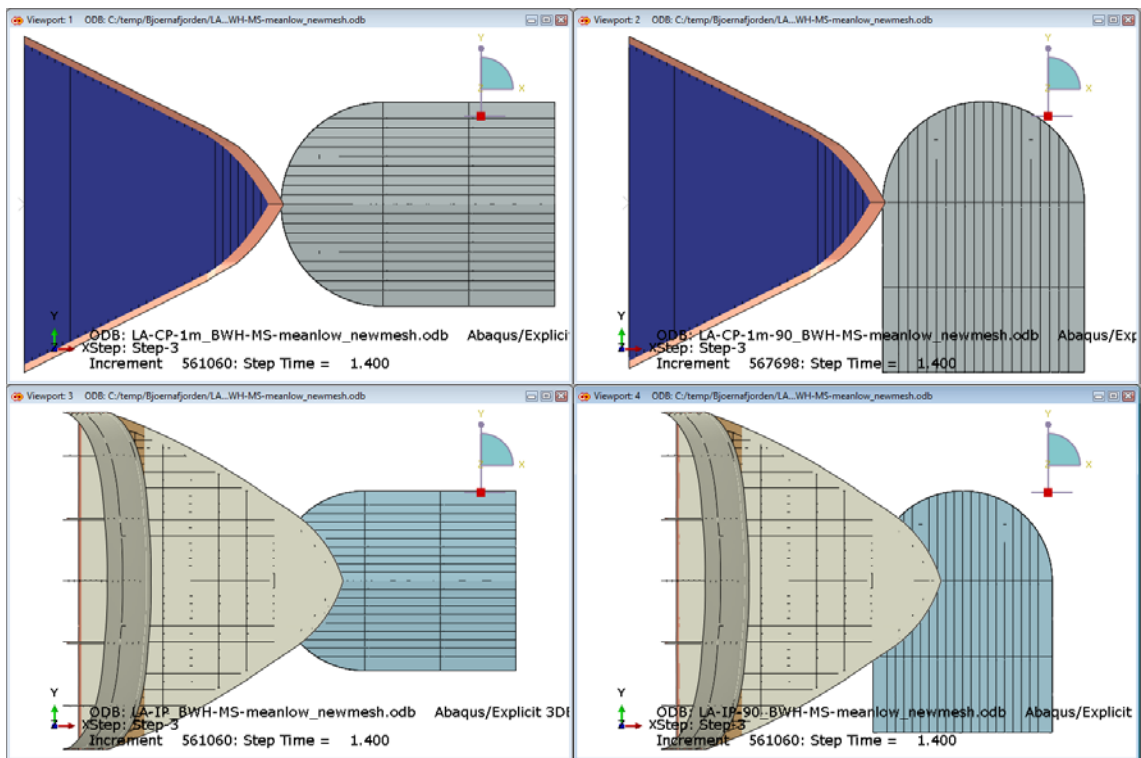


> Figure 5-2 Load cases A-D of bow-pontoon collision seen from above: Container bow (upper), ice-strengthened bow (lower), head-on (left), 90-degree (right)

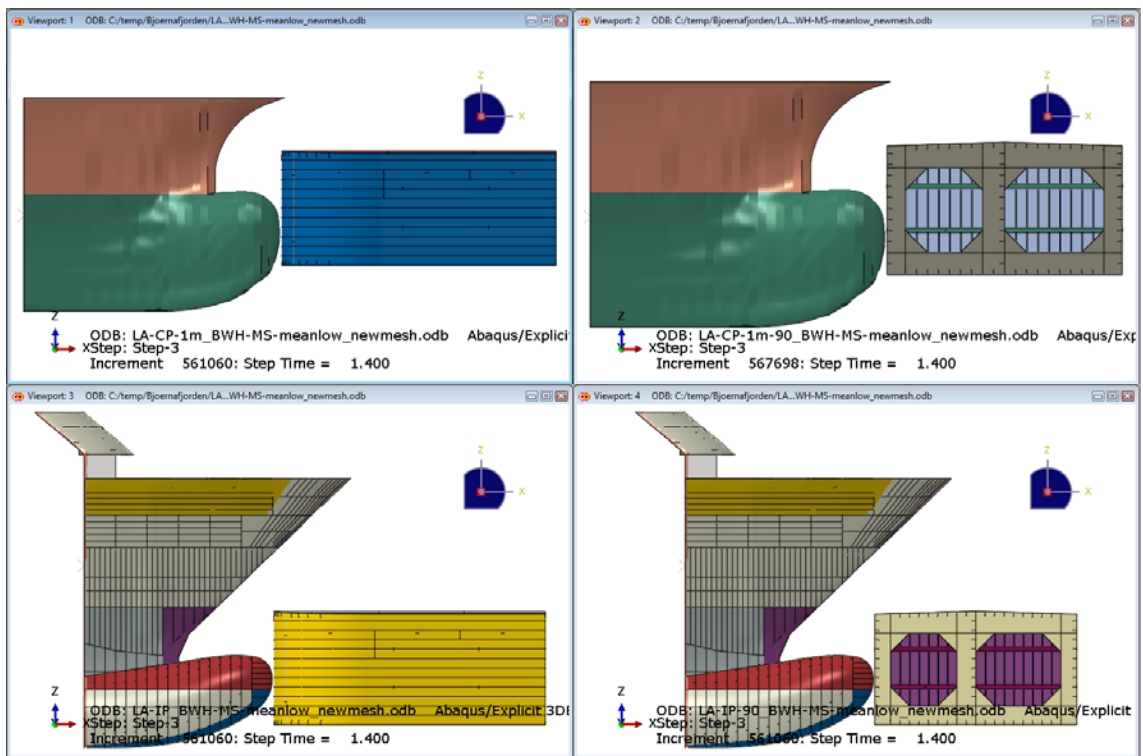


> Figure 5-3 Load cases A-D of bow-pontoon collision side view: Container bow (upper), ice-strengthened bow (lower), head-on (left), 90-degree (right)

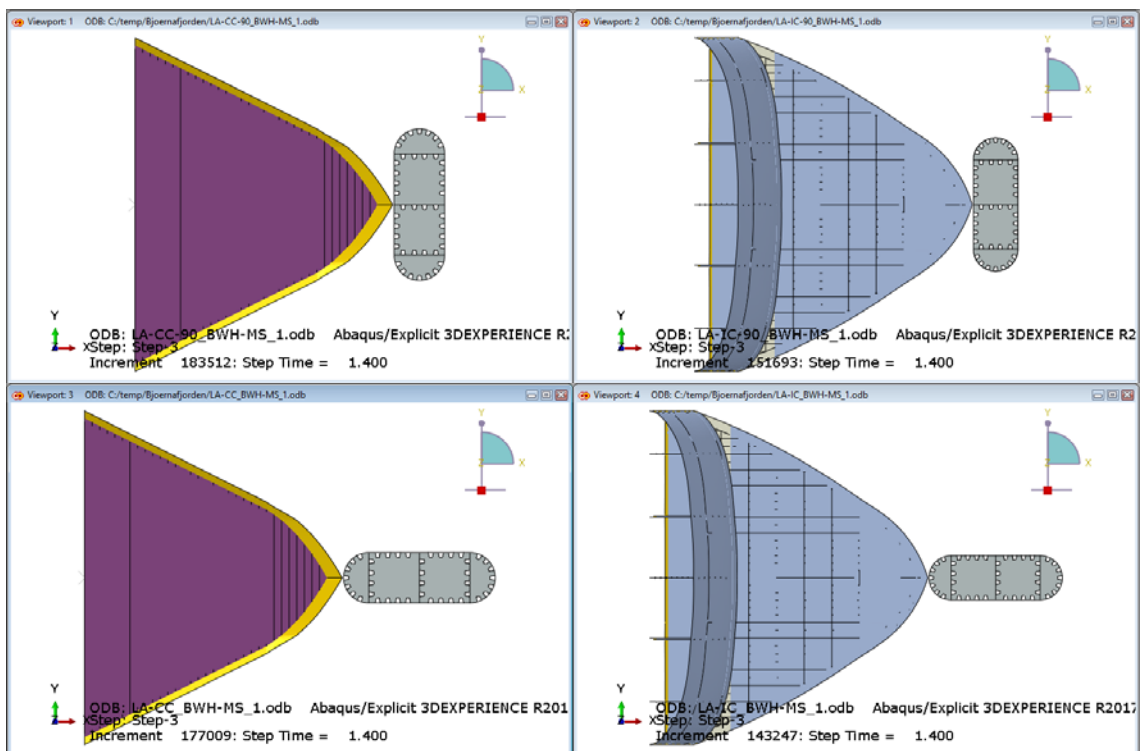


> Figure 5-4 Load cases A-D of forecastle-column collision seen from above: 90-degree (upper), head-on (lower), container bow (right), ice-strengthened bow (right)

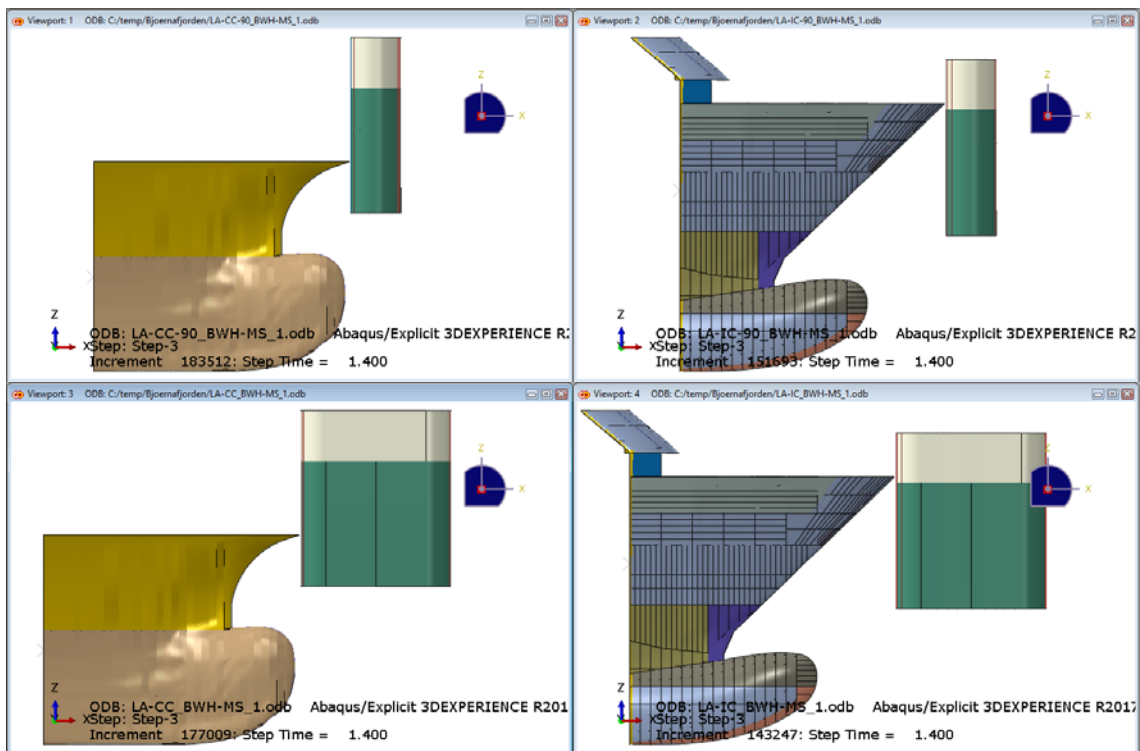


> Figure 5-5 Load cases A-D of forecastle-column collision side view: 90-degree (upper), head-on (lower), container bow (right), ice-strengthened bow (right)

Impact with the container bow is also performed at scantling draught (9.6 m), since this is the known height of the container bow [1]. The design draught is assumed 1.0 m above the scantling draught. The pontoon draught is 5.0 m.

Sensitivity analyses have been performed related to material model, material quality, mesh size, element type and ship velocity. The impact velocity on the pontoon in axis 3 is 5.6 m/s [1].

Modifications to the pontoon geometry have been conducted to investigate possible reduction options to the impact force level.

5.2 Response parameters

The goal of the local response simulations is to evaluate the force-displacement curves for load input to the global response simulations [2].

The extent of damage to the pontoons and columns is also obtained from the local simulations. This must be calibrated with the global simulations to reaffirm the amount of energy that is dissipated locally.

When the local damage is known, reduced stiffness (number of filled compartments and thus reduced water plane stiffnesses) can also be given as input to evaluate the damaged condition with a 100-year environmental loading applied to the bridge.

5.3 Response

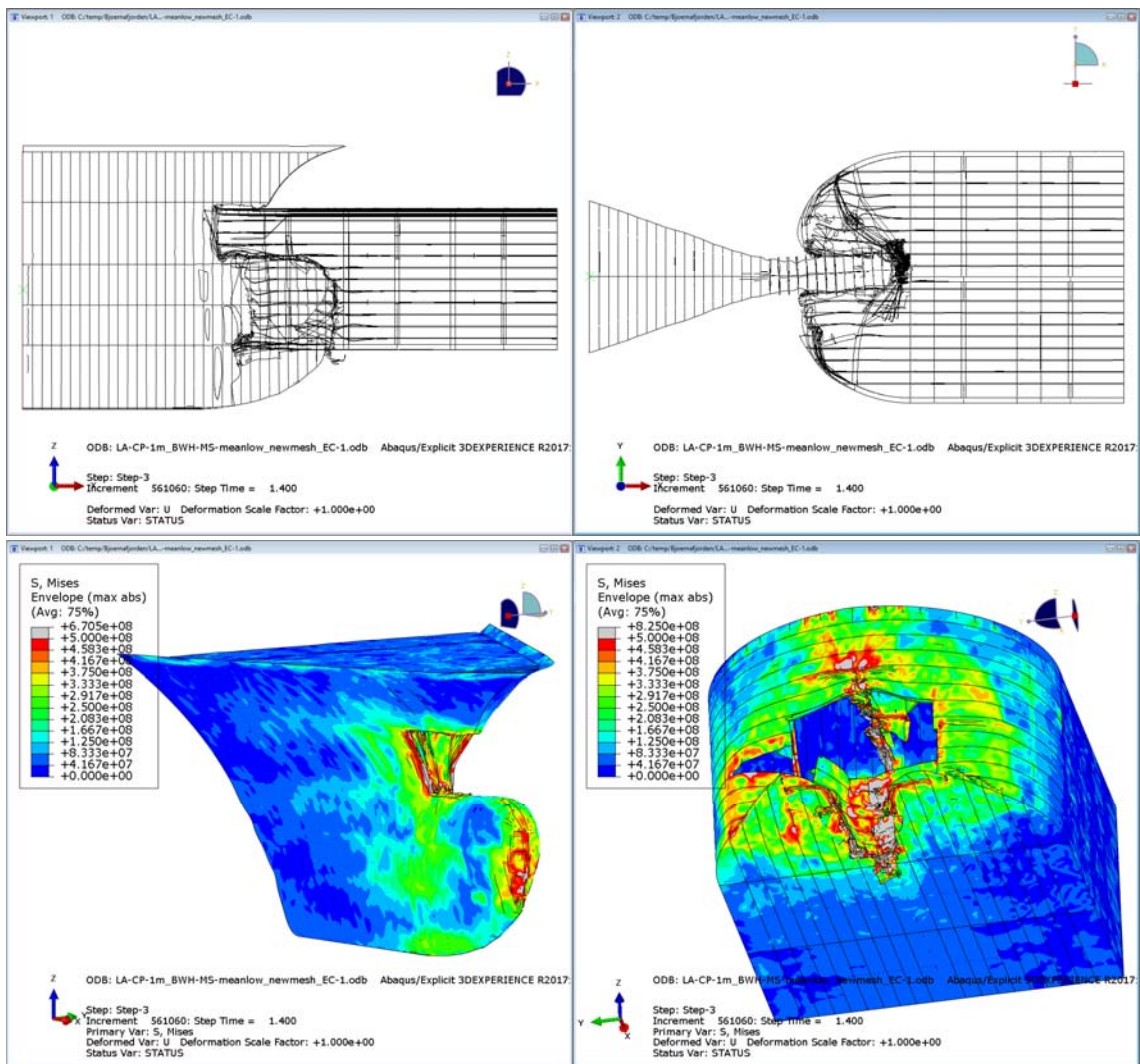
5.3.1 Damage illustrations of base impact cases

Figure 5-6 to Figure 5-10 show the ship bow and pontoon damage for the load cases in Table 5-2 at 8 m ship displacement. The pontoon is subjected to severe damage for both the container bow and the ice-strengthened bow. Deformations are not scaled.

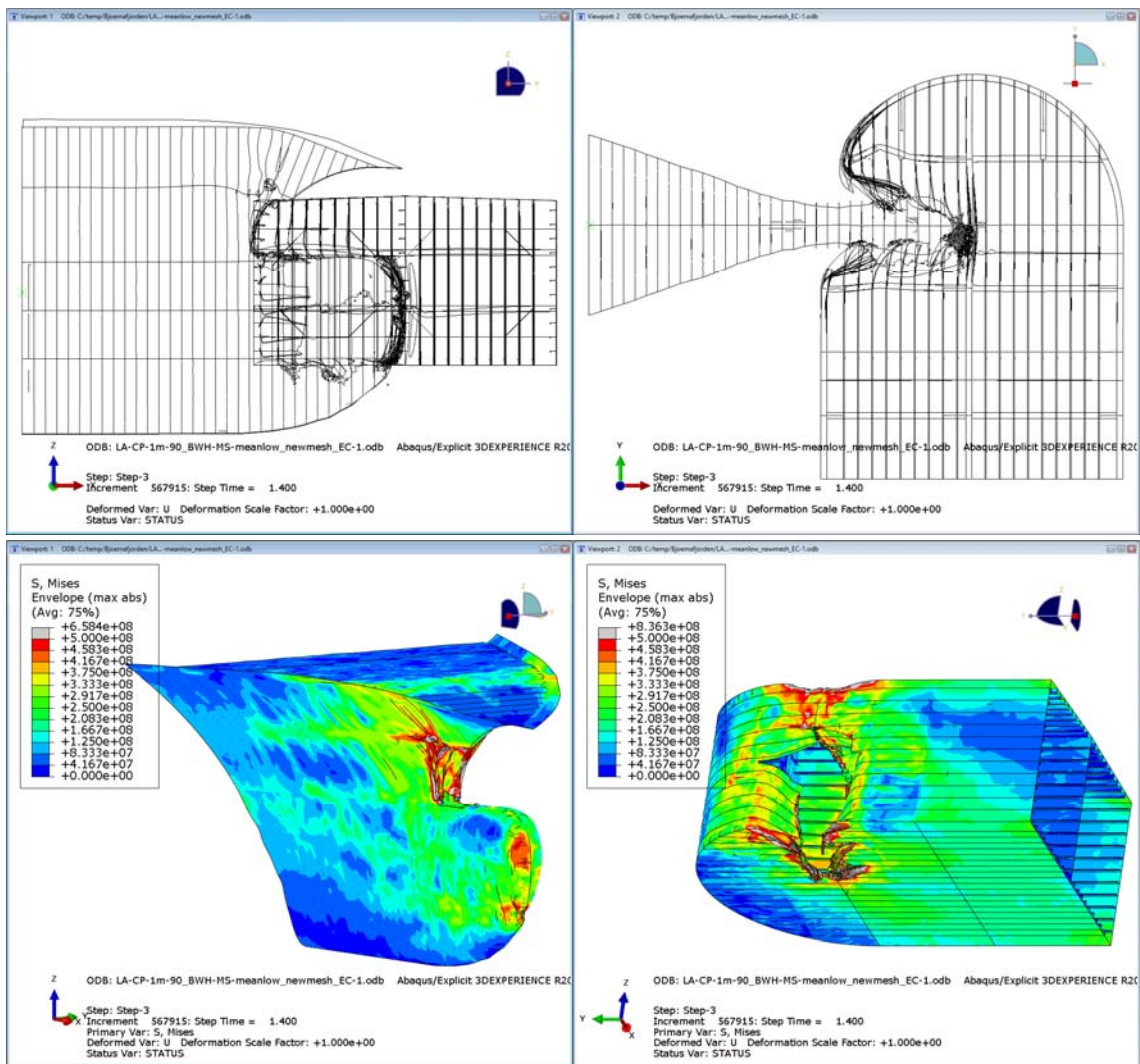
The damage caused by the container bow comprises a large area where the bulb hits the pontoon. The frames and bulkheads are crushed. At the upper part, the forecastle of the container bow is crushed, while the pontoon is less damaged.

The bulb of the container bow twists a bit to one side of the pontoon for head-on impact. This can be random or may be because the frames and stiffeners of the pontoon are facing the other side of the pontoon and thus a bit stiffer.

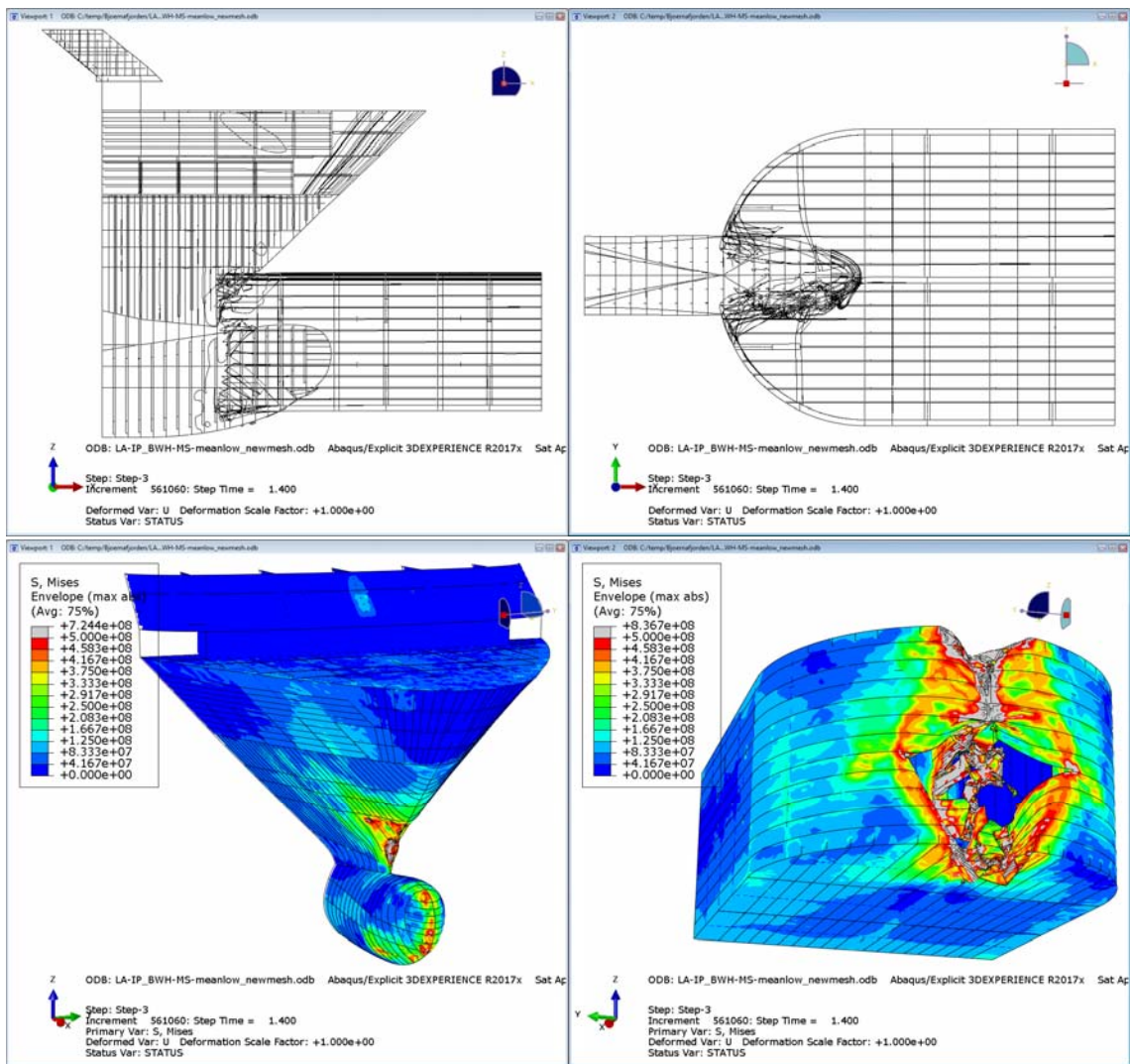
The impact area caused by the ice-strengthened bow is a bit more compressed. However, the ice-strengthened bow results in larger damage to the upper part of the pontoon, especially when the hit is between bulkheads and frames.



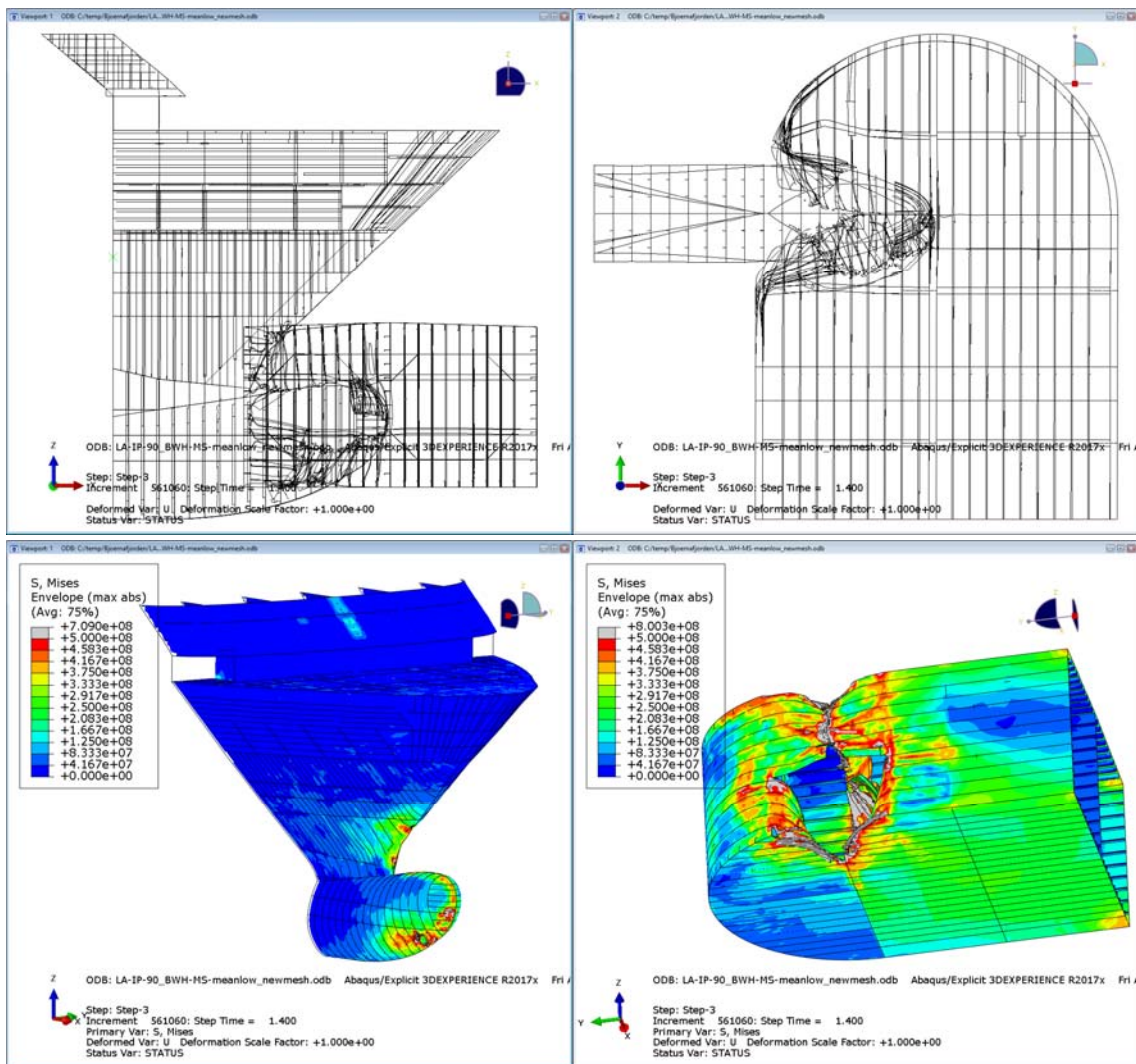
- > Figure 5-6 von Mises stress [MPa] load case A: Container bow at design draught (8.6 m), head-on impact on pontoon



- > Figure 5-7 von Mises stress [MPa] load case B: Container bow at design draught (8.6 m), 90-degree impact on pontoon



- *Figure 5-8 von Mises stress [MPa] load case C: Ice-strengthened bow at design draught (6.8 m), head-on impact on pontoon*



- > Figure 5-9 von Mises stress [MPa] load case D: Ice-strengthened bow at design draught (6.8 m), 90-degree impact on pontoon

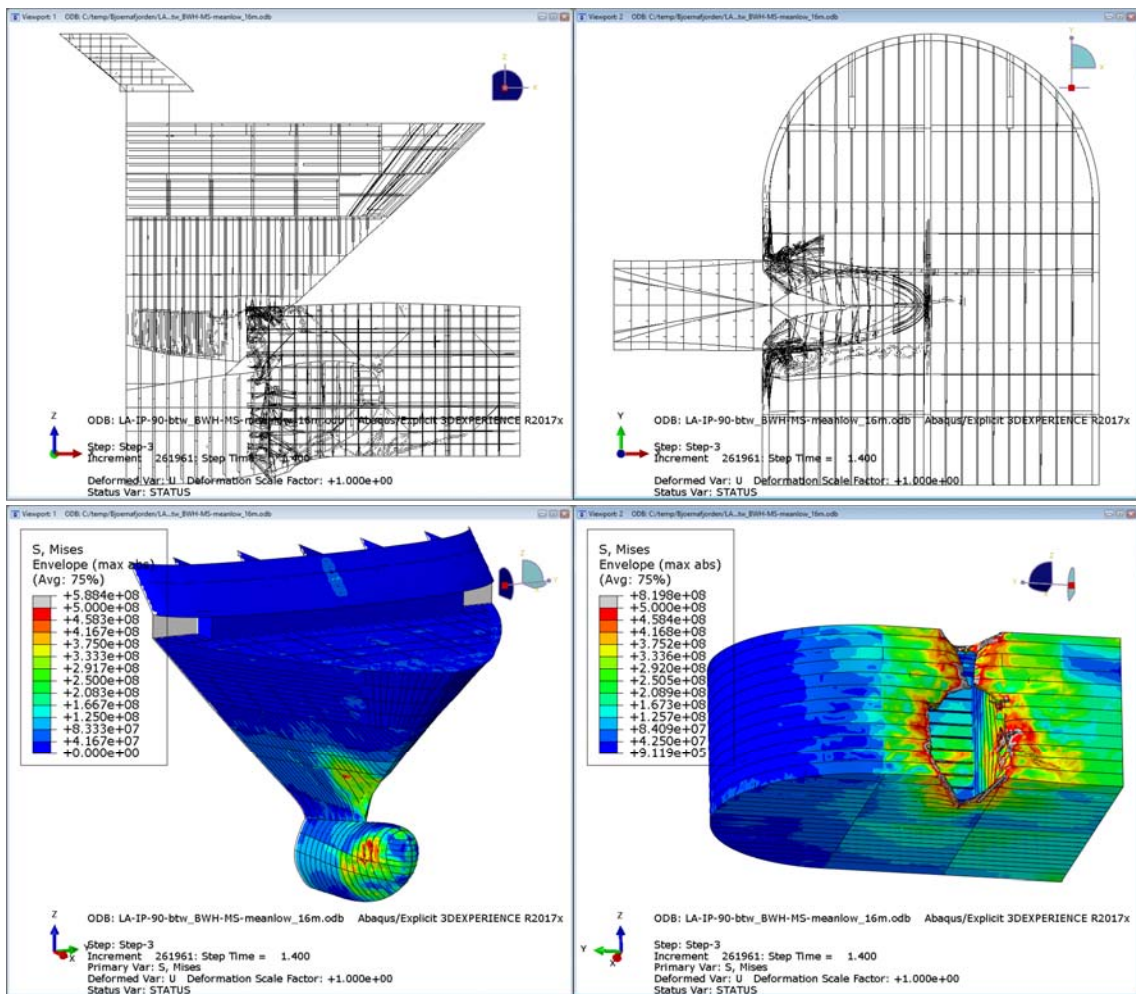


> Figure 5-10 von Mises stress [MPa] load case E: Ice-strengthened bow at design draught (6.8 m), 90-degree impact on pontoon between bulkheads and frames

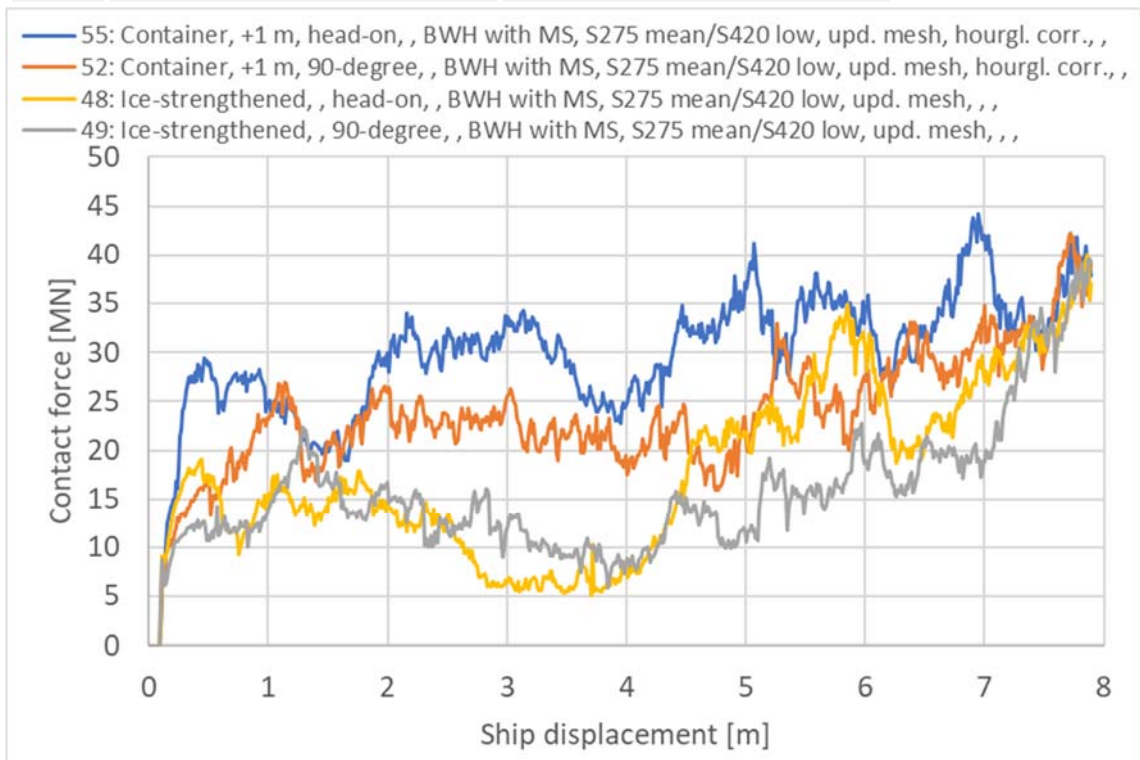
5.3.2 Base impact cases

Figure 5-11 shows the force-displacement curves for the load cases in Table 5-2 with “mean-low” material parameters described in section 4.2. The maximum and mean contact force is for comparison given for the period up to 4 m ship displacement.

Sensitivity of material parameters is investigated in Appendix C sections 2 and 3 [22].

The impact force level is higher for the container bow than the ice-strengthened bow. For the container bow, head-on impact gives higher force level than 90-degree impact. This seems to be because a larger impact area is involved if the surface hit is curved. The head-on impact results also in a steeper force-displacement relation in the early impact stage. The difference between head-on and 90-degree impact is not that prominent for the ice-strengthened bow.

ID-no.	Max. contact force [MN] 0-4 m	Mean contact force [MN] 0-4 m
55	34	27
52	27	21
48	19	11
49	22	13



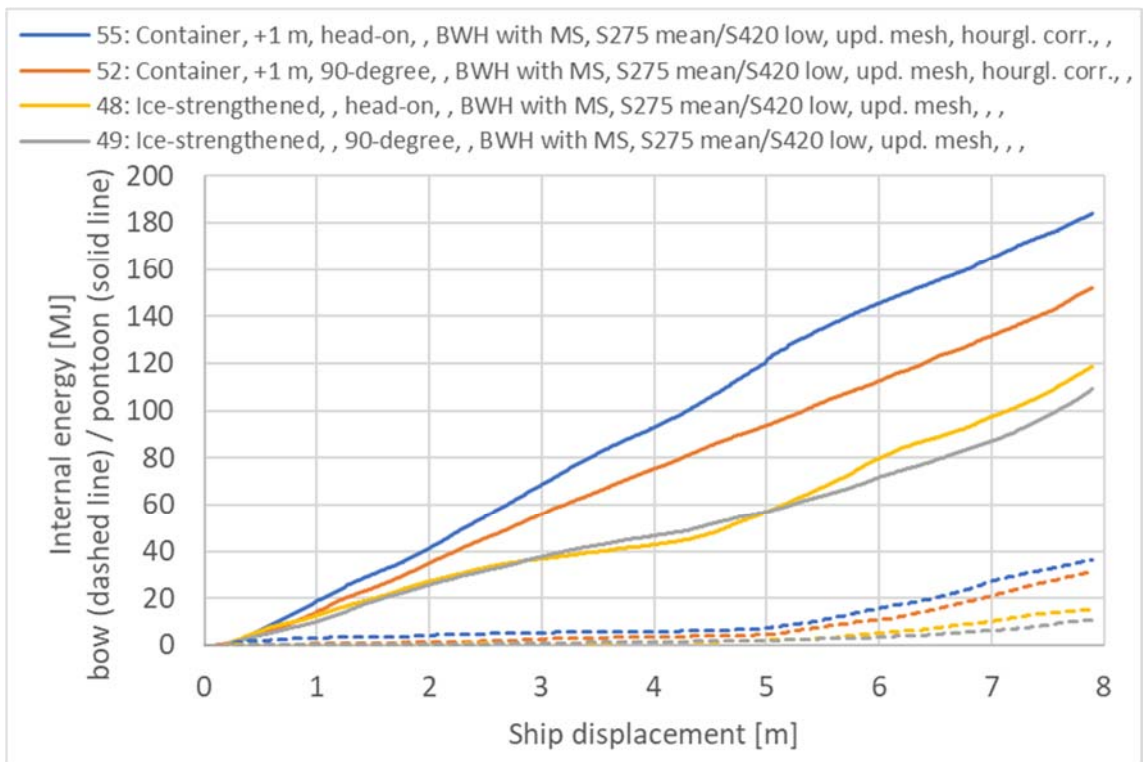
> Figure 5-11 Contact force [MN] impact bow-pontoon

Figure 5-12 shows the internal energy dissipated in the bow with dashed line and the pontoon with solid line. Here, the internal energy is the sum of strain energy, plastic dissipation and artificial energy. The largest proportion of the internal energy is the plastic dissipation.

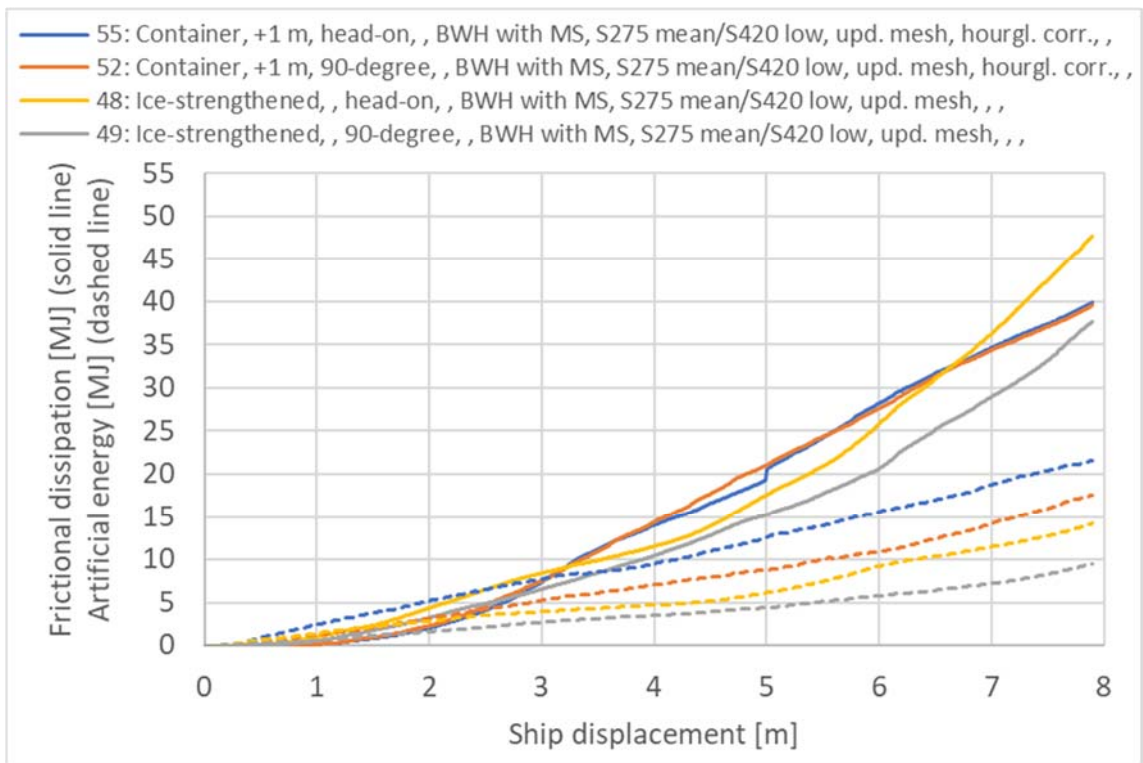
It is seen that the pontoon dissipates most of the energy. The container bow causes a significantly larger energy dissipation in the pontoon than the ice-strengthened bow, reflecting the area under the force-displacement curve. The internal energy in the ship bows is low for both types of bows and impact directions. The impact energy to be dissipated in axis 3 is 246 MJ. The local dissipated energy does not reach this level at 8 m ship displacement.

Figure 5-13 shows the frictional dissipation and artificial energy in the models. The proportion of artificial to internal energy is 8-11 % for the displayed models, which is a bit high. The artificial energy reduces when utilizing elements with full integration, but this is time demanding.

The effect of reduced integration is investigated in Appendix C section 5 [22].

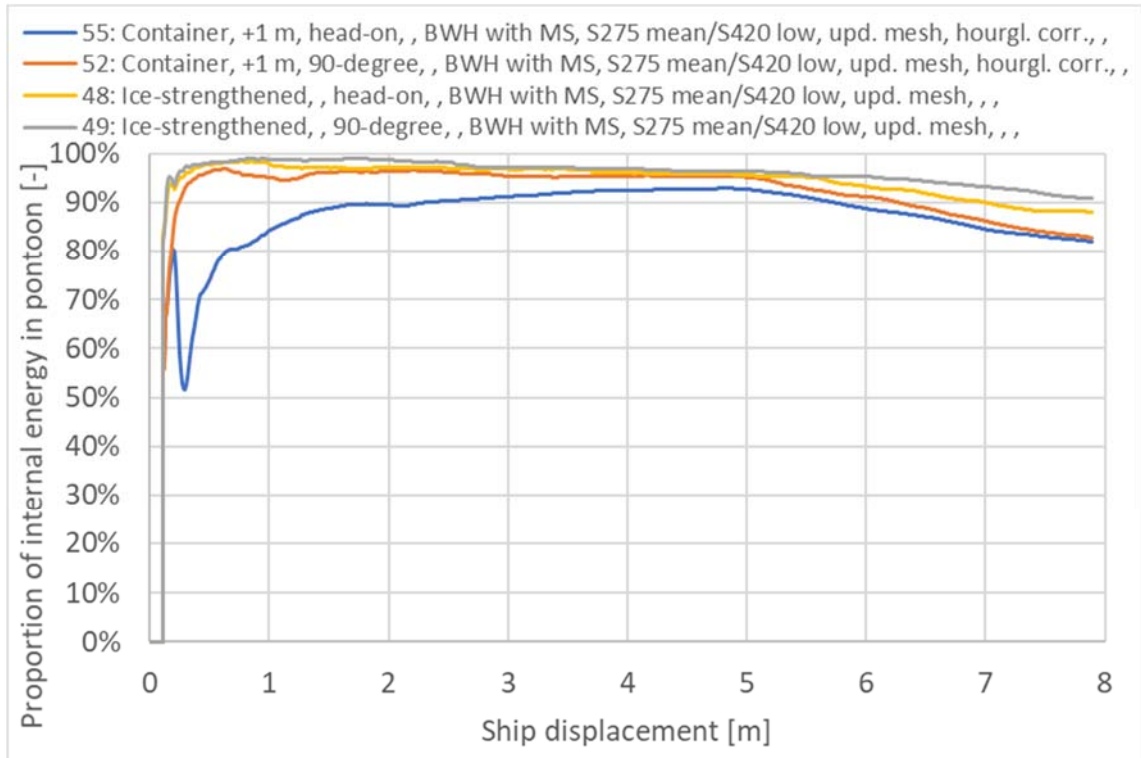


> Figure 5-12 Internal energy [MJ] impact bow-pontoon



> Figure 5-13 Frictional dissipation and artificial energy [MJ] impact bow-pontoon

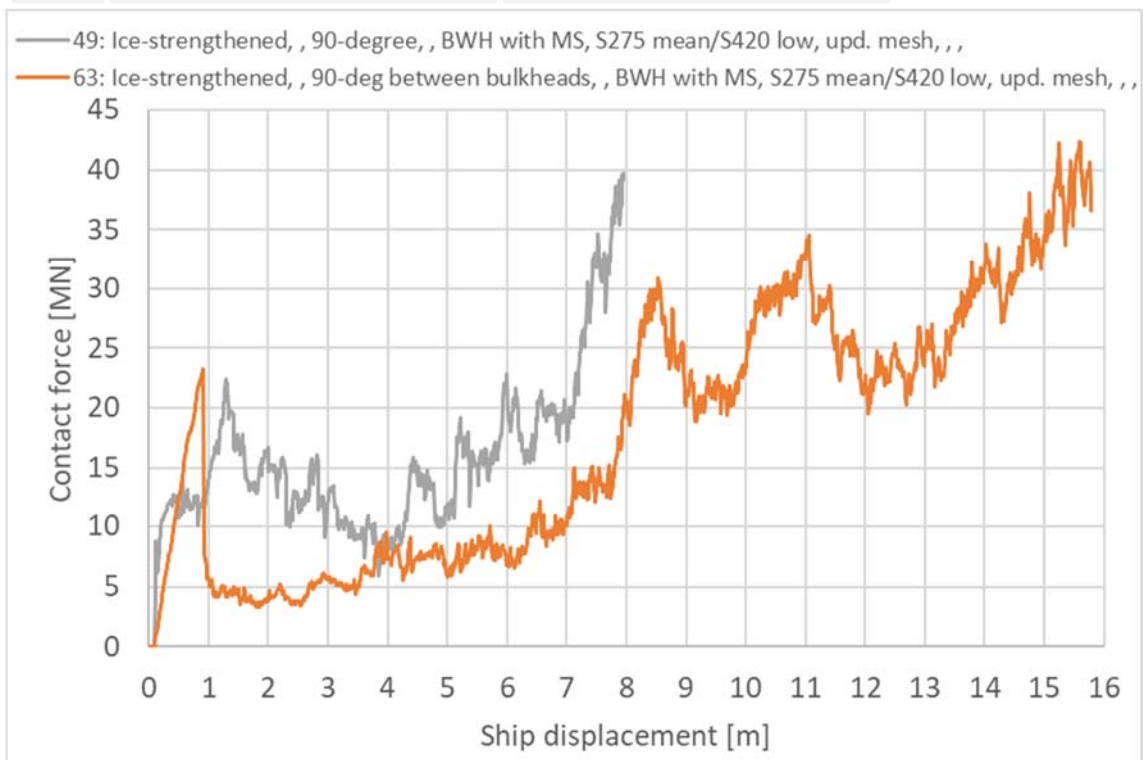
Figure 5-14 shows that the proportion of internal energy dissipated in the pontoon is high for all load cases. The head-on impact with the container bow displays lower energy dissipation in the pontoon in the early stage of the impact.



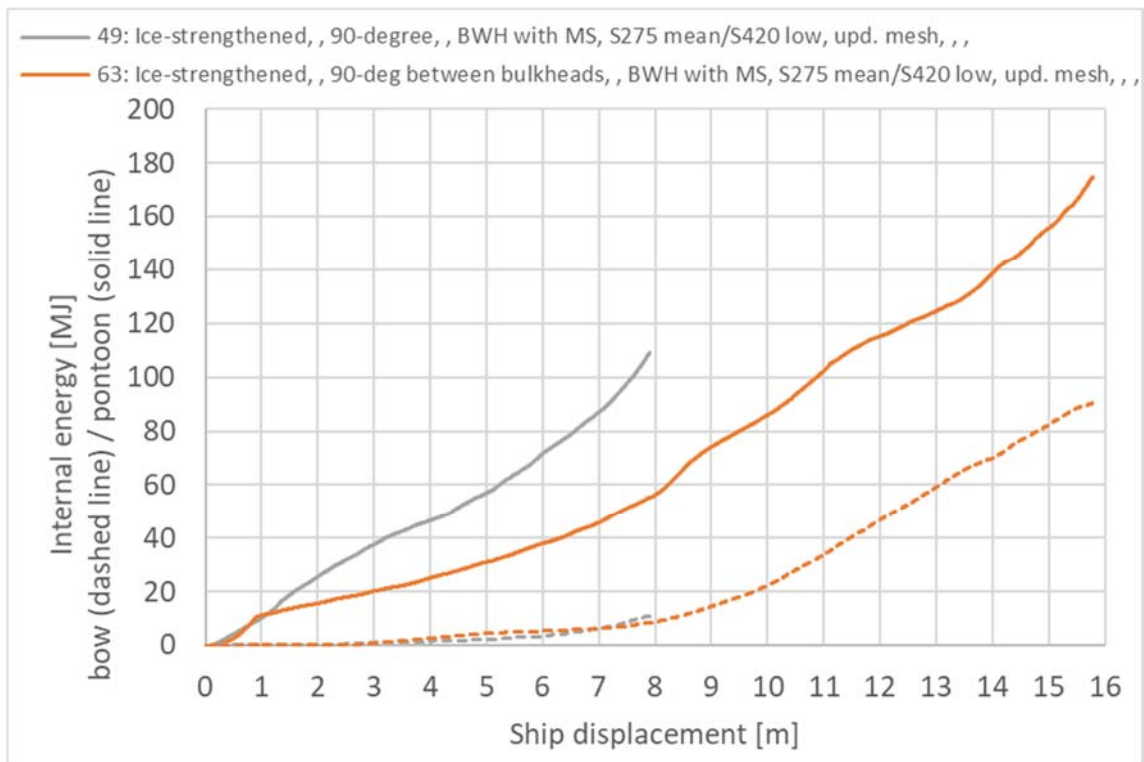
> Figure 5-14 Proportion of internal energy in pontoon [-] impact bow-pontoon

Figure 5-15 to Figure 5-18 show the results for 90-degree impact with the ice-strengthened bow at two different locations: On the bulkhead and between bulkheads and frames. See Figure 5-1 for locations. The purpose is to obtain the lowest possible force-indentation curve. Note that the frictional dissipation increases much, and the proportion of internal energy dissipated in the pontoon decreases for impact between bulkheads and frames beyond 8 m ship displacement.

ID-no.	Max. contact force [MN] 0-4 m	Mean contact force [MN] 0-4 m
49	22	13
63	23	7



- > *Figure 5-15 Contact force [MN] impact ice-strengthened bow-pontoon 90-degree on bulkhead or between bulkheads/frames*



> Figure 5-16 Internal energy [MJ] impact ice-strengthened bow-pontoon 90-degree on bulkhead or between bulkheads/frames

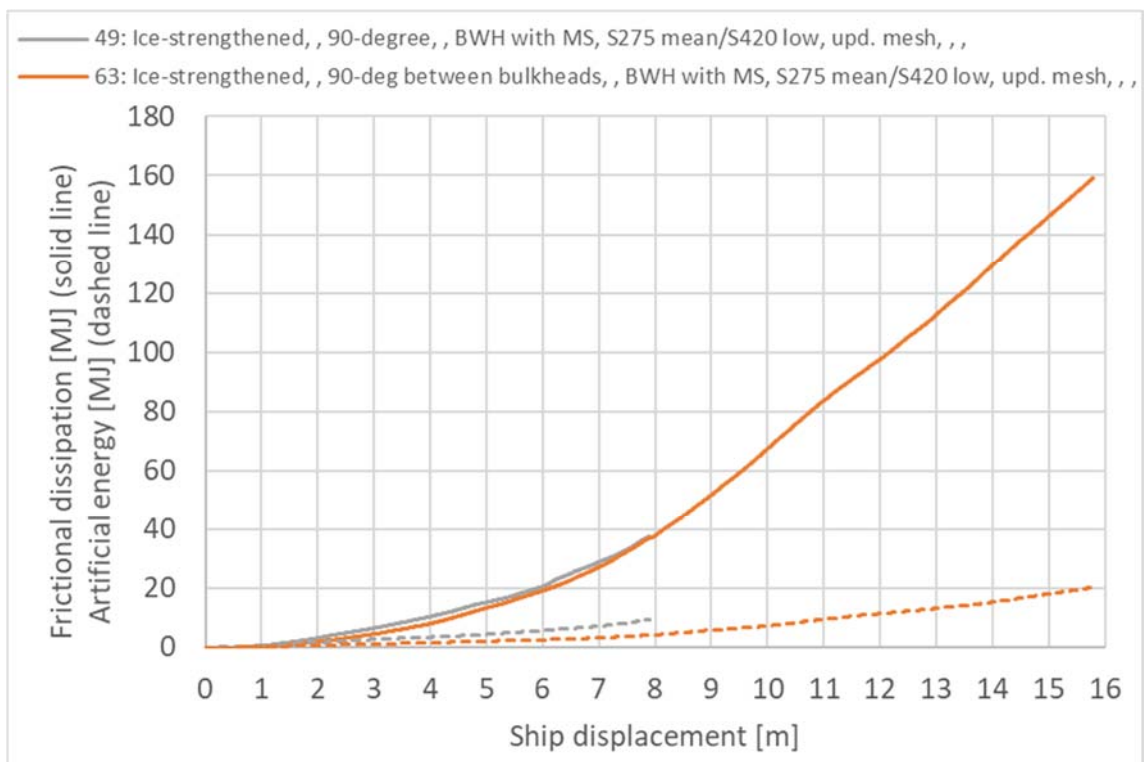


> Figure 5-17 Frictional dissipation and artificial energy [MJ] impact ice-strengthened bow-pontoon 90-degree on bulkhead or between bulkheads/frames

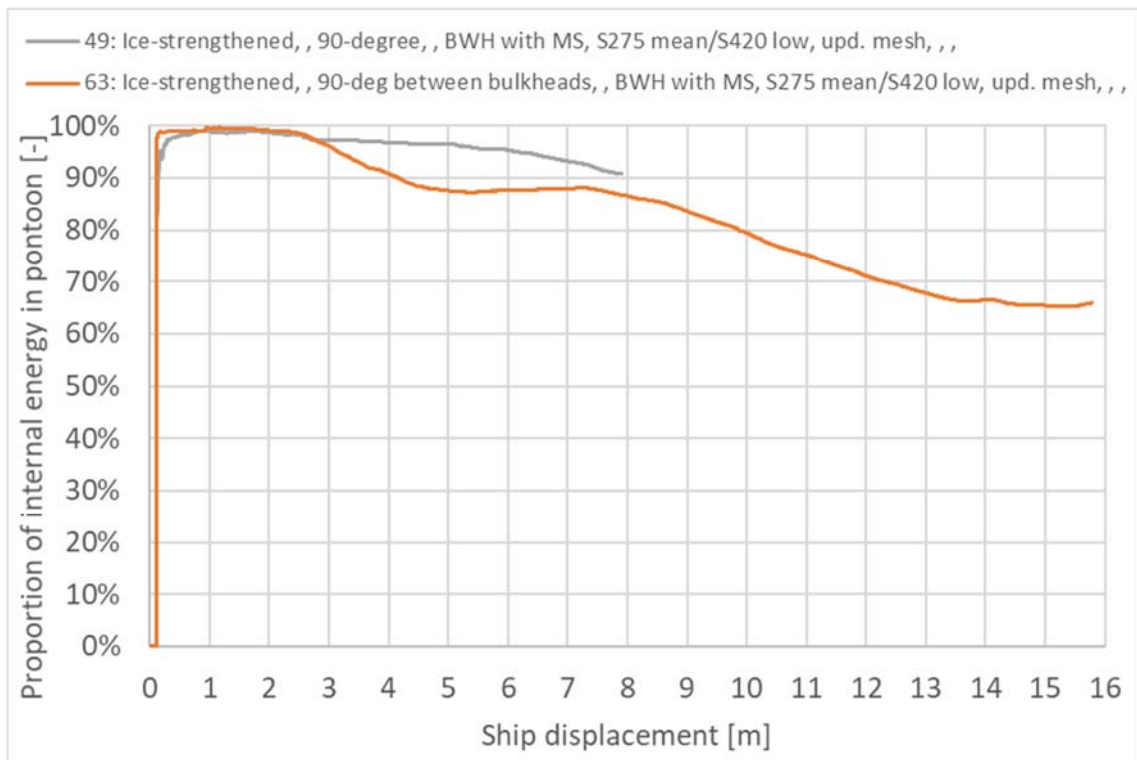


> Figure 5-18 Proportion of internal energy in pontoon [-] impact ice-strengthened bow-pontoon 90-degree on bulkhead or between bulkheads/frames

5.3.3 Comparison impact force reduction options

This section shows the result for different modifications to the pontoon geometry:

1. Reduced plate thicknesses with 2 mm to the top, bottom, walls and bulkheads of the pontoon
2. Reduced stiffeners to HP240x12 for all plates in the pontoon
3. Corrugated bulkheads in the front of the pontoon, shown in Figure 4-6 and Figure 4-7

Figure 5-19 to Figure 5-21 show the force-displacement curves for the modifications above compared with the reference curves.

Note that the force reduction investigations have been performed utilizing the low fractile set of material parameters as described in section 4.2. There is a disturbance in the reference model of the head-on impact (no. 56), with a sudden higher energy dissipation in the ship bow seen in Figure 5-22 at 5.5 m. This is reflected in the force-displacement curve in Figure 5-19 with the peak seen at 5.5 m. There is also a single peak in Figure 5-20 which is not realistic.

The reductions of the force level for the different modifications are:

1. Reduced plate thickness 2 mm: about 10 %
2. Reduced stiffeners to HP240x12: about 10 %
3. Corrugated bulkheads: from 0-20 %, dependent on evaluation

The corrugated bulkheads are more effective for the head-on impact than the 90-degree impact. This is because the longitudinal frames at the front of the pontoon (effective when

head-on impact) are softer than the transverse frames (effective when 90-degree impact). The corrugated bulkheads have the largest reduction at the first state of the impact for both directions, better than the options with reduced thickness or stiffeners. However, the reduction of the force level is uncertain dependent on the variable chosen for consideration. This is discussed further below.

ID-no.	Description	Max. contact force [MN] 0-4 m	Mean contact force [MN] 0-4 m
56	Head-on base case	33	24
32	90-degree base case	25	17
67	Head-on reduced plate thickness	28	21
66	90-degree reduced plate thickness	21	15

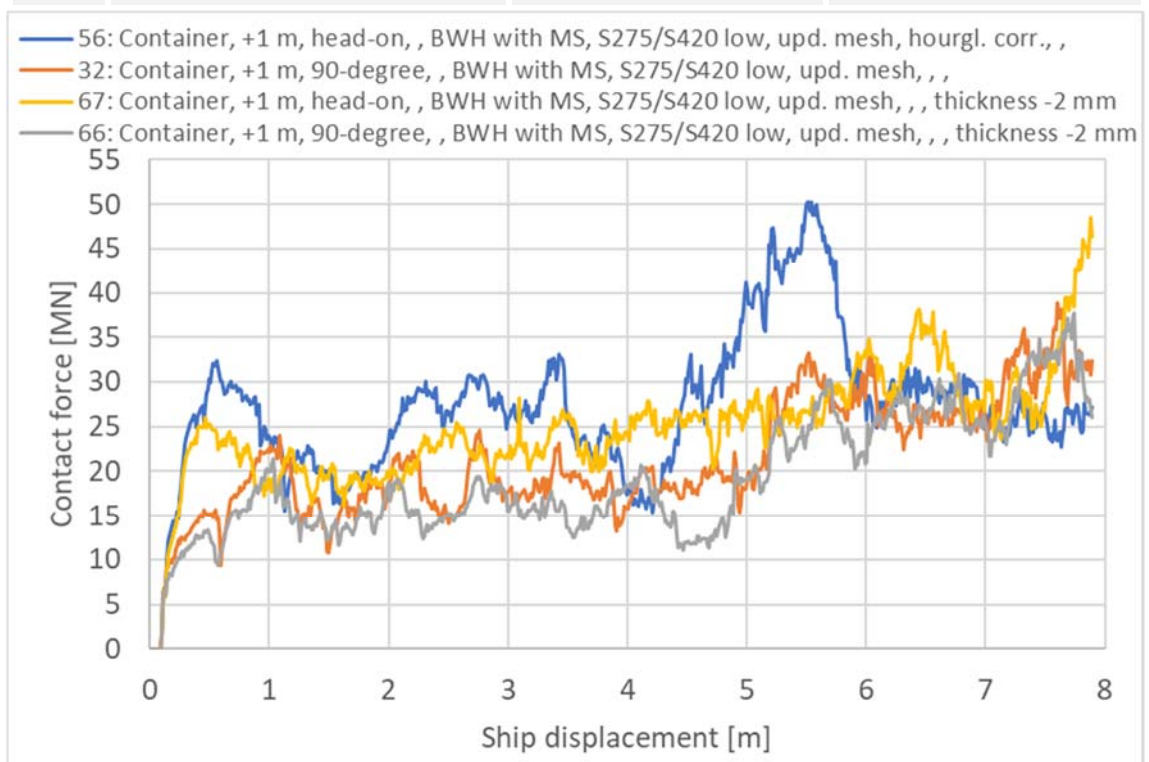


> Figure 5-19 Contact force [MN] impact bow-pontoon, plate thickness reduction

ID-no.	Description	Max. contact force [MN] 0-4 m	Mean contact force [MN] 0-4 m
56	Head-on base case	33	24
32	90-degree base case	25	17
64	Head-on reduced stiffener height	30	21
61	90-degree reduced stiffener height	25	16

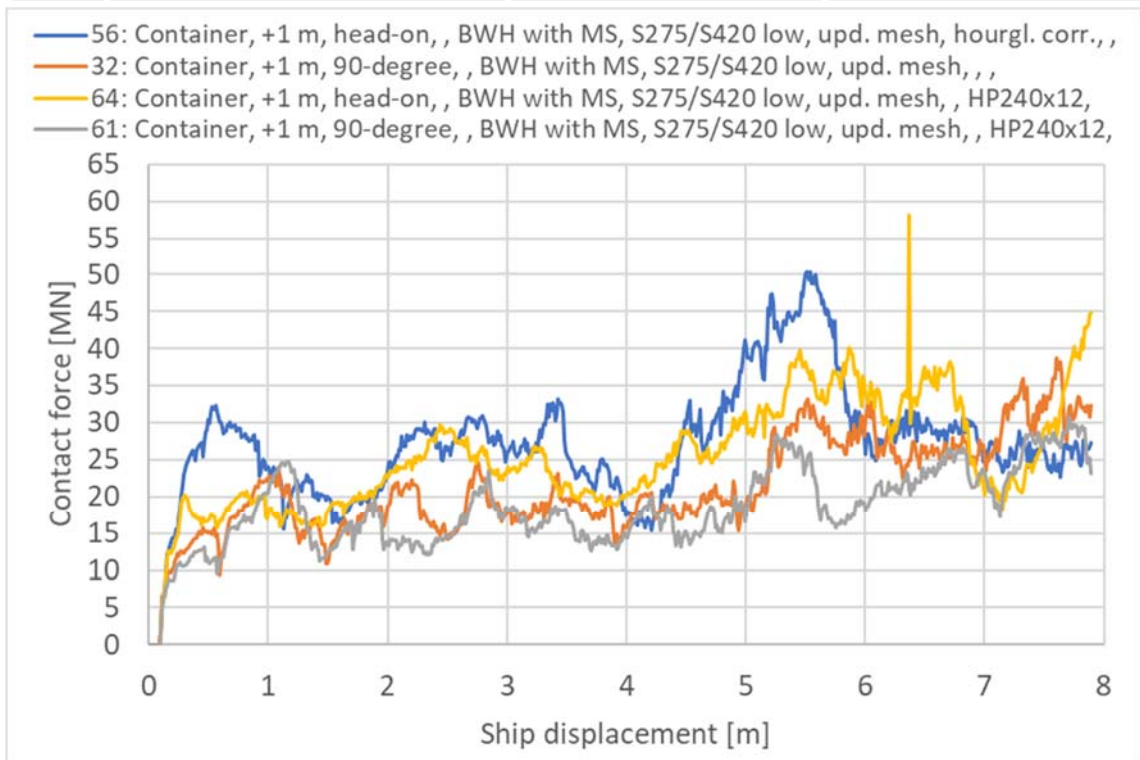


> Figure 5-20 Contact force [MN] impact bow-pontoon, stiffener reduction

ID-no.	Description	Max. contact force [MN] 0-4 m	Mean contact force [MN] 0-4 m
56	Head-on base case	33	24
32	90-degree base case	25	17
33	Head-on corrugated bulkheads	25	19
34	90-degree corrugated bulkheads	24	17

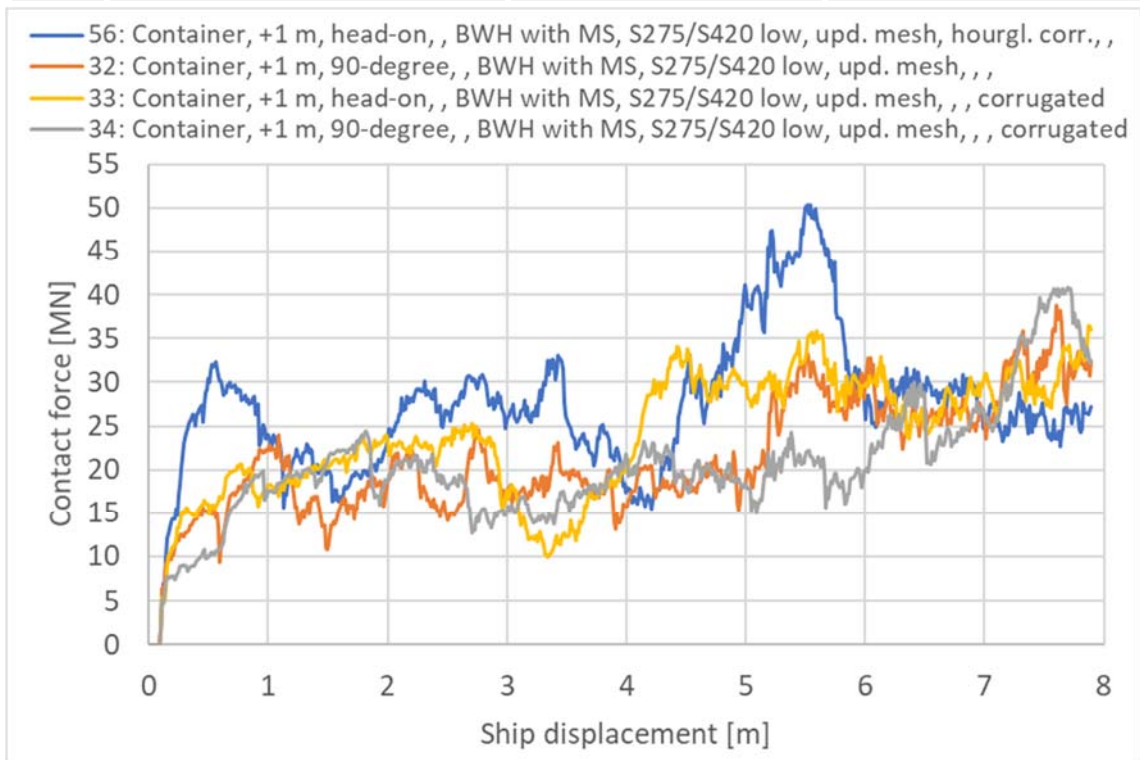
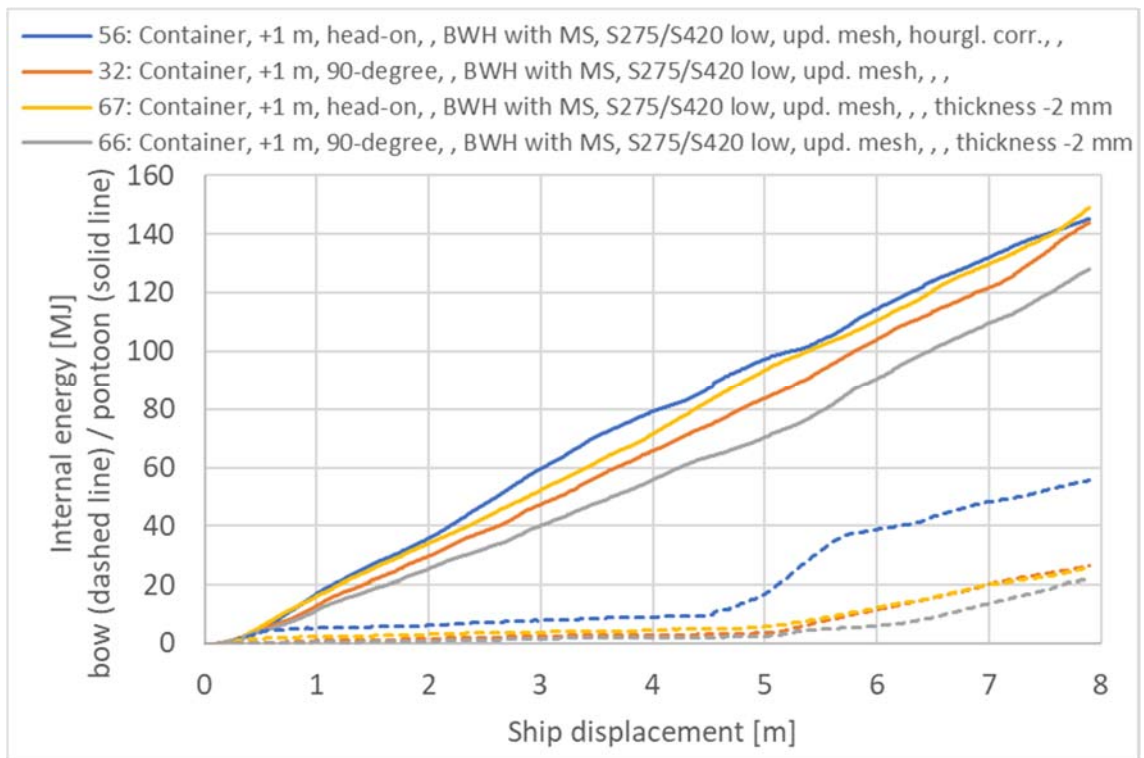


> Figure 5-21 Contact force [MN] impact bow-pontoon, corrugated bulkheads

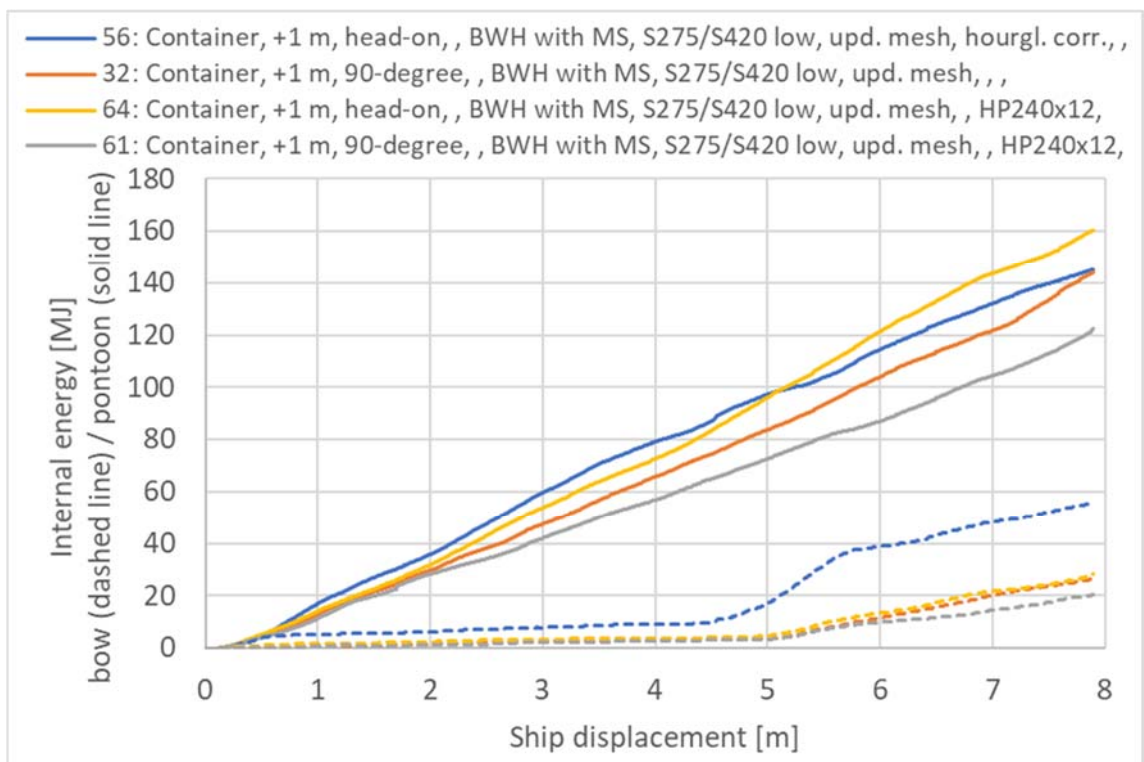
Figure 5-22 to Figure 5-24 show the internal energy dissipated in the bow with dashed line and the pontoon with solid line for the different modifications.

Figure 5-25 to Figure 5-27 show the frictional dissipation and artificial energy in the models. The proportion of artificial to internal energy is 9-12 % for the displayed models.

Figure 5-28 to Figure 5-30 show that the force reduction options does not change the proportion of internal energy dissipated in the pontoon much. The head-on impacts display lower energy dissipation in the pontoon in the early stage of the impact, except for the model with corrugated bulkhead. The corrugated bulkhead leads to high energy dissipation in the pontoon also for head-on impact.



> Figure 5-22 Internal energy [MJ] impact bow-pontoon, plate thickness reduction



> Figure 5-23 Internal energy [MJ] impact bow-pontoon, stiffener reduction

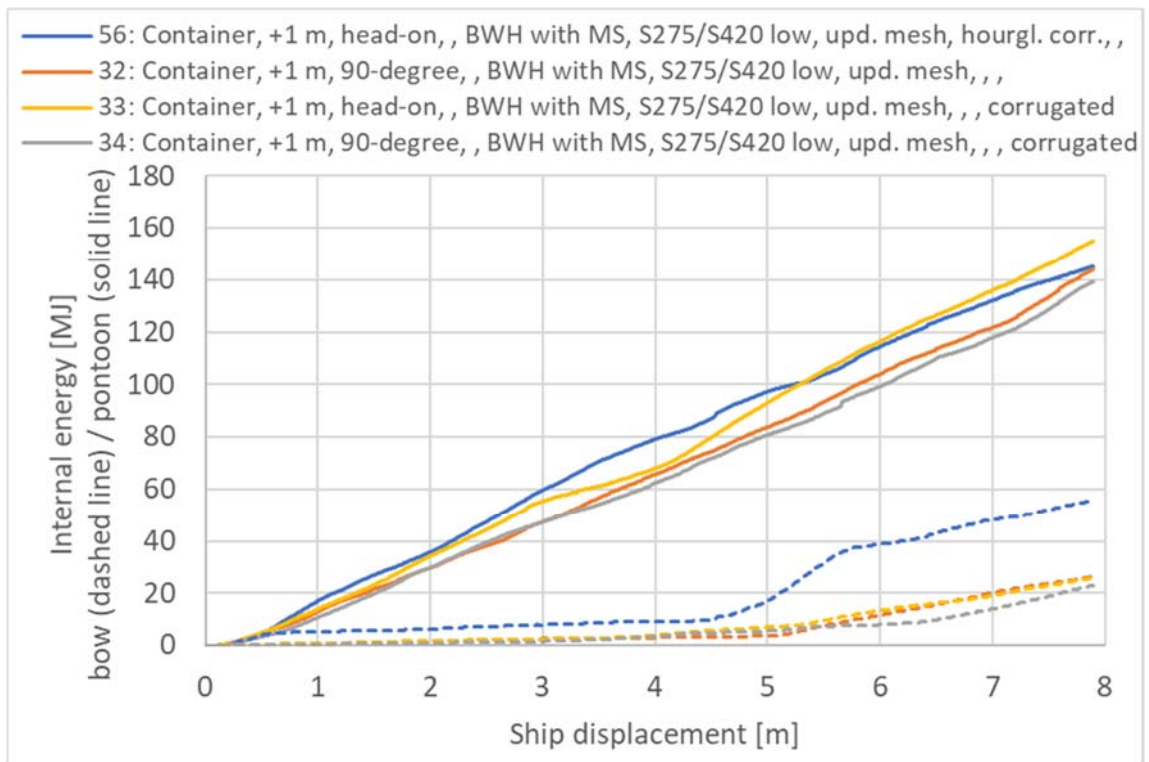


> Figure 5-24 Internal energy [MJ] impact bow-pontoon, corrugated bulkheads

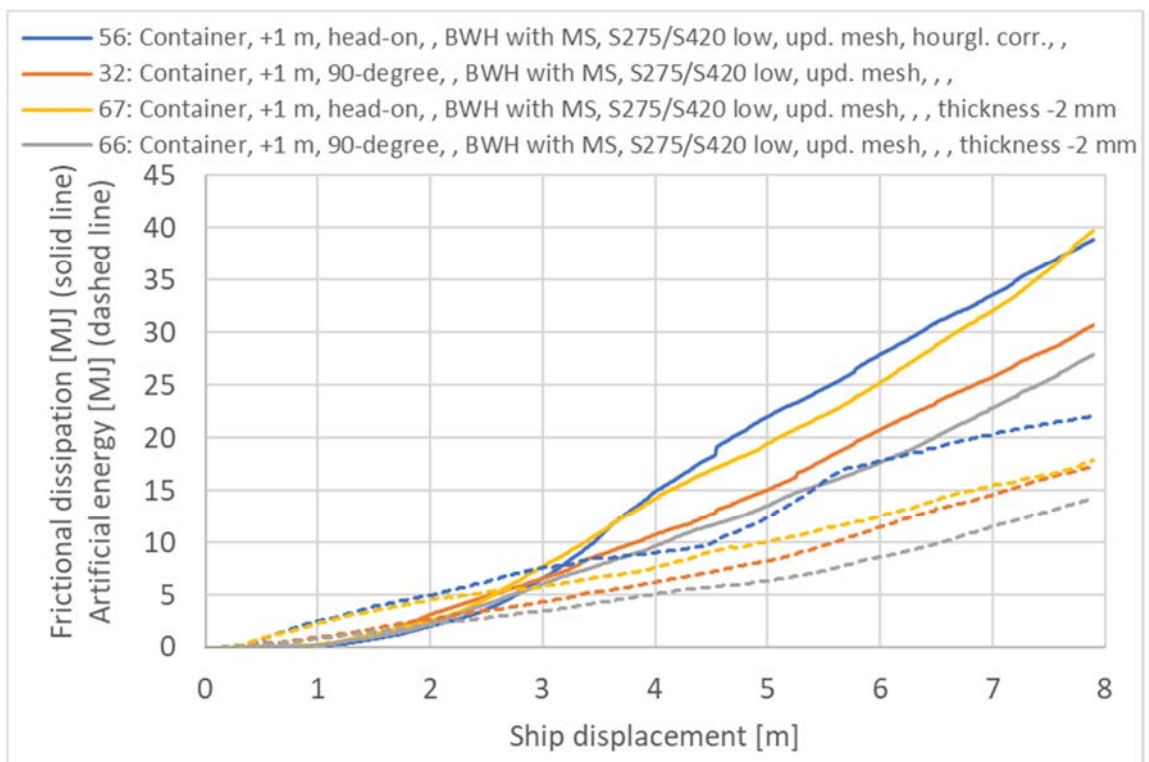


> Figure 5-25 Frictional dissipation and artificial energy [MJ] impact bow-pontoon, plate thickness reduction

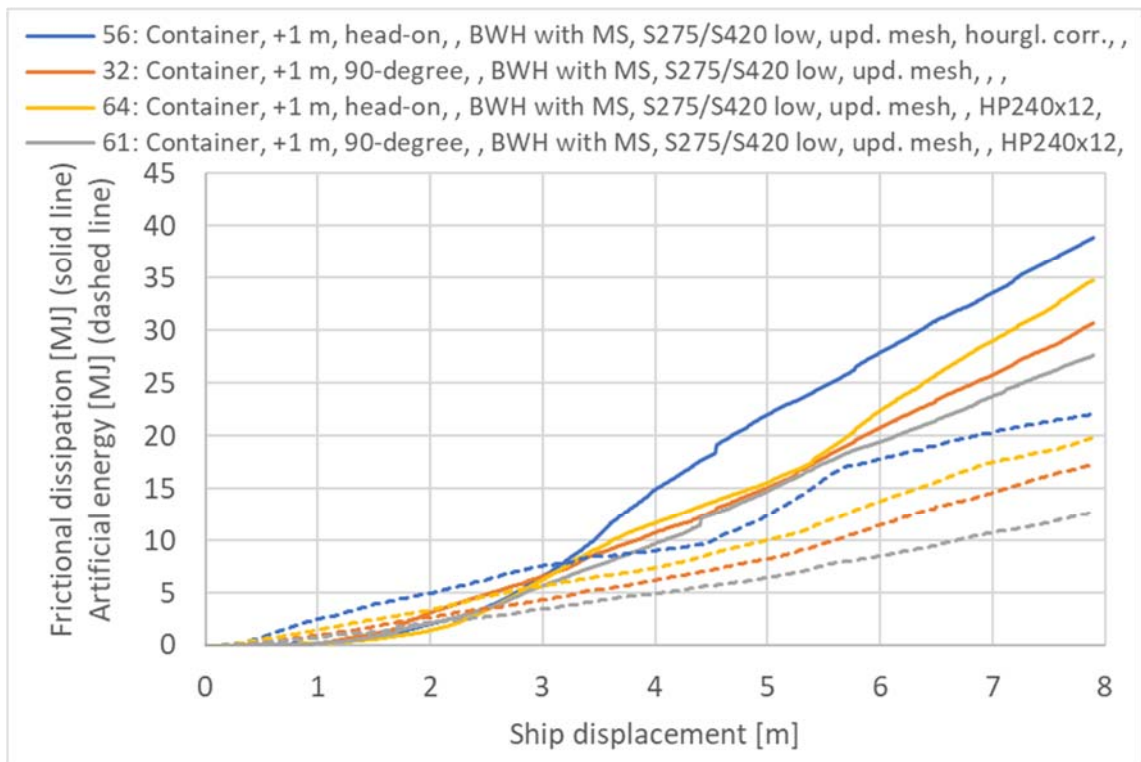


> Figure 5-26 Frictional dissipation and artificial energy [MJ] impact bow-pontoon, stiffener reduction

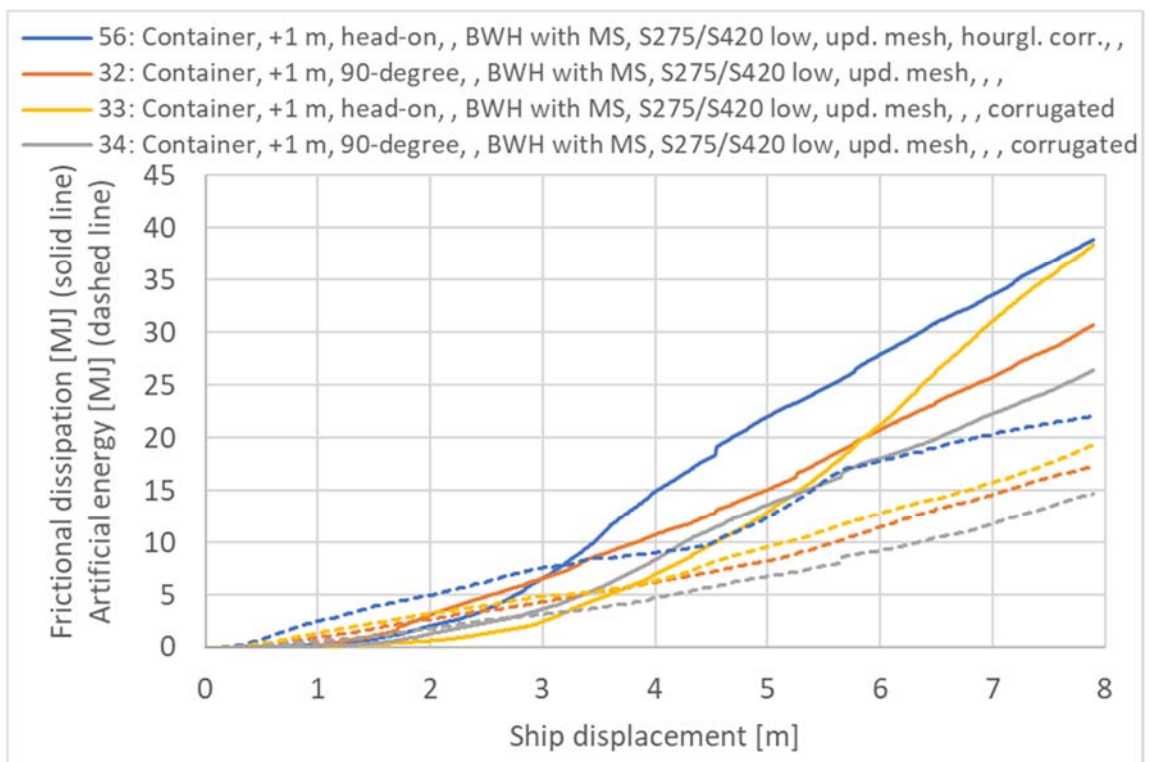


> Figure 5-27 Frictional dissipation and artificial energy [MJ] impact bow-pontoon, corrugated bulkheads

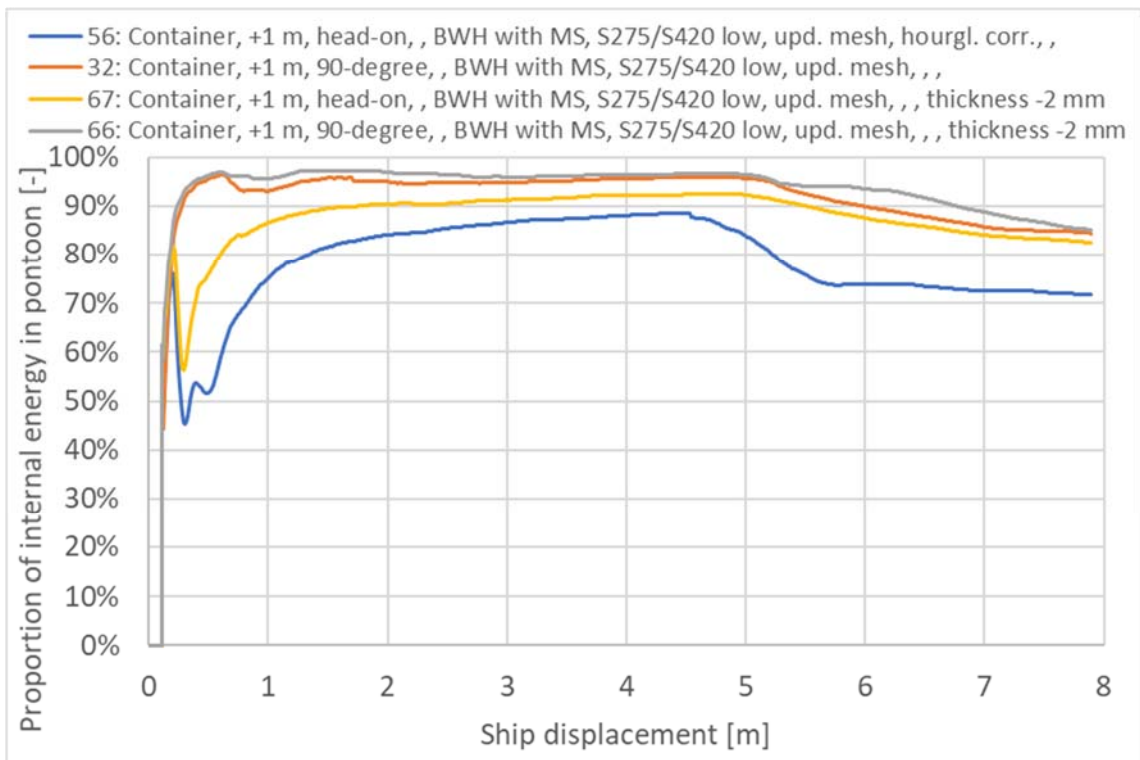


> Figure 5-28 Proportion of internal energy in pontoon [-] impact bow-pontoon, plate thickness reduction

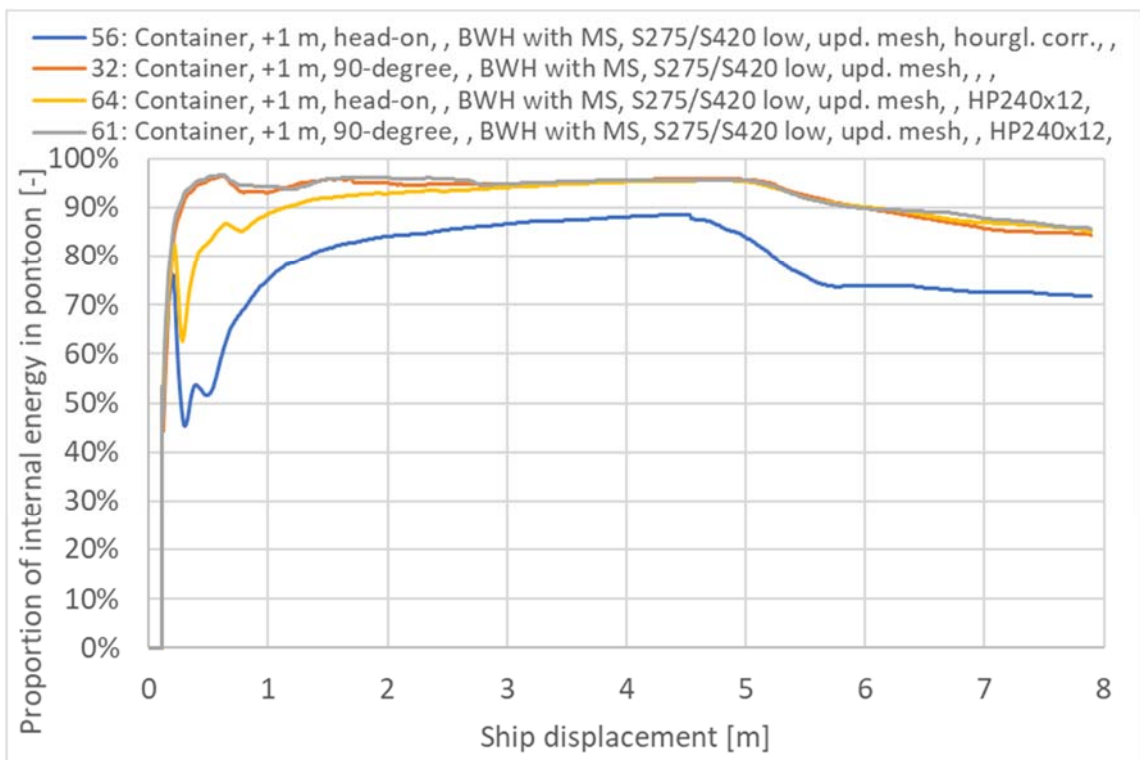


> Figure 5-29 Proportion of internal energy in pontoon [-] impact bow-pontoon, stiffener reduction

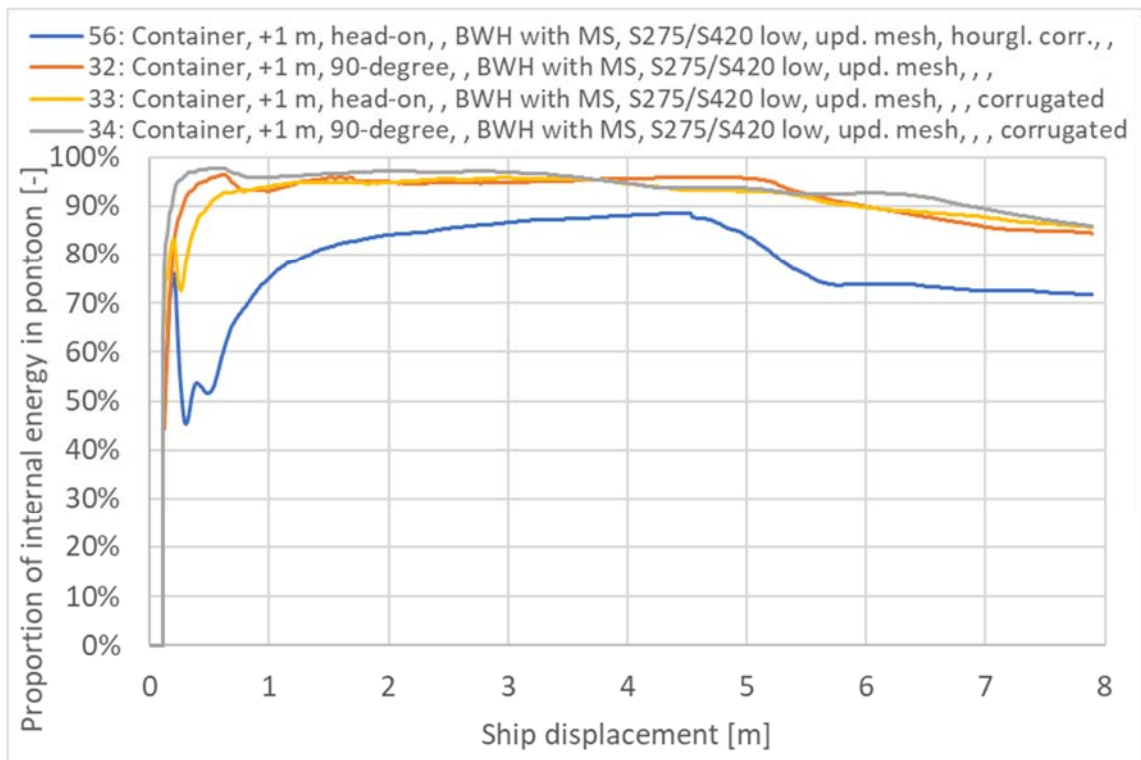


> Figure 5-30 Proportion of internal energy in pontoon [-] impact bow-pontoon, corrugated bulkheads

Figure 5-31 shows a graphical presentation of the sensitivity of the three force reduction options investigated. An equal value of the dissipated internal energy in the local simulations is chosen, 100 MJ. This is about 40 % of the energy to be dissipated in axis 3 (246 MJ). Then, the maximum contact force occurred from 0 m ship displacement to ship displacement corresponding 100 MJ for the respective simulation is evaluated. I.e. the maximum force from Figure 5-19 to Figure 5-21, defined by a cut-off at 100 MJ for the respective simulation.

It is seen that the base geometry gives the shortest ship displacement at 100 MJ and mostly also the highest maximum contact force. The head-on impact with corrugated bulkhead gives higher maximum force because the impact reaches a higher force level at about 4.5 m, seen in Figure 5-21, since the corrugated geometry is only modelled in the front 4 m.

The force reduction seems high for the 90-degree impact with corrugated bulkhead, however this is mostly because this impact is softer up to 6 m ship displacement, while the other simulations are only softer up to 4-5 m ship displacement and with higher force level after this.

The reductions of the force level are therefore uncertain for the option with corrugated bulkhead. The corrugation should be throughout the pontoon for a noticeable effect. The damage of the pontoon is nevertheless severe, but a reduced force level for pontoon collision can be beneficial for the bridge girder and column.

Generally, the reduction of the force level is limited for the modifications investigated. The type of ship that hits the pontoon and the direction of the impact is of greater importance but cannot be controlled.

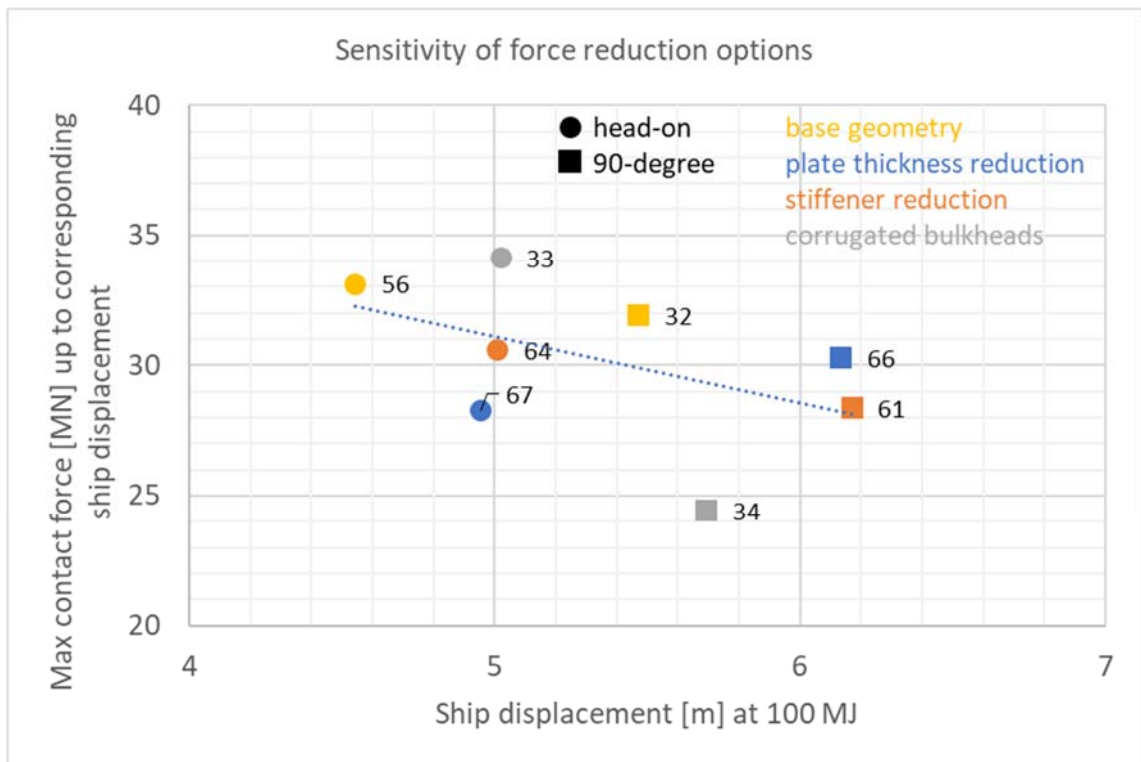


> Figure 5-31 Sensitivity of force reduction options, impact container bow-pontoon

5.3.4 Impact with column

This section presents results for forecastle impact with bridge column. "Mean-low" material parameters have been utilized.

The load cases are equal to the load cases for impact with the pontoon in Table 5-2. However, the head-on impact is not very relevant since the indentation in the pontoon must be larger than 23 m to hit the column head-on. For the 90-degree impact, the column is hit if the indentation in the pontoon is larger than 4 m given the smallest pontoon with width 12 m. See Figure 5-32. The different indentations in the pontoon are results from the global assessment [2].

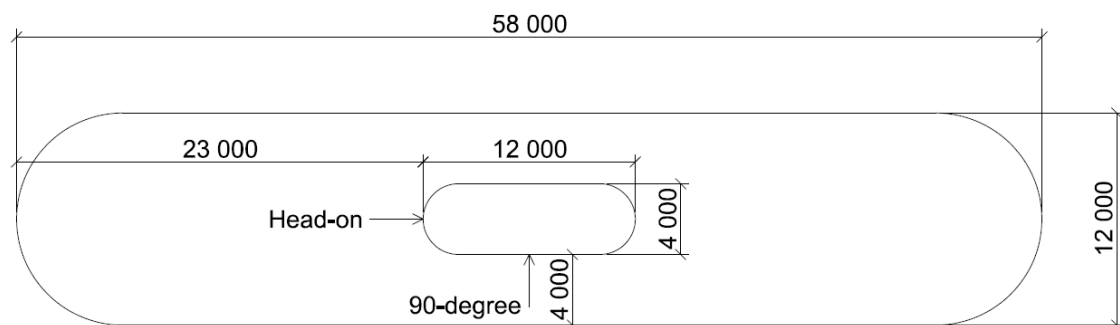
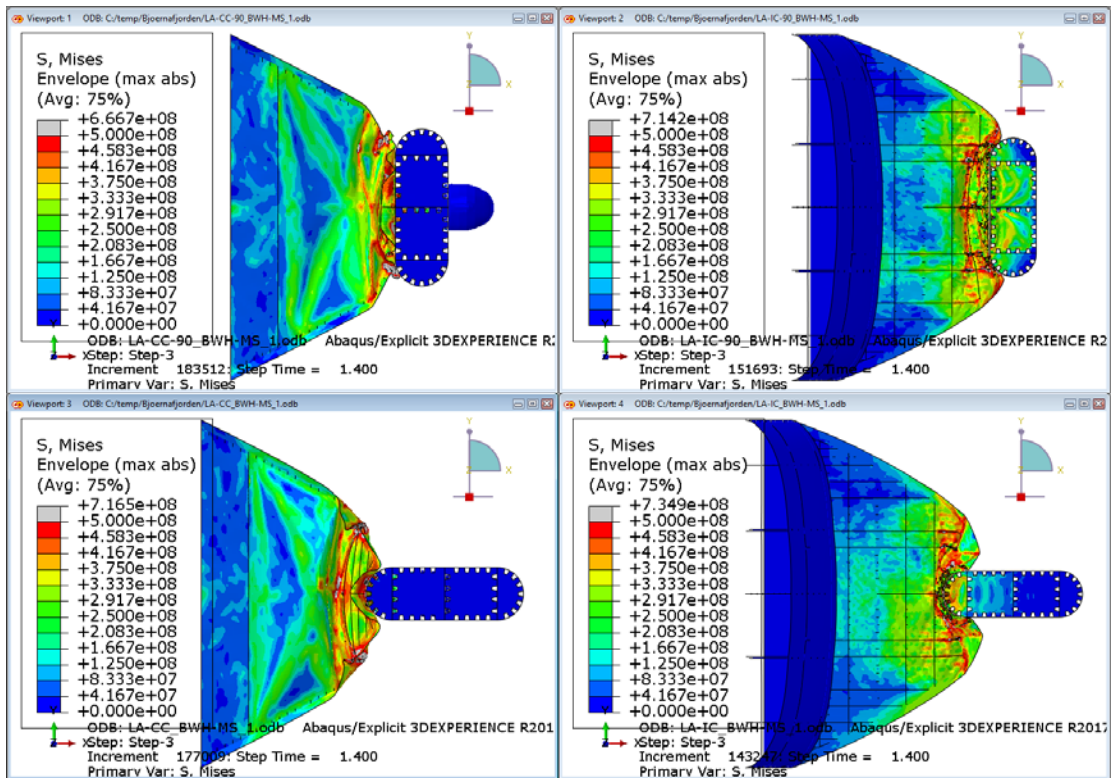


> Figure 5-32 Plan of smallest pontoon and column [mm]

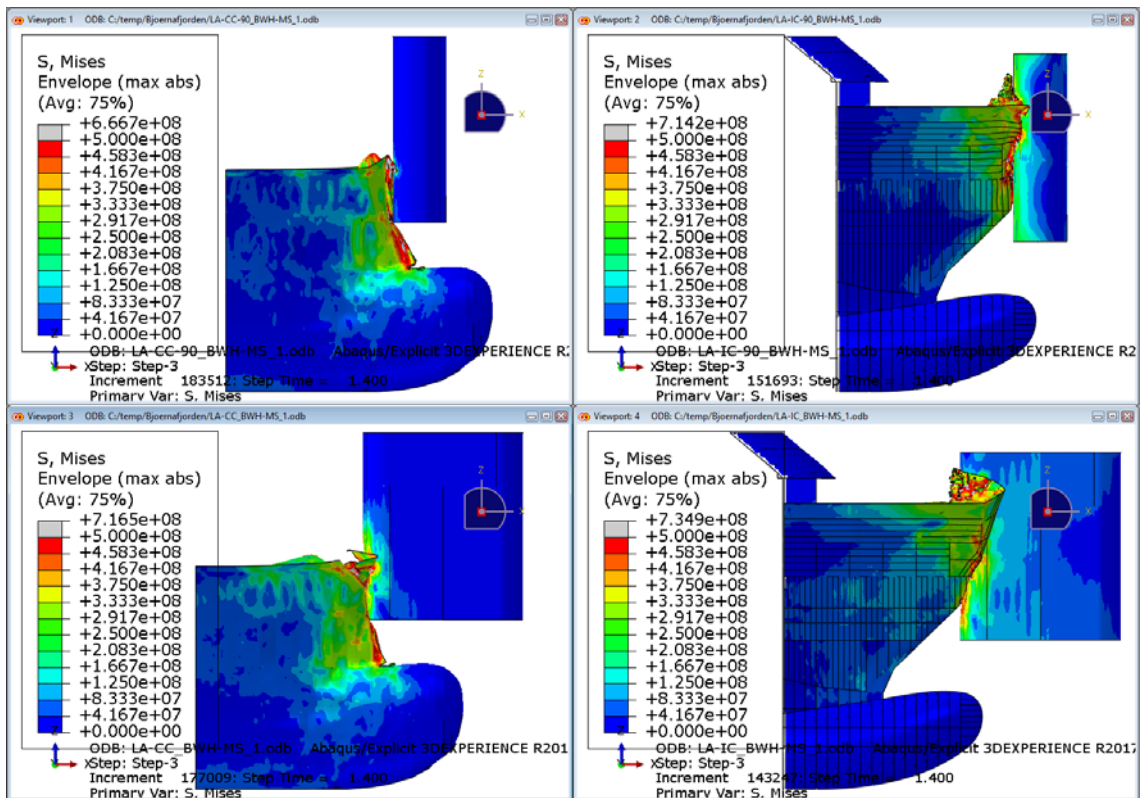
Figure 5-33 and Figure 5-34 show the ship bow and column damage at 8 m ship displacement. The forecastle of the ship bow is subjected to severe damage, while the column is mostly spared. Damage in the column is a bit higher for impact with the ice-strengthened bow than the container bow. Note that the column wall is modelled with thickness 20 mm. A higher wall thickness will prevent even more damage to the column.

Note that the maximum indentation is 13 m for the 90-degree ice-strengthened bow-pontoon collision in the "K12 - Ship impact, Global assessment" report [2]. This corresponds to $(13-4) \text{ m} = 9 \text{ m}$ ship displacement for the forecastle-column collision.

Figure 5-35 shows the resulting force-displacement curves. All impacts have a low force level in the early state of the collision. The impact force level becomes very high for the 90-degree impact with the ice-strengthened bow. This is because the ice-strengthened bow has large stiffeners at the front of the forecastle. The container bow is believed to be more representative for the column impact.



➤ Figure 5-33 von Mises stress [MPa] forecastle-column collision seen from above: 90-degree (upper), head-on (lower), container bow (left), ice-strengthened bow (right)



➤ Figure 5-34 von Mises stress [MPa] forecastle-column collision side view: 90-degree (upper), head-on (lower), container bow (left), ice-strengthened bow (right)

ID-no.	Max. contact force [MN] 0-4 m	Mean contact force [MN] 0-4 m
1	17	9
2	45	20
3	18	8
4	22	11

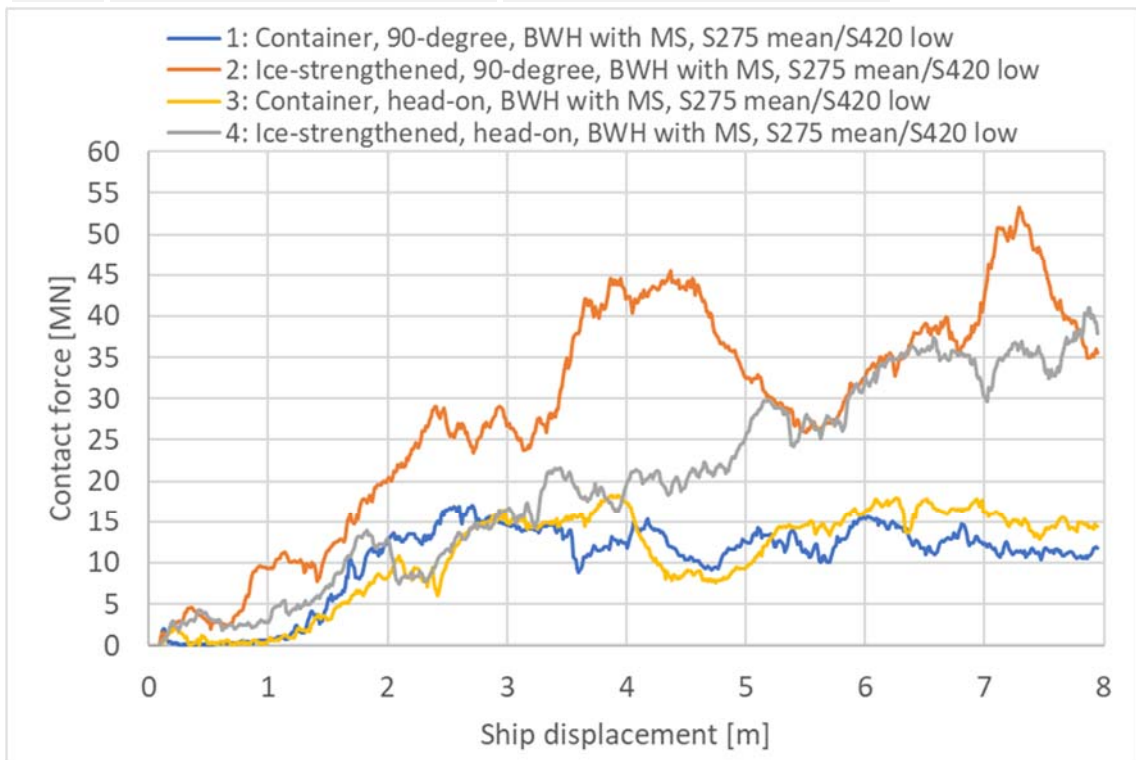
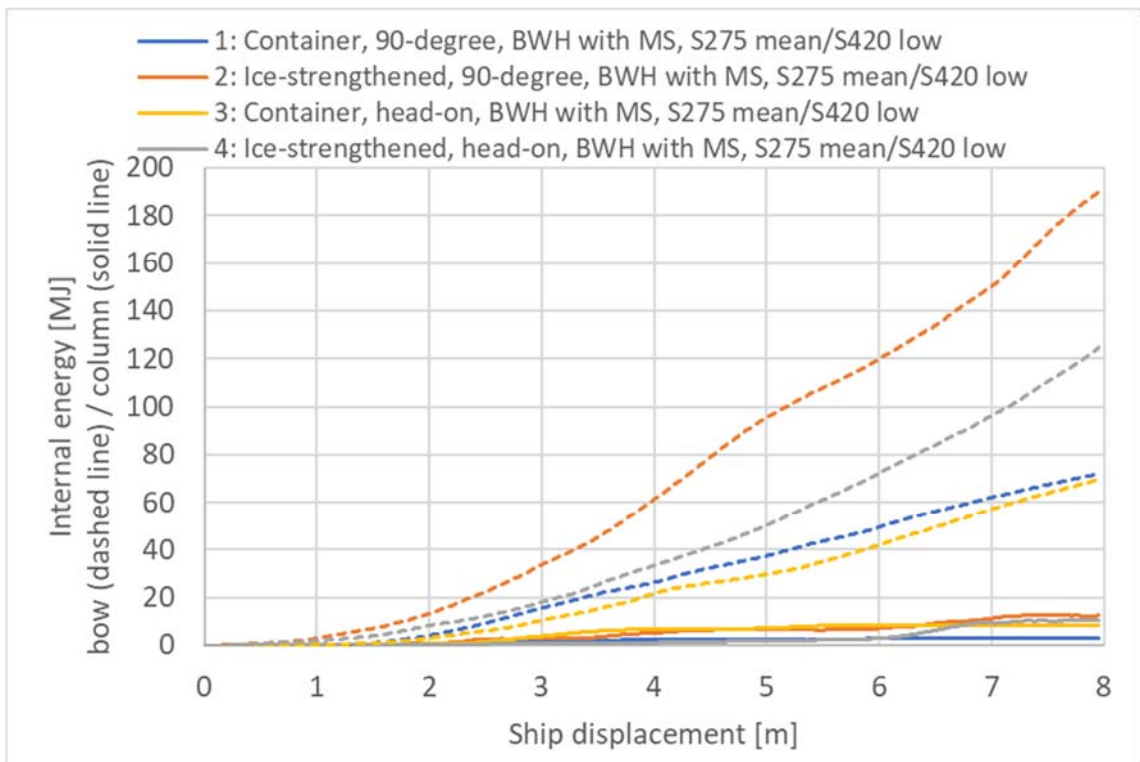


> Figure 5-35 Contact force [MN] impact forecastle-column

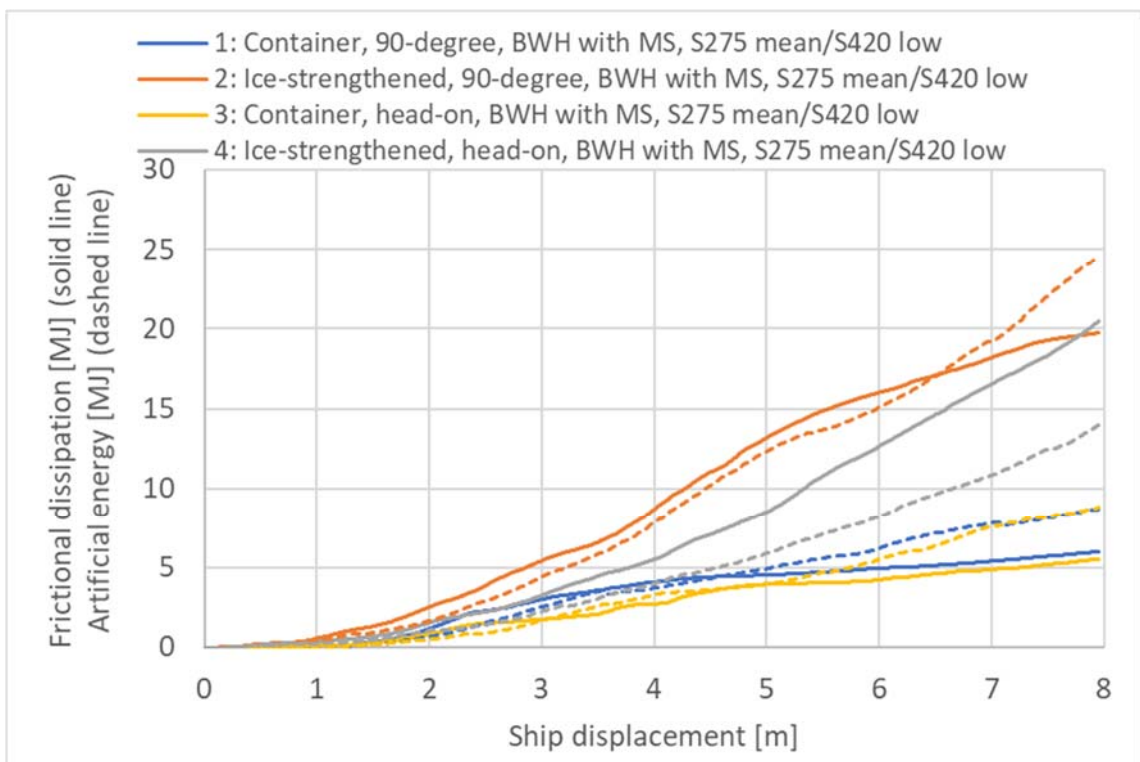
Figure 5-36 shows the internal energy dissipated in the forecastle with dashed line and the column with solid line. The internal energy is high in the forecastle and low in the column.

Figure 5-37 shows the frictional dissipation and artificial energy in the models. The proportion of artificial to internal energy is maximum 15-19 % for the displayed models shown in Figure 5-39, which is very high. This is because the internal energy is low at the early state of the impact, while the artificial energy is present early on. The proportion of artificial to internal energy stabilizes at 10-12 %, which is closer to a satisfactory level. With full integration, the proportion of artificial to internal energy reduces to 4-5 %.

Figure 5-38 shows that the proportion of internal energy dissipated in the columns is low for all load cases. The head-on impact with the container bow displays higher energy dissipation in the column, but it is not likely that the column will experience impact from the head-on direction with a bow like the container bow.



> Figure 5-36 Internal energy [MJ] impact forecastle-column



> Figure 5-37 Frictional dissipation and artificial energy [MJ] impact forecastle-column

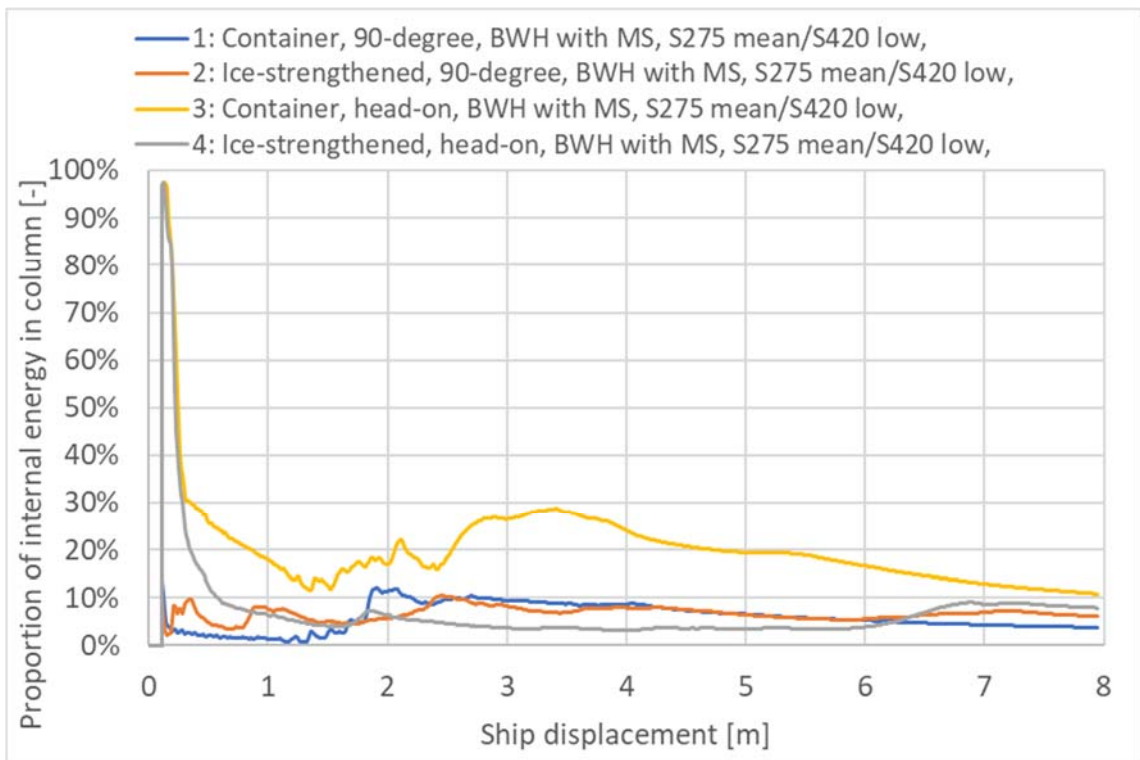


> Figure 5-38 Proportion of internal energy in column [-] impact forecastle-column

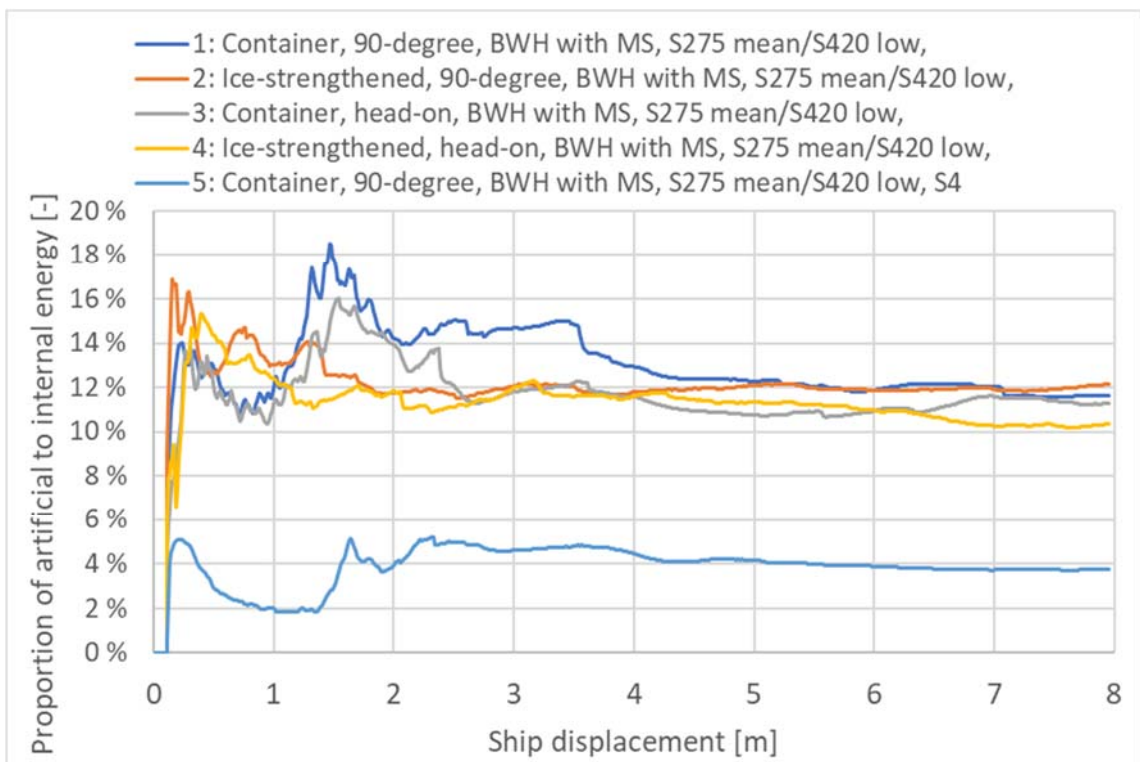
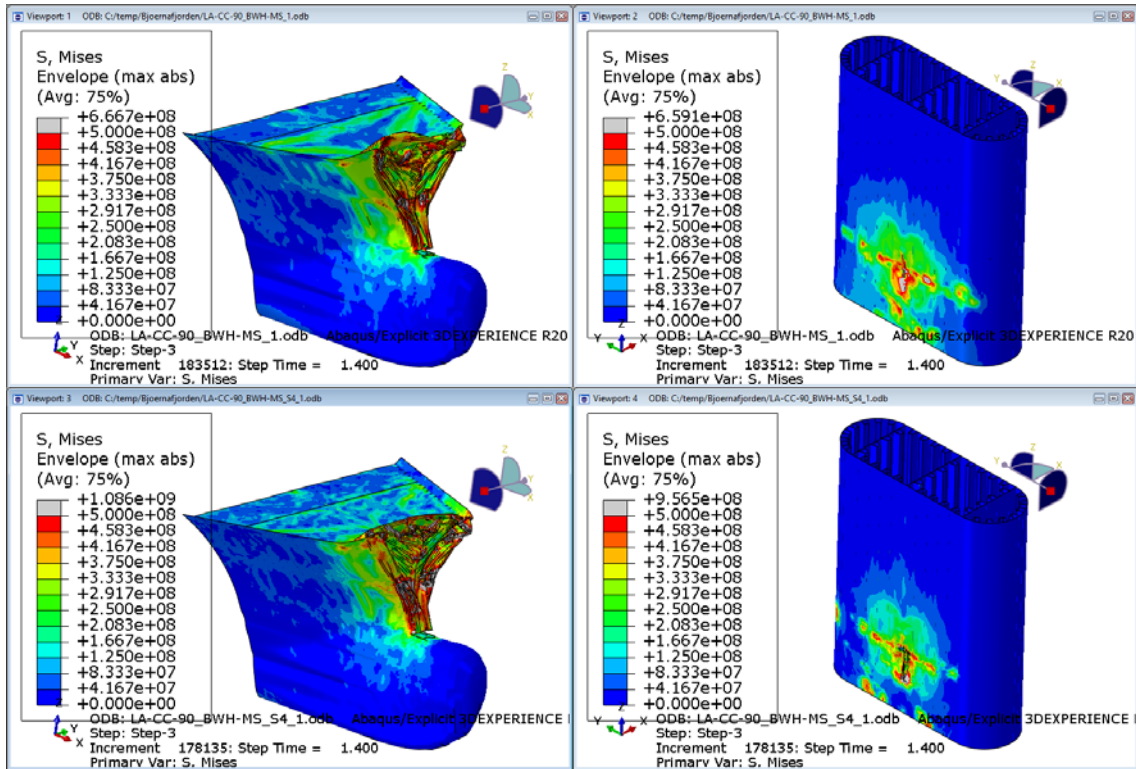


> Figure 5-39 Proportion of artificial energy to internal energy [-] impact forecastle-column: The low curve is with full integration

Figure 5-40 to Figure 5-44 show that reduced integration gives approximately the same results as full integration, except for internal energy in the ship bow which is a bit higher with reduced integration.



- > Figure 5-40 von Mises stress [MPa] forecastle-column collision: Comparison reduced integration (upper) with full integration (lower), container bow (left), column (right)

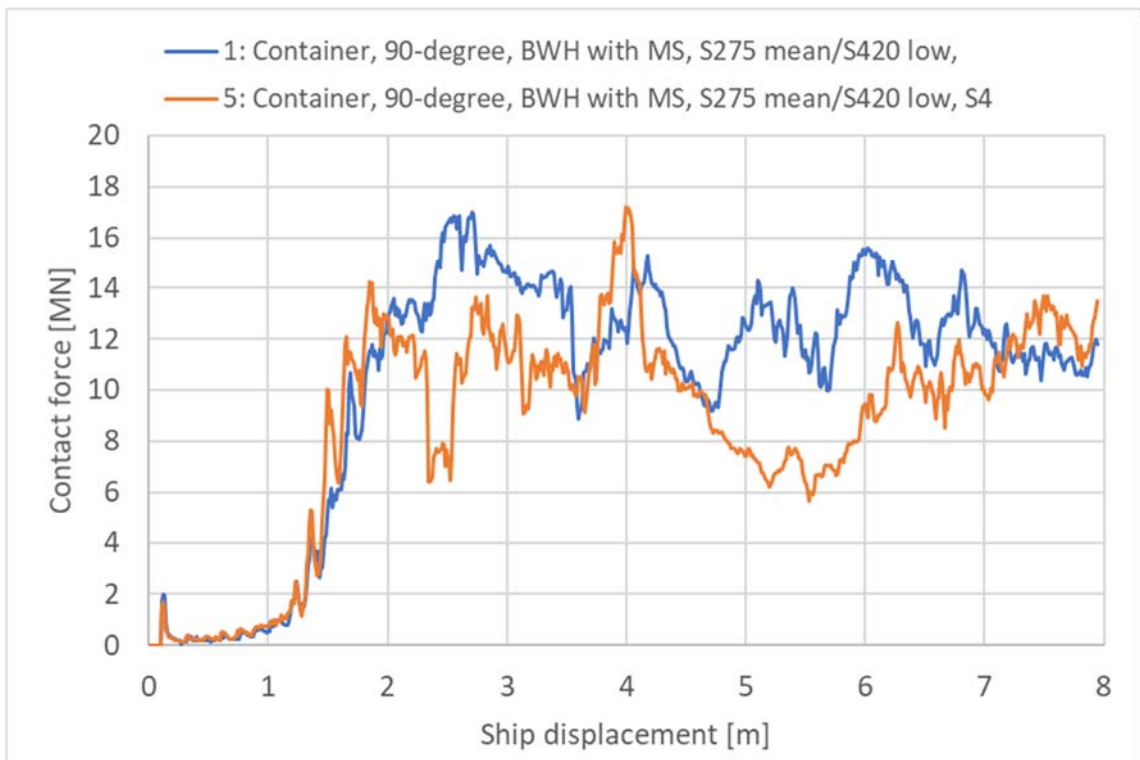


> Figure 5-41 Contact force [MN] impact forecastle-column, sensitivity of element type

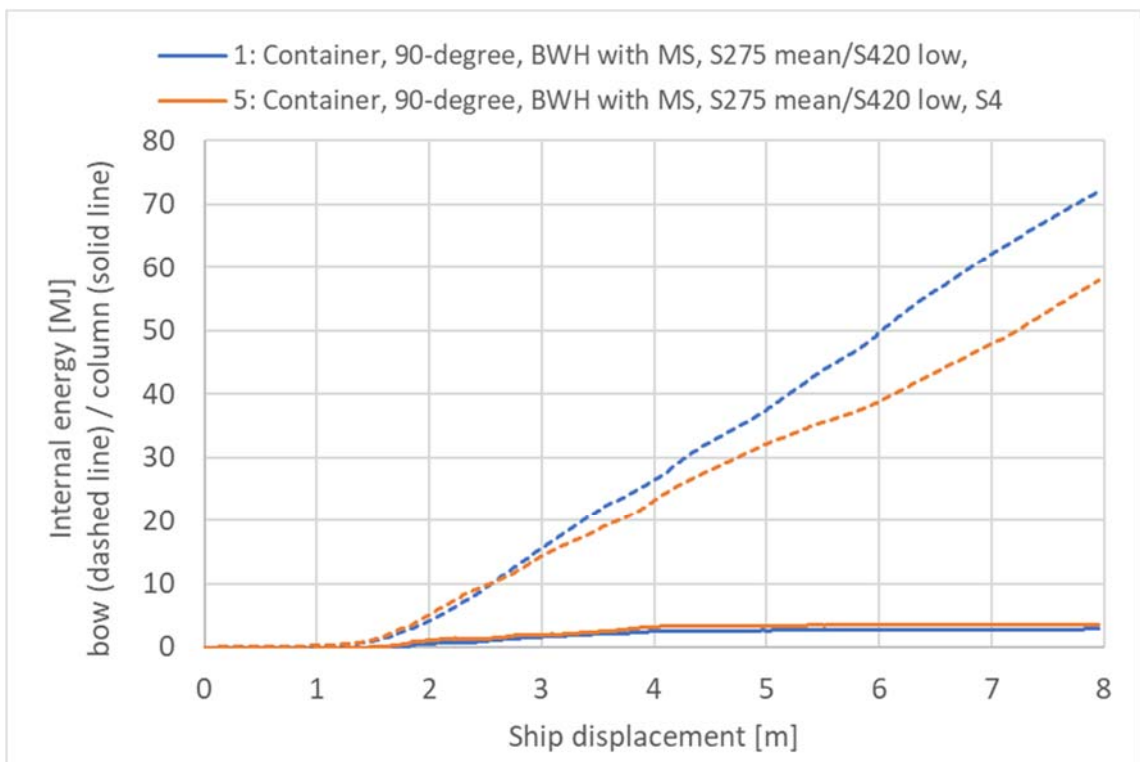


> Figure 5-42 Internal energy [MJ] impact forecastle-column, sensitivity of element type

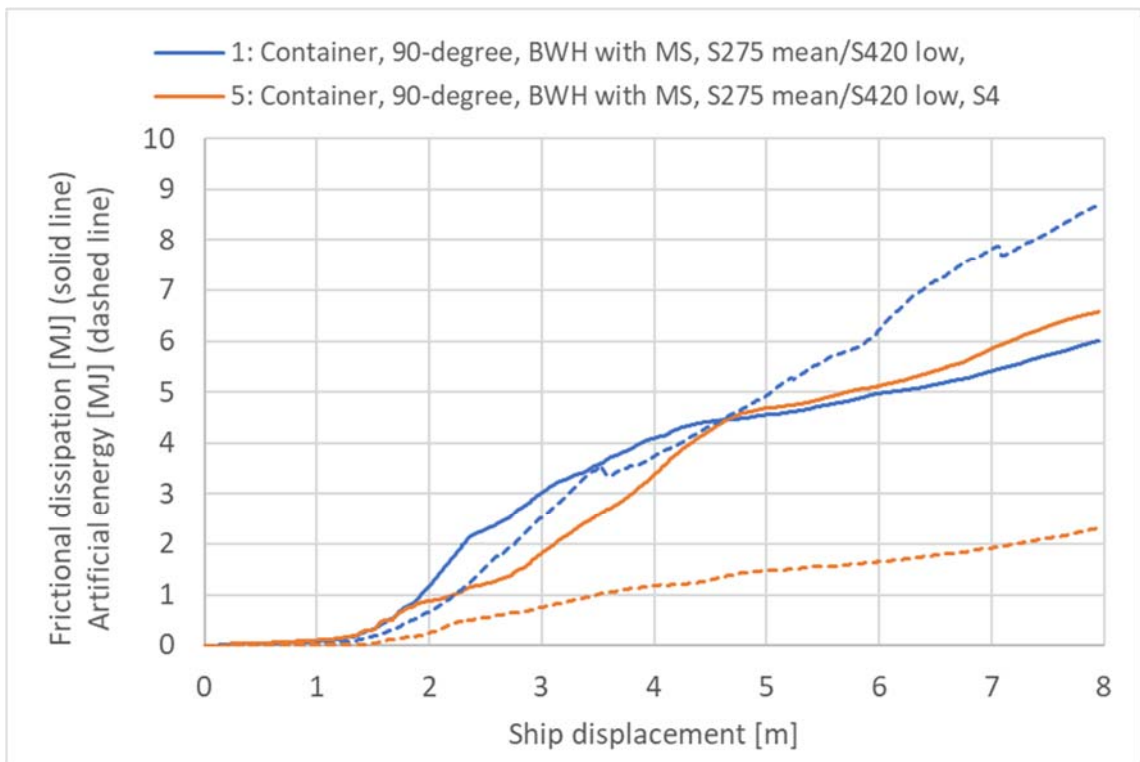


> Figure 5-43 Frictional dissipation and artificial energy [MJ] impact forecastle-column, sensitivity of element type

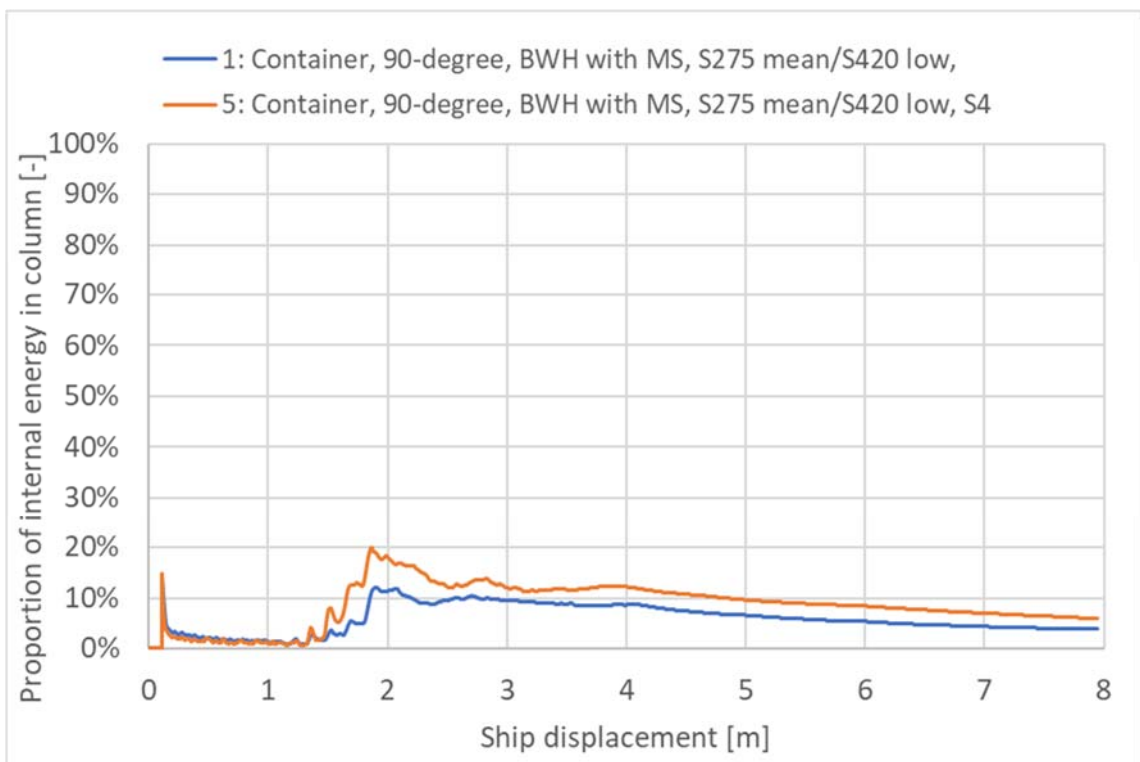


> Figure 5-44 Proportion of internal energy in column [-] impact forecastle-column, sensitivity of element type

6 INPUT TO GLOBAL COLLISION ASSESSMENT

Global collision assessment has been performed with “mean-low” material parameters. Impact with the container bow, load cases A and B from Table 5-2, gives the highest impact force level. The resulting force-displacement curves are given in Figure 6-1.

If a low force-displacement curve is desired, the green curve may be utilized, which is 90-degree impact with the ice-strengthened bow between bulkheads and frames.

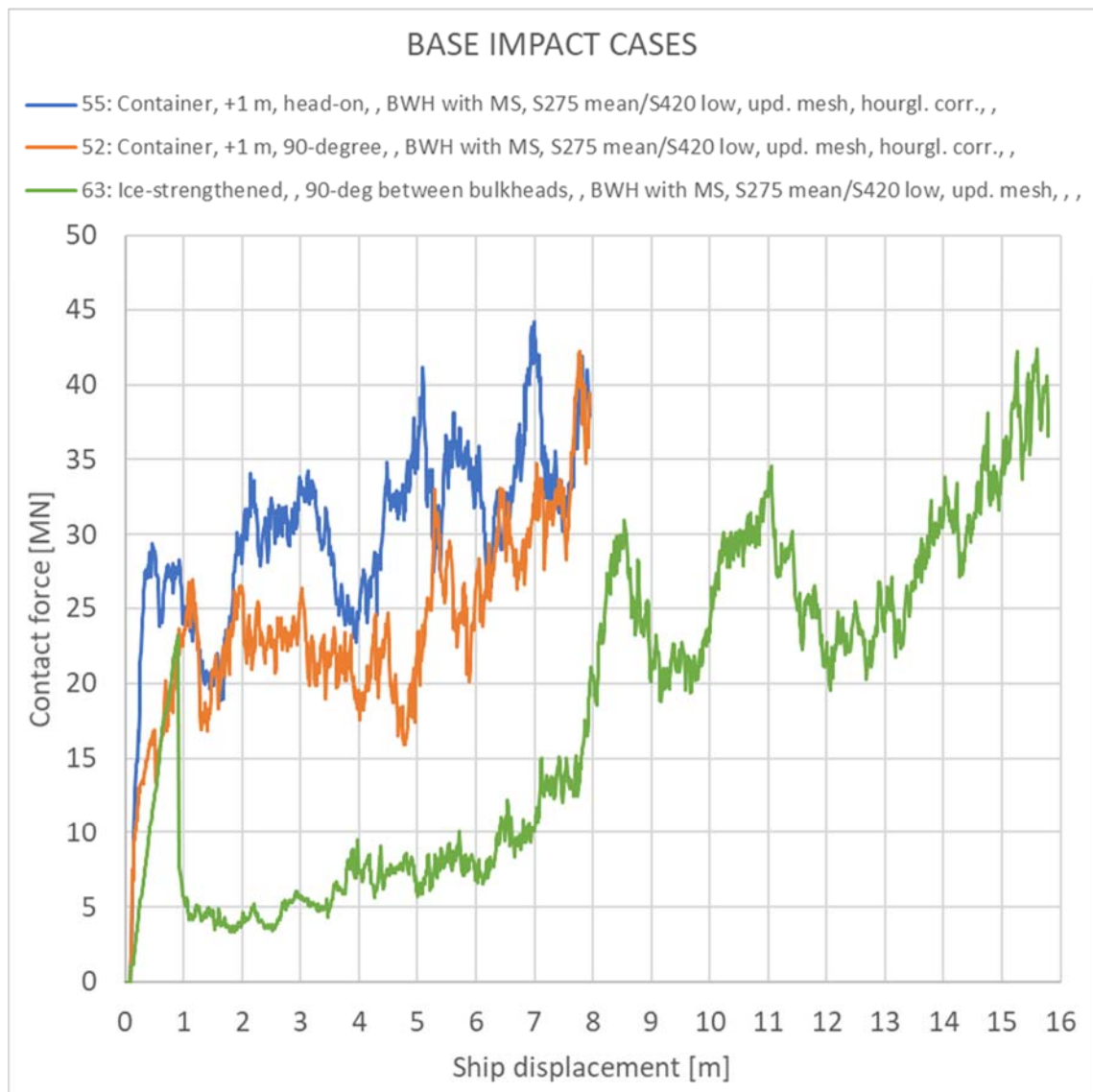


> Figure 6-1 Contact force [MN] base impact cases bow-pontoon

7 SUMMARY AND CONCLUSIONS

7.1 Compilation of response

Local response of bow-pontoon collision with “mean-low” material parameters is considered as the most reliable simulations performed. Further, the height of the container bow used is 1.0 m above scantling draught as defined in the Design Basis [1]. The response of the load cases in Table 5-2 are shown in Figure 7-1.

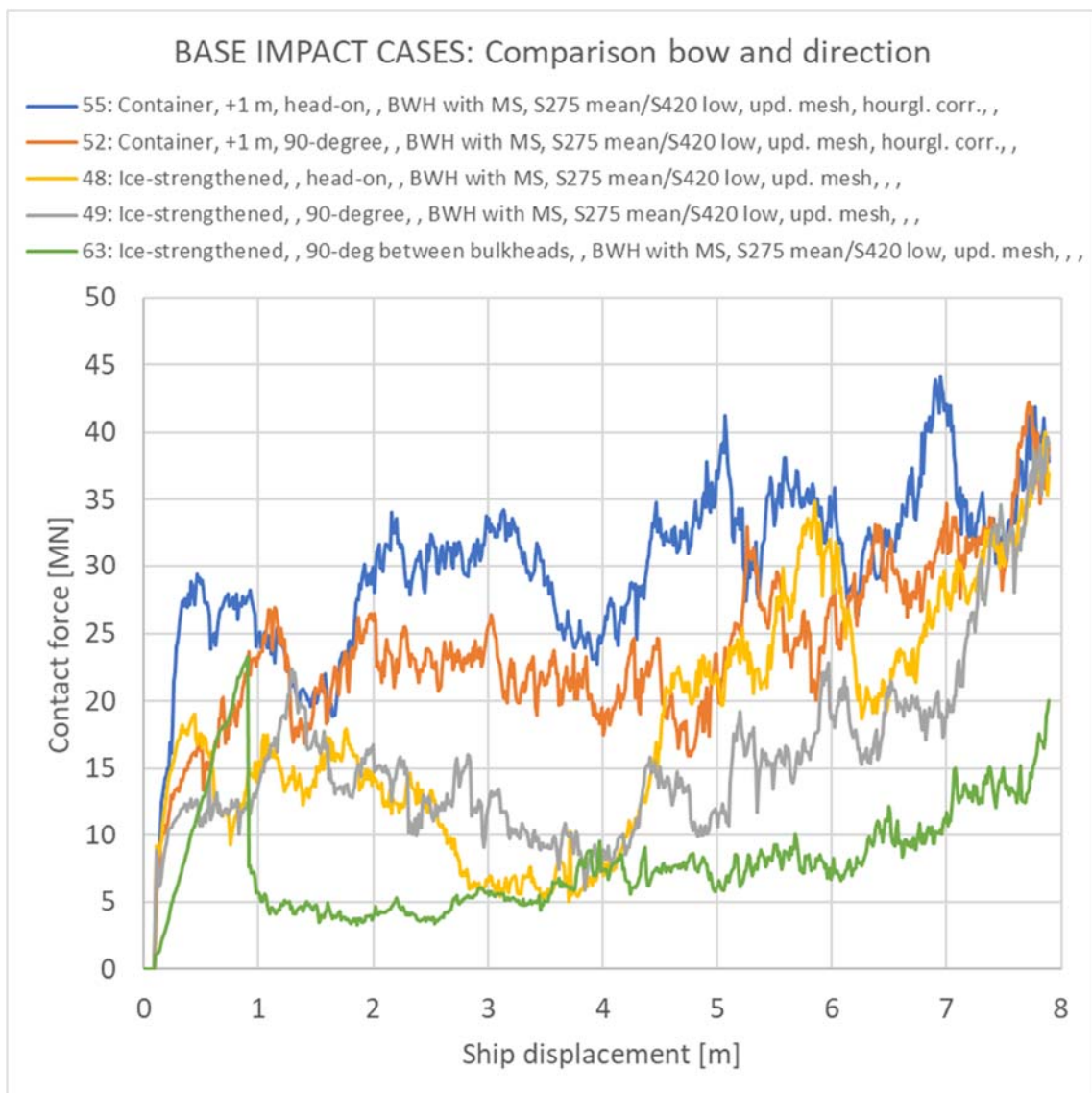


> Figure 7-1 Contact force [MN] impact bow-pontoon

Forecastle impact with column is not governing for the forecastles that have been investigated. The local collision simulations to 8 m forecastle displacement show that the forecastle of the ship bow is subjected to severe damage, while the column is mostly spared. The maximum indentation is 13 m for the 90-degree ice-strengthened bow-pontoon collision with the lowest force-displacement curve in Figure 7-1. This corresponds to 9 m ship displacement for the forecastle-column collision (4 m from pontoon wall to column wall).

7.2 Discussion

7.2.1 Interaction with global assessment

Input from local collision response to global collision assessment is the force-displacement curves. These curves are put into the global finite element model of the bridge structure by a non-linear connector representing the ship and pontoon. Details to this workflow are explained in the global assessment report [2].

When global assessment has been conducted, several response parameters are revealed for further local damage evaluation. This includes as the most important the amount of energy that is dissipated locally and the displacement of the connector.

In the local simulations performed, the pontoon dissipates most of the energy, about 80-90 %, while the ship bow is less damaged. This means that the displacement of the connector obtained from the global assessment can almost be transferred directly as the indentation in the pontoon.

When the local damage is known, reduced stiffness (number of filled compartments and thus reduced water plan stiffness) can be given as input to evaluate the damaged condition with a 100-year environmental loading applied to the bridge.

External dynamics is accounted for, and this report does not quantify the exact damage of the pontoon. Reference is made to the global assessment report [2]. Results for local impact response are rather given for chosen parameters as basis for comparison.

7.2.2 Sensitivity of results

The ship impact simulations performed are sensitive to several parameters.

When studying the force-displacement relation, the impact force level is higher for the container bow than the ice-strengthened bow. For the container bow, head-on impact gives higher force level than 90-degree impact. This seems to be because a larger impact area is involved if the surface hit is curved. The head-on impact results also in a steeper force-displacement relation in the early impact stage. The difference between head-on and 90-degree impact is not that prominent for the ice-strengthened bow.

Figure 7-2 shows a graphical presentation of the sensitivity of bow and direction. The maximum contact force defined by a cut-off at ship displacement corresponding 100 MJ is plotted.

When studying the force-displacement relation up to an equal energy dissipation, the ice-strengthened bow results in slightly higher maximum contact force and considerably higher ship displacement than the container bow. For equal energy dissipation, head-on impact results in higher maximum contact force than 90-degree impact for both ship bows. Impact between bulkheads and frames gives large displacement before the same amount of energy is dissipated. This impact also results in high maximum contact force which occurs at a later stage of the impact, see Figure 6-1.

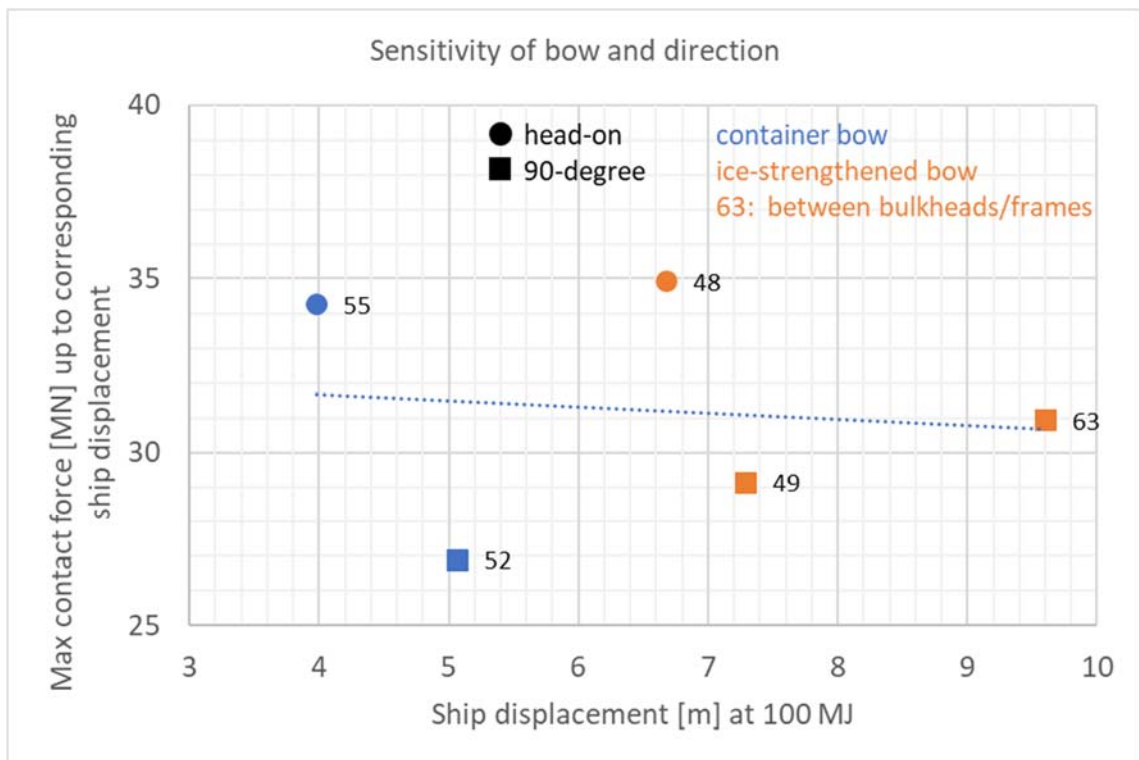


> Figure 7-2 Sensitivity of ship bow and direction of impact

Different impact force reduction options have been tested. The damage of the pontoon is regardless severe for a slender design, which is preferred for other load cases and limit states. However, a reduced force level for pontoon collision is beneficial for the bridge girder.

Figure 7-3 (equal to Figure 5-31) shows the sensitivity of the three force reduction options investigated. A 2 mm reduction to plate thickness and reduced stiffener height from 320 mm to 240 mm display similar results; a moderate reduction at about 10 %. Reduction of the force level with corrugated bulkhead is uncertain and dependent on the variable chosen for consideration.

The corrugated bulkhead is more effective for the head-on impact than the 90-degree impact when considering the maximum and mean contact force up to 4 m ship displacement. When considering the maximum contact force up to ship displacement at 100 MJ, the findings are opposite. The 90-degree impact with corrugated bulkhead seems favorable and the head-on impact gives no reduction. The corrugated bulkheads have nevertheless the largest reduction at the first state of the impact for both directions. The corrugation should be throughout the pontoon for a noticeable effect.

Generally, the reduction of the force level is limited for the modifications investigated. The type of ship that hits the pontoon and the direction of the impact is of greater importance but cannot be controlled.

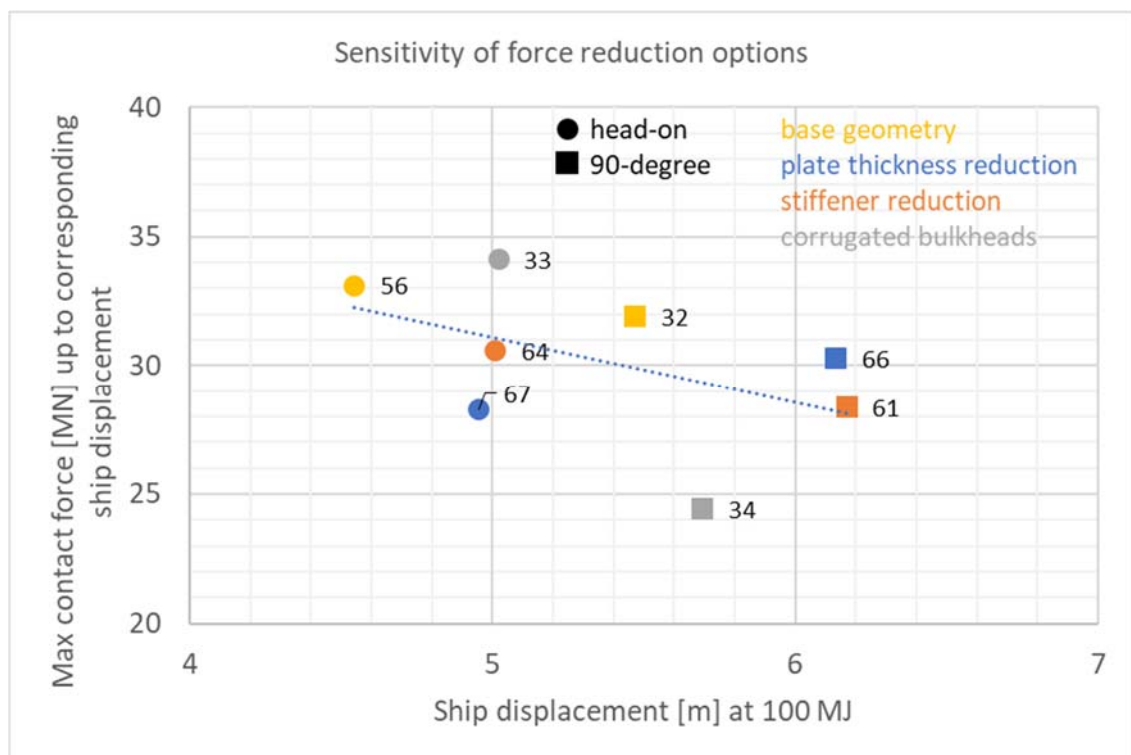


> Figure 7-3 Sensitivity of force reduction options, impact container bow-pontoon

The following sensitivity studies are documented in Appendix C [22]:

- Superduplex steel material in the splash zone (Appendix C section 1 [22])
- Material parameters defining the isotropic hardening (App. C sections 2 and 3 [22])
- Material damage model (Appendix C section 4 [22])
- Mesh size and element type (Appendix C section 5 [22])
- Impact height and ship velocity (Appendix C section 6 [22])

The models with superduplex steel affect the impact results to both lower and higher force and energy level, but the differences are not prominent.

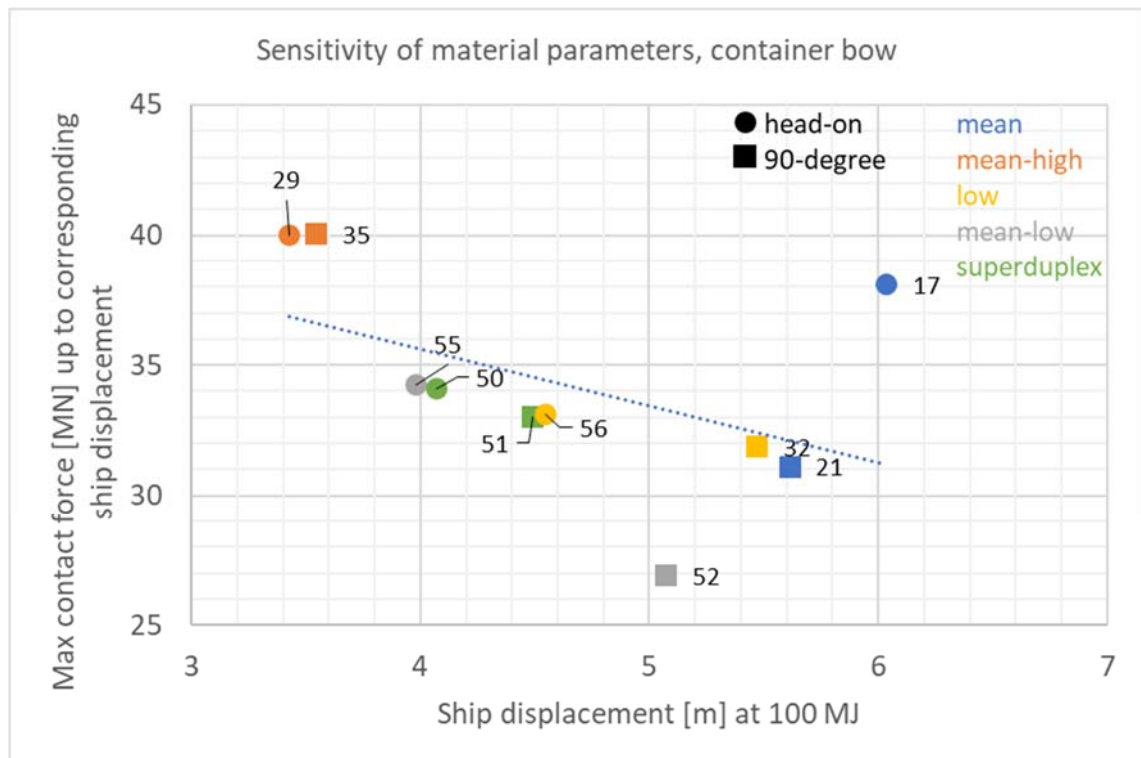
The choice of material parameters defining the isotropic hardening affects the collision response. Generally, a higher material curve also represents a higher force and energy level. However, the initial impact can be almost identical given a medium variation to the material parameters of the pontoon (about 100 MPa to hardening strength K), while a large variation (300 MPa to K) results in higher initial impact force. Since the pontoon is more damaged than the ship bow, the pontoon is also more sensitive for the choice of material parameters.

A low set of materials parameters is intended for design calculations. The design parameters may result in too low capacity for structures when the goal is to evaluate the impact forces. On the other hand, a high set of material parameters is considered too conservative.

Consciousness should be addressed when choosing the hardening parameters. To lower the uncertainties regarding higher material quality than accounted for, an opportunity is to specify the maximum values to yield and ultimate tensile stress to the supplier of the bridge steel materials. Experimental test can be performed to verify the actual material quality.

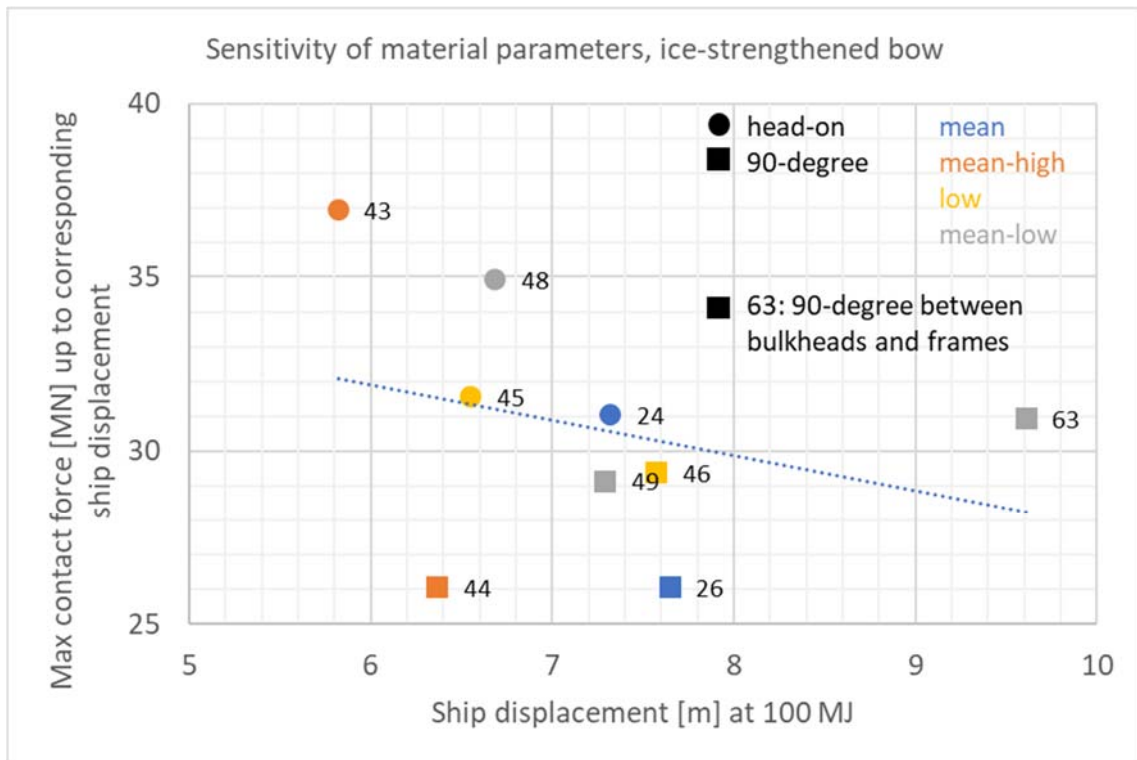
Figure 7-4 shows the sensitivity of the material parameters investigated for impact with the container bow.

It is seen that the "mean-high" set of material parameters gives the shortest ship displacement at 100 MJ and the highest maximum contact force. The simulation is sensitive to especially the "mean-high" set of material parameters. In addition, head-on impact with the "mean" material according to DNVGL-RP-C208 [6] gave deviant results.



> Figure 7-4 Sensitivity of material parameters, impact container bow-pontoon

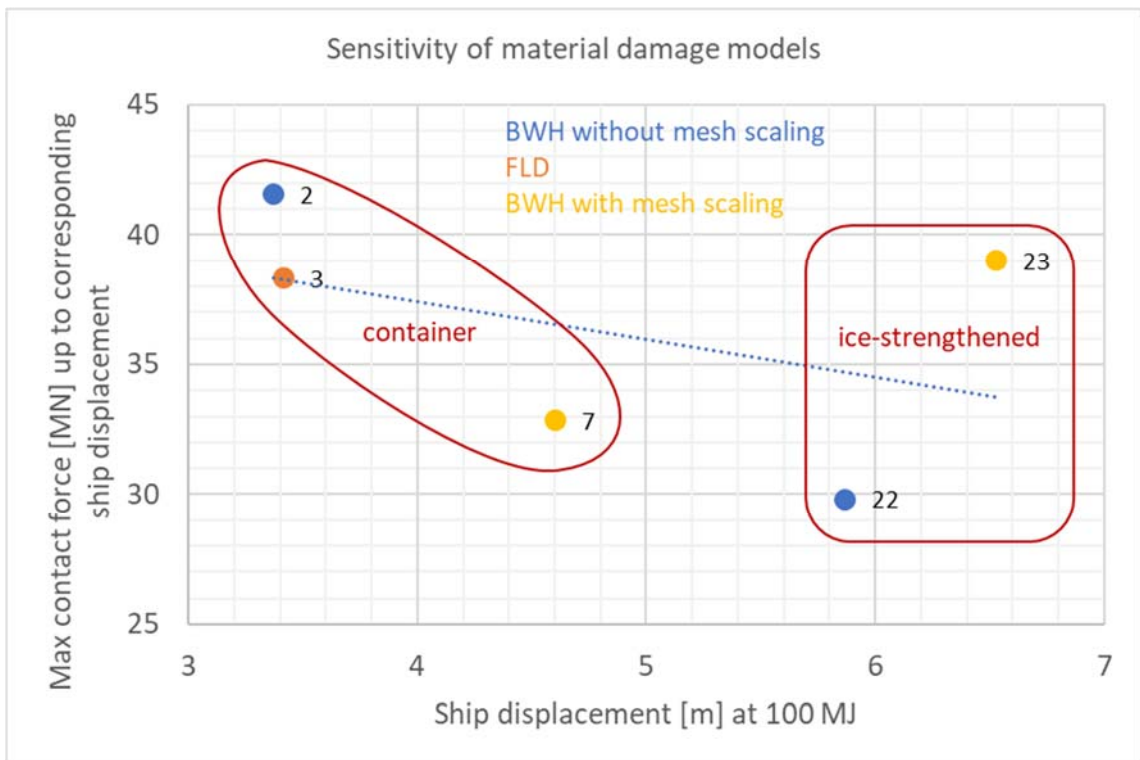
Figure 7-5 shows the sensitivity of the material parameters investigated for impact with the ice-strengthened bow. The simulations with the ice-strengthened bow are not that sensitive to the “mean-high” set of material parameters as seen for the container bow impact simulations.



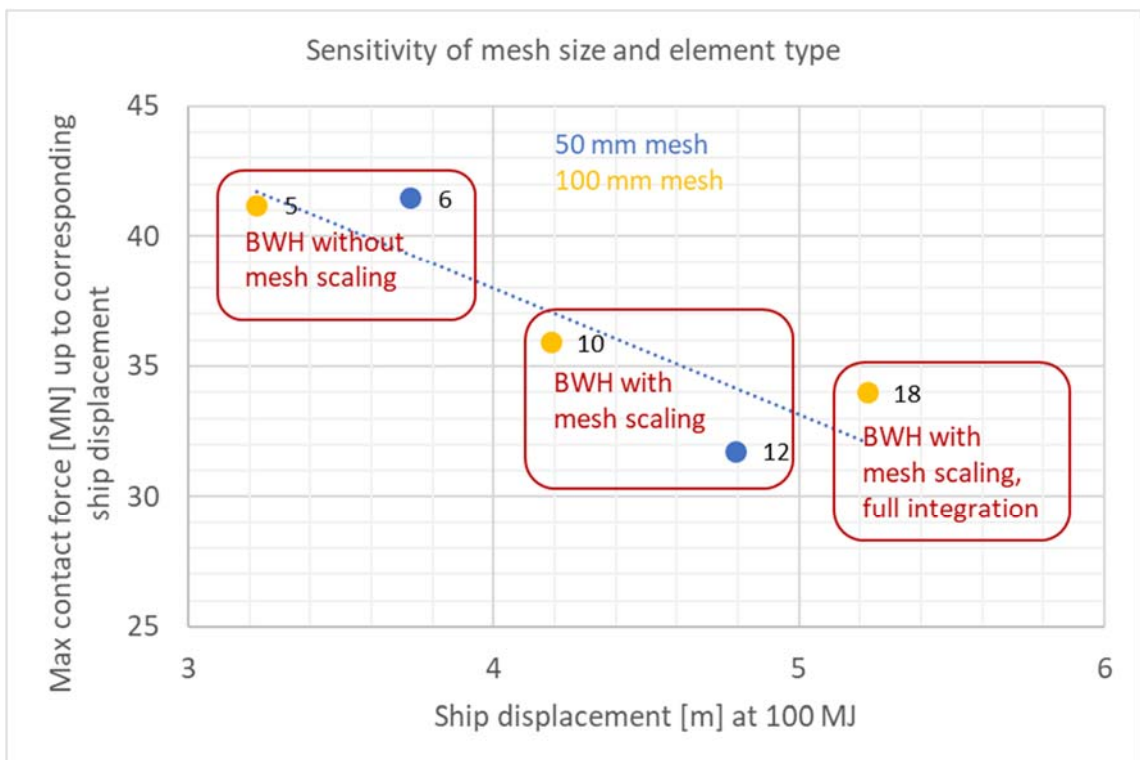
> Figure 7-5 Sensitivity of material parameters, impact ice-strengthened bow-pontoon

Figure 7-6 shows that the local impact simulation is sensitive to the material damage models investigated. The material damage model utilized is mainly the BWH model with mesh scaling. The finite element model behaves more independently of the mesh size when mesh scaling is applied. The FLD material model display similar results to the BWH model without mesh scaling. Both these models are sensitive to coarse mesh by predicting fracture at a later state. In addition, these two models predicted larger damage to the ship than the BWH model with mesh scaling. The latter model is conservative when considering damage of the pontoon.

Figure 7-7 shows that the simulation is more sensitive to the material damage model and the element type utilized than the mesh size.

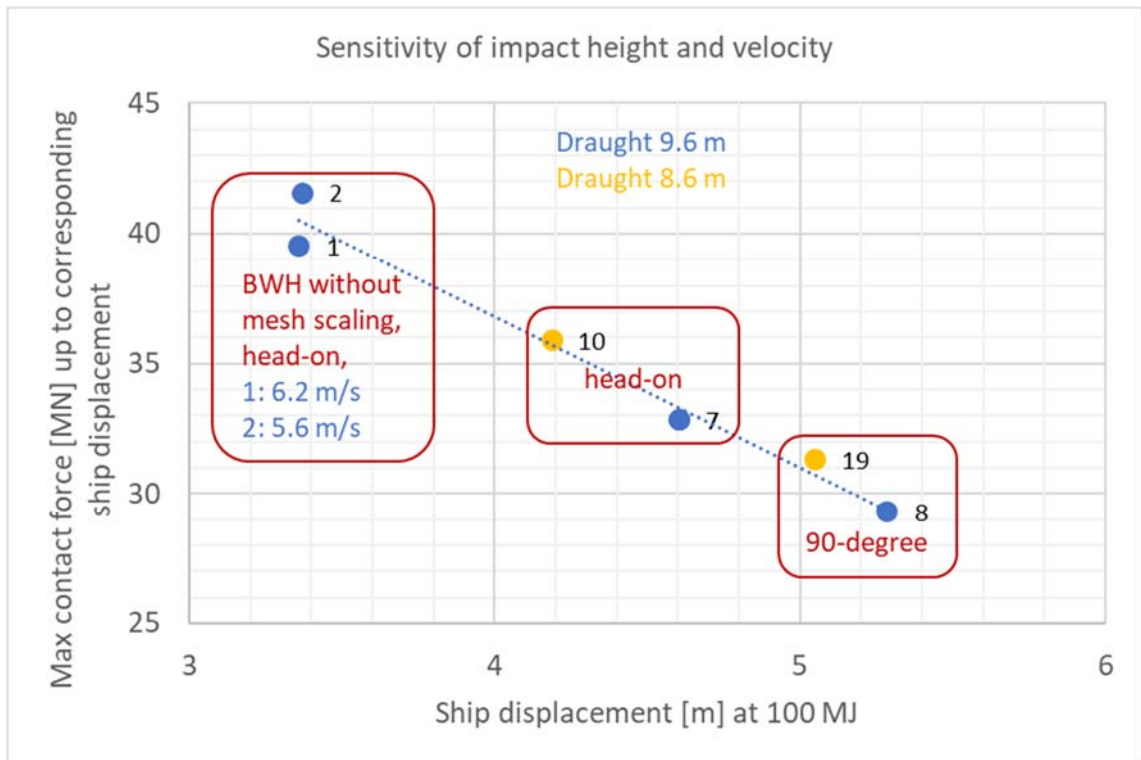


> Figure 7-6 Sensitivity of material damage models



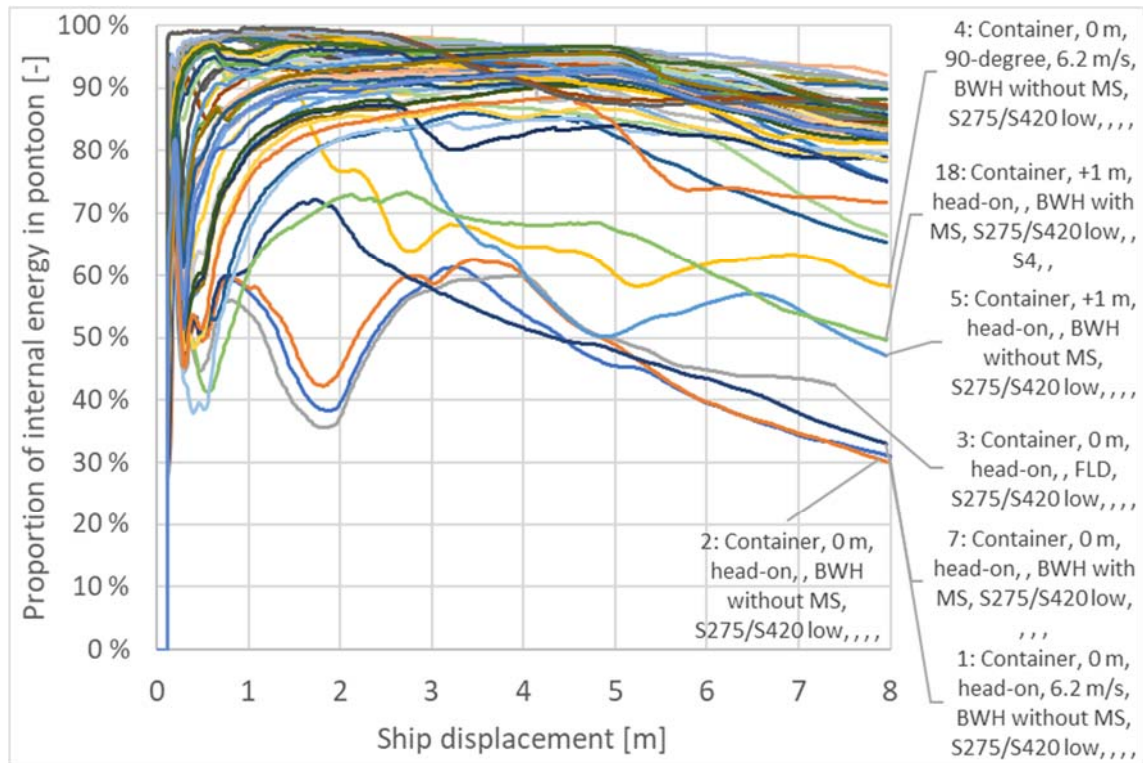
> Figure 7-7 Sensitivity of mesh size and element type

Figure 7-8 shows that the simulation is not very sensitive to a small change of the impact velocity. In terms of the maximum contact energy, the simulation is not very sensitive to draught height of the container bow either. However, impact at scantling draught of the container bow resulted in much higher energy dissipation in the bow than in the pontoon, which is non-conservative for the pontoon design. It has been chosen to use 1.0 m above the scantling draught ("design draught") as the base impact height for the container bow.



> Figure 7-8 Sensitivity of impact height and velocity, impact container bow-pontoon

Figure 7-9 shows the proportion of internal energy in the pontoon for all simulations conducted. Generally, the pontoon dissipates most of the energy while the ship bow is spared. This is conservative when considering damage of the pontoon. There are some exceptions where the ship bow is more damaged. These are head-on impact with draught height 9.6 m of the container bow, the simulations with material damage model FLD or BWH model without mesh scaling and the simulation with full integration of elements.



- > *Figure 7-9 Proportion of internal energy in pontoon [-] impact bow-pontoon, series name of the non-conservative simulations with low proportion of dissipated energy in the pontoon is displayed*

A minor mass scaling is applied to the models to reduce computation time. This is performed by applying an automatic mass scaling which limits the minimum time increment to the ship bows, scaling 0.6 % of the total mass of the container bow-pontoon impact model and 1.1 % of the ice-strengthened bow-pontoon impact model. The mass scaling is low, and the sensitivity of mass scaling is not investigated for the pontoon impact models. Sensitivity of mass scaling is investigated for the bridge girder impact model in [24].

7.2.3 Submarine impact

Submarine impact is discussed in the global assessment report [2].

7.3 Further work

Further work should include updating finite element models to the final geometry of the pontoons and columns. Changes to ship impact design loads should be implemented. A smaller pontoon should be checked to see if this results in more damage to the pontoon. The damage evaluation must be performed in context with the global assessment.

Semi-local impact simulation of the pontoon-column interface can be done, like the column-bridge girder model reported in [2]. Such a model can clarify more detailed how energy from ship impact is absorbed at this interface.

Assessment of ship and/or submarine impact on pontoons with mooring system can be investigated.

Sensitivities to the local impact simulations can be addressed further to minimize the uncertainties. However, this is difficult if not material specification, material tests and experimental tests are performed to calibrate the local simulations. Sensitivity should be investigated for other type of ship bows that can hit the pontoon and impact at lower velocities.

In the next phase, detailed design of the pontoon, pontoon-column interface, column and column-bridge girder interface must be conducted. This to make sure that the bridge's resistance against ship impact meets the requirements defined.

- [1] SBJ-32-C4-SVV-90-BA-001, "Design Basis Bjørnafjorden floating bridges," Statens Vegvesen, 2018.
- [2] SBJ-33-C5-OON-22-RE-013-B, "Concept development floating bridge E39 Bjørnafjorden - K12 - Ship impact, Global assessment," Norconsult, Dr. Techn. Olav Olsen, 2019.
- [3] Håndbok N400 , "Bruprosjektering," Statens vegvesen Vegdirektoratet, 2015.
- [4] NS-EN 1991-1-7:2006+NA:2008, "Eurocode 1: Actions on structures - Part 1-7: General actions - Accidental actions," Standard Norge, 2006.
- [5] DNVGL-RP-C204, "Design against accidental loads," DNV GL, 2017.
- [6] DNVGL-RP-C208, "Determination of structural capacity by non-linear finite element analysis methods," DNV GL, 2016.
- [7] DNVGL-OS-B101, "Metallic metals," DNV GL, 2015.
- [8] Simulia, "Abaqus/CAE 2017," Dassault Systèmes, 2016.
- [9] K. M. Ofstad, "Finite element modelling of steel bridge structures exposed to ship collisions (Matster thesis)," NTNU, Trondheim, 2018.
- [10] A. S. Hagbart, O. S. Hopperstad, R. Törnqvist and J. Amdahl, "Analytical and numerical analysis of sheet metal instability using a stress based criterion," *International Journal of Solids and Structures*, vol. 45, no. 7-8, pp. 2042-2055, 2008.
- [11] M. Storheim and J. Amdahl, "On the sensitivity to work hardening and strain-rate effects in nonlinear FEM analysis of ship collisions," *Ship and Offshore Structures*, vol. 12, no. No. 1, pp. 100-115, 2017.
- [12] Y. Sha, I. F. Osvoll and J. Amdahl, "Ship-pontoon collision analysis of the floating bridge concepts for Bjørnafjorden," NTNU, 2018.
- [13] Y. Sha and J. Amdahl, "Local deckhouse-girder collision analysis of the floating bridge concept for Bjørnafjorden," NTNU, 2018.
- [14] H. S. Alsos, J. Amdahl and O. S. Hopperstad, "On the resistance to penetration of stiffened plates, Part II: Numerical analysis," *International Journal of Impact Engineering*, vol. 36, pp. 875-887, 2009.
- [15] SBJ-20-C3-AAS-27-RE-002, "Bjørnafjorden Suspension Bridge - K1 Impact Report - Local," Aas-Jakobsen, NGI, Johs Holt, Moss Maritime, Plan Arkitekter, Cowi, Aker Solutions, 2017.
- [16] SBJ-33-C5-OON-22-RE-014-B App. B, "K12 - Ship Impact, pontoons and columns, Appendix B - Mesh and material sensitivity study," Norconsult, Dr. Techn. Olav Olsen, 2019.
- [17] H. S. Alsos and J. Amdahl, "On the resistance to penetration of stiffened plates, Part I - Experiments," *International Journal of Impact Engineering*, vol. 36, pp. 799-807, 2009.
- [18] Drawing no. K7-057, "E39 Bjørnafjorden K7 End-anchored Floating Bridge," Norconsult, Dr. Techn. Olav Olsen, Aker Solutions, 2017.
- [19] Drawing no. K7-063, "E39 Bjørnafjorden K7 End-anchored Floating Bridge," Norconsult, Dr. Techn. Olav Olsen, Aker Solutions, 2017.
- [20] SBJ-33-C5-OON-22-RE-018-B, "Concept development floating bridge E39 Bjørnafjorden - K12 - Design of pontoons and columns," Norconsult, Dr. Techn. Olav Olsen, 2019.

- [21] M. Storheim, "Structural Response in Ship-Platform and Ship-Ice Collisions (Doctoral theses)," NTNU, Trondheim, 2016.
- [22] SBJ-33-C5-OON-22-RE-014-B App. C, "K12 - Ship Impact, pontoons and columns, Appendix C - Sensitivity of ship impact response," Norconsult, Dr. Techn. Olav Olsen, 2019.
- [23] E-mail by Fredrik Lindqvist from SSAB, "Teknisk forespørsel - materialegenskaper ved stålbestilling?," Borlänge, received 2019-04-15.
- [24] SBJ-33-C5-OON-22-RE-015-B, "Concept development floating bridge E39 Bjørnafjorden - K12 - Ship impact, Bridge girder," Norconsult, Dr. Techn. Olav Olsen, 2019.